（Annual Report）1997-1998

1.PHYSICS

1.1 Track Sensitivity Analysis of CR-39 Using Atomic Force Microscope

AMikio Yamamoto, Nakahiro Yasuda, Mieko Kurano, ATatuaki Kanai[1], Kuniaki Amemiya,Hiroyuki Takahashi[1], Masaharu Nakazawa[1],Atsushi Kyan[2], Tadayoshi Doke[2] and Koichi Ogura[3]

([1]CUniv. of Tokyo, [2]DWaseda Univ., [3]ENihon Univ.)

Keywords: CR-39, track detector, etch pit, track sensitivity, atomic force microscope

We have studied application of an atomic force microscope (AFM) to measurements and sensitivity analysis of minute etch pits on CR-39 plastic nuclear track detectors. The objective size of AFM measurements is about 1/100-1/1000 that of ordinary optical microscope (OPT) measurements. In contrast to the OPT method, by the AFM technique observations of the three-dimensional profile of the track in the early stage of the etching process can be made. Therefore AFM is a very useful tool to study the track etching mechanisms of the track detector. Moreover AFM observations make it possible to observe high density tracks produced by heavy ions of more than 10^7 ions/cm^2, which, due to the overlapping of tracks, are difficult to make using OPT for samples irradiated with higher density than 10^4 ions/cm^2. Therefore AFM observations would be applicable to in vivo measurements of an ion's LET and the absorbed dose for carbon ion cancer treatments at NIRS, because the order of the exposure density for the cancer treatment is 10^6 ions/cm^2.

Several pieces of CR-39 (HARZLAS (TD-1); Fukuvi Chemical Industry Co. Ltd., Japan) were exposed to 490 MeV/n Si ions and 290 MeV/n C ions from NIRS-HIMAC (Heavy Ion Medical Accelerator in Chiba). The irradiation was done at normal incidence at a density of $\sim 10^7$ ions/cm^2 for AFM measurements and 3×10^3 ion/cm^2 for OPT measurements.

After the irradiation, the CR-39 pieces were etched in 7N NaOH solution kept at 70 degrees using a water bath incubator. The etching time was varied from 3 to 180 minutes.

The AFM (Nanoscope III; Digital Instruments) was equipped with a 125 μm cantilever having a typical tip length of 10 μm and was operated in the tapping mode which has been developed as a method to achieve high resolution without inducing destructive frictional forces. The cantilever was oscillated near its resonant frequency (∼250kHz) which allowed the whole surface of the sample to be scanned.

It is well known that the track sensitivity S is a function of REL (Restricted Energy Loss) and is denoted by the etch rate ratio of the track etch rate VTto the bulk etch rate VB. S for 490 MeVn Si ions (REL=284 MeV cm^2/g) and 290 MeV/n C (REL=70 MeV cm^2/g) ions were calculated by the following two formulas: where D,L and B are the track diameter, the track length and amount of bulk etch, respectively.

$$S_1=\frac{1+\left(\frac{D}{2B}\right)^2}{1-\left(\frac{D}{2B}\right)^2}-1 \quad (1), \qquad S_2=\frac{L+B}{B}-1 \quad (2),$$

The variations of S1 and S2 for C and Si tracks are summarized in Fig.1, as a function of B. Sensitivities S1 at different depths of CR-39 were almost the same value within statistical error. In contrast to S1, and as was predicted from the progression of track profiles, sensitivities S2 calculated by using B and L were smaller than S1 especially for a short etching time, but it seemed that the values of S2 increased gradually with the etching time and approached S1. This tendency was almost the same for C and Si tracks in spite of having different REL values. In the early stage of the track evolution, the track sensitivity calculated by using formula (1) will be more reliable than that from formula (2).

Fig. 1 Variations of sensitivities of S1 (circles) and S2 (triangles) as a function of the amount of bulk

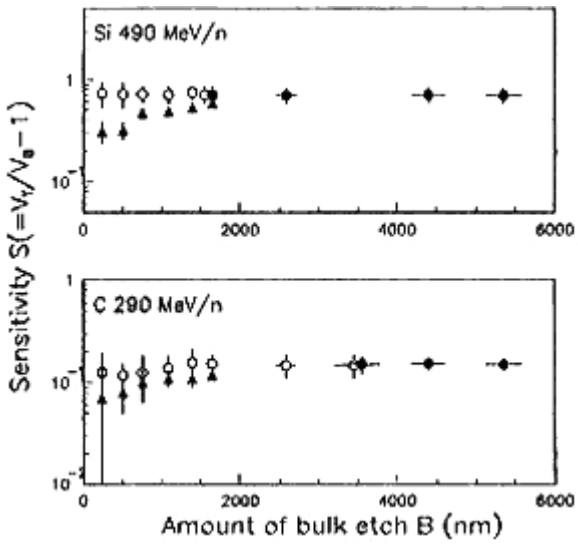

etch.S81DB indicated by open and closed circles were measured by AFM and OPT, respectively.

Publications:

1) Yamamoto M., Yasuda N., Kaizuka Y., Yamagishi M., Kanai T., Ishigure N., Furukawa A., Kurano M., Miyahara N., Nakazawa M., Doke T., and Ogura K.: Radiat. Meas, 227-230, 1997.

2) Yasuda N., Yamamoto M., Miyahara N., Ishigure N., Kanai T., and Ogura K.: Nucl. Inst. and Meth.B, 111-116, 1998.

1.2Measuring System for nT-order Magnetic Field near Human Hands

Hideyuki Kokubo, Mikio Yamamoto, Masahiko Hirasawa, Hideaki Sakaida, Masahide Furukawa, Kimiko Kawano[1], Tsuyoshi Hirata[2] and Nobuo Fukuda

([1]Nippon Medical School, Tokyo, Japan; [2]C&C Media Research Laboratories, NEC Corporation, Kawasaki, Japan)

Keywords: magnetic field, nT, qigong, human hands, living body, measuring system, somatic science, anomalous

Some reports suggest that special qigong masters or students can generate a strong magnetic field under the subjects' control. In these reports, an nT-order to 100nT-order magnetic field is detected at palms, the forehead, the top of the head, etc. However, there are few experts who can generate an nT-order magnetic field even in an experiment on bio-magnetism with SQUID which can detect 1.2 pT, therefore anomalous bio-magnetic fields have not been researched well yet.

We developed a pilot system to measure the magnetic field caused by human hands (Fig. 2). The pilot measuring system consists of a small magnetic shielding case (double box type) which shields human hands, magnetometers, amplifiers, a data sampling system and a monitoring system. Geomagnetic field was decreased about 1/1500 in the shielding case. Moreover, for easy carrying, the magnetic shielding case could be disassembled into some parts and placed in a handling packet.

A preliminary test was done with nearly 70 ordinary Japanese persons and about 15 Japanese and Chinese qigong masters/students. The standard trial of the preliminary test consisted of three parts: 1) 2 minute control; 2) 2 minute qi-emitting; 3) 2 minute control.

Through the test, we examined the following points. 1) Regarding portability of the case, the measuring system achieves the useful level expected. 2) For long time experiments, an air conditioning system was needed. 3) It was easy to detect a magnetic field not caused by the hands. For example, in the case of a qigong master, it was considered that the detected magnetic field was caused near the subject's stomach. In an interview after the experiment, moreover, we heard he had often eaten some metal objects, such as a small knife as part of the qigong training. 4) For ordinary persons, there was no detection of nT-order anomalous magnetic field caused by the hands.

Results of the test confirmed that we should develop this system by further studies on certain aspects; e.g. analyzing methods or using diffrent sensors.

Publication

: Kokubo, H., Yamamoto, M., Hirasawa, M., Sakaida, H., Furukawa, M., Kawano, K., Hirata, T. and Fukuda, N.: J. Int. Soc. Life Info. Sci.,16, 134-147, 1998.

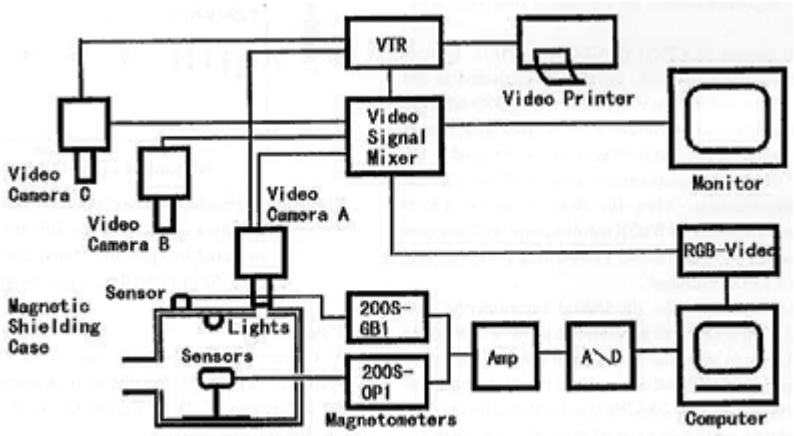

Fig. 2 Measuring system for nT-order magnetic field near human hands

1.3Measurement of Physiological States duringQigong

Hideaki Sakaida, Hideyuki Kokubo, Mikio Yamamoto, Masahiko Hirasawa and Kimiko Kawano*

(*ANippon Medical School, Tokyo, Japan)

Keywords: various simultaneous measurements (VSM), respiration, photoplethysmogram, electrodermal activity, electroencephalogram, alpha wave, qigong

Modern scientific research on qigong started in 1978 in China. We have tried to measure the physiological state emitting qi during qigong by Various Simultaneous Measurements (VSM). The difference between emitting qi during qigong and at rest, and moreover the change while emitting qi during qigong, were measured.

The subject was a healthy woman, 32 years old who had practiced Tai- ji-quan and Tong-bei-quan-qigong for about 1.5 years about 5 years ago. Measurement were done at pre-rest for 2.5 minutes, emitting qi for 2 minutes and post-rest for 2 minutes. Measurement items were RSP (ReSPiration), PPG (PhotoPlethysmoGram), EDA (ElectroDermal Activity), 2 poles of EEG (ElectroEncephaloGram) (Fp1, Fp2). RSP was measured on the abdomen. PPG was measured for the right-hand middle finger. EDA was measured between the index finger and the third finger of the right-hand. Based on the international electrode guiding method (10-20 method), EEG was measured with the single pole guiding method. Reference electrode was placed on an earlobe. The grounding electrode was Fpz.

Results from separately analyzing each item showed periods of RSP and PPG lengthened, the EDA value increased and a peak appeared, and the alpha wave amplitude increased while emitting qi during qigong as compared to at rest. In the emitting qi trial, after the EDA peak, periods of RSP and PPG became short and the alpha wave amplitude decreased. Because the subject consciously made the period of RSP long at the time of emitting qi during qigong, this was seen in the data as a matter of course. EDA suggested that the subject was straining while emitting qi. This may be the result of passive concentrating and imaging emitting qi. It has been reported that the alpha wave of the front head increases at the time of concentrated consciousness such as when doing mental arithmetic. So the increase may be a result of passiveconcentration.

Publication:

Sakaida, H., Kokubo, H., Yamamoto, M., Hirasawa, M. and Kawano, K.:
J. Int. Soc. Life Info. Sci., 16, 29-41, 1998.

1.4Dosimetry of Radiosurgery Beams Using Several Detectors with Different Sensitive Volumes

Takeshi Hiraoka, Akifumi Fukumura, Kaname Omata and Mitsue Takeshita

Keywords: dosimetry, radiosurgery beam, small detector, stereotactic radiotherapy, stereotactic radiosurgery

To investigate the dosimetry method for very small fields in stereotactic radiosurgery and stereotactic radiotherapy using a photon beam, several different types and sizes of detectors have been used for the measurements of high energy photon beams. The detectors used consisted of three ionization chambers, [type and nominal ionizing volume: PTW-23323 (0.1ml), Markus (0.05ml), Exradin-Al (0.05ml)], four silicon diodes [type and effective diameter: F-1796 (2.5mmφ), EDD-2 (1.5mmφ), EDD-5 (1.5mmφ), 96111 (0.6mmφ),]and a diamond detector[(RIGA (4.5mmφ)]. An Exradin-A14 and a Farmer ionization chamber were used for comparison purposes.

The field sizes for the measurements gave 7.5, 10, 15, 20, 25mm diameter using additional collimators. The depth dose curve (Tissue Maximum Ratio, TMR) and lateral dose distributions (Off Axis Ratio, OAR and Output Factor, OPF) were obtained with a 10MV X-ray beam. To check the energy dependency of the detectors, measurements were also performed using a 6MV X-ray beam. An in-house phantom system was designed using two stepping motor controlled by a lap top computer to measure the accurate dose distributions with accuracy in positioning of ±50μm.

Before measurements of dose distributions for radiosurgery beams, the response of the detectors to be used for such a field were checked. A TMR in water for 5cm x 5cm field with a 10MV X-ray beam was measured using the detectors. All curves were normalized at the peak depth. The data were then fitted by a polynomial function for each detector in order to compare the value at a particular depth in the phantom. Almost all points at the same depth agreed within ±0.5% when located at a depth of less than 20cm in water. The same values were obtained for 6MV X-ray beam. For very small collimator sizes, the TMR values measured with the detector having a volume of less than 0.1ml agreed within 1% except for one chamber.

Measurement of lateral dose distributions, OCR and OPF, were influenced significantly by the detector size. The relative OCRs determined from a variety of radiation detectors were compared. The widths at 70, 50 and 30% dose levels for each detector were determined from the OCR curves measured at the depth of the peak dose in the water phantom. The changes in the curve with detector size could be quantified and extrapolated to zero detector size to obtain a corrected curve for distributions measured with detectors of different sizes. The correction factors for other dose levels could be obtained by using the same method.

To calculate an absorbed dose at an arbitrary field, it is also important to consider output factor. Measurements of this factor for the 10MV X-ray with different size detectors were carried out. As the output factor is affected directly by detector size, a detector with a diameter of a few mm is needed for the field of less than 20mm beam collimation for precise measurement. Then the detector size correction factor was also obtained from the extrapolation for each collimator size. However, for a smaller collimator

the data were widely scattered because the detector size was only explained by its diameter. For the lateral dose distributions with a very small field the detector response could be affected by not only by size but also by energy dependency, directional response, and electron transport process.

We concluded that the relative energy dependency with depth for all detectors investigated was less than 1% between the peak and 20cm depth in water. The TMR values were obtained with sufficient accuracy with these small detectors. The size of the chamber should be small, but not too small to avoid an adverse effect on measuring the ionization charge. For lateral dose distributions, the detector size should be small enough with respect to the size of the radiation field since the size of the detector directly affected the measurement. Accurate dose distributions must be determined by an extrapolation technique using several detectors with different sizes.

1.5Simple Range Measurement of Therapeutic Ion Beams Using Visible Rays Generated in a Bare Plastic Scintillator Block

Akifumi Fukumura, Yutaka Noda, Kaname Omata, Takeshi Hiraoka, Yasuyuki Futami, Naruhiro Matsufuji, Takeshi Murakami and Tatsuaki Kanai

Keywords: range of ion beam, plastic scintillator, scintillation light, CCD camera, ion beam therapy

Therapeutic ion beams exhibit a flat depth-dose distribution until near the end of their range where there is a marked increase in dose, called the Bragg peak. To superimpose the Bragg peak on a tumor precisely, it is necessary to measure the range of the beams with enough accuracy. A combination of a detector and a tissue-equivalent phantom of variable thickness is normally employed in most charged-particle therapy facilities including HIMAC. This process is indispensable before patient treatment, and it consumes considerable beam time since it is comprised of a series of sequential measurements. Then we have developed a simple method to measure the range, using a bare scintillator and a CCD camera.

Usually a scintillator is housed in a container, viewed with photo multiplier tubes and operated in a pulsed mode. We, however, tried to irradiate a bare scintillator block with a high-energy ion beam of the high dose rate employed in therapy.

A plastic scintillator is equivalent to water with a density close to 1.0/gcm^3 and consists of hydrogen and carbon. Because of the equivalence, it is expected that the range in a plastic scintillator can be converted to that in water with just a minor correction. A homogeneous plastic scintillator block, 5cm×5cm×30cm, was irradiated by 290 MeV/u carbon beams from HIMAC. The scintillator was not wrapped by light shielding material. A ruler was placed on the scintillator to measure the range of the beam in the scintillator. A CCD video camera was focused on the scintillator 6m away and perpendicular to the beam axis. The image was monitored on CRT during the irradiation. We also used absorbers, when changing the residual range of the beams.

Fig. 3 is a picture instantly recorded by the CCD camera during irradiation by the carbon beam with an intensity of 10^6 ions per second, which is much higher than that of a counter experiment. We could clearly observe a stripe of light generated along the beam track in the plastic scintillator. In a close-up picture near the end of the range, we could recognize the falloff of the dose within about 0.5mm. We also found that the relation between observed ranges in the scintillator and the residual ranges in water showed very good lineanty. As we expected, the bare plastic scintillator is applicable to measure range of high intensity heavy ion beams.

In an ordinary measurement using a combination of a phantom and a detector, the range must be kept constant during a measurement. The scintillator method, however, offers a value of the range in a fraction of a second, since a CCD video camera records thirty frames per second. This feature enables us to observe variation of the ranges consecutively. The method provides information not only on the range but also on the position and shape of beams simultaneously by viewing the emitted light perpendicular to and along a beam axis when pencil beams are employed.

Compared to the usual range measurement method, this method is very simple, realizes measurement in

a fraction of a second and consecutively, and provides information on shape and position of the beam simultaneously.

Publication:

Fukumura, A., Noda, Y., Omata, K., Hiraoka, T., Futami, Y., Matsufuji, N., Murakami, T. and Kanai, T.: Nucl. Instr. Meth. Phys. Res. A, 416, 148-151, 1998.

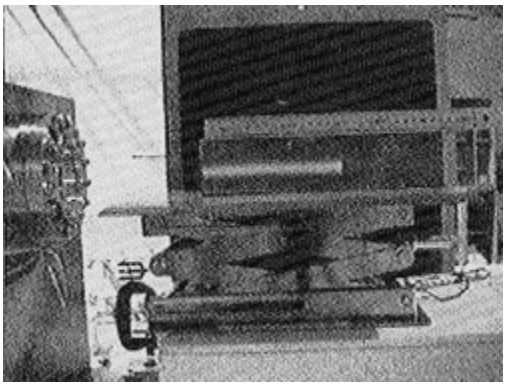

Fig. 3 Visible scintillon light genereted by 290 MeVu carbon beam in the plastic scintillator.

1.6Dose Evaluation of Patients Receiving Paranasal Sinus Radiography

AKanae Nishizawa, Masaki Matsumoto, Tetsuo Ishikawa and Kazuo Iwai

Keywords: patient exposure, effective dose, CT examinationComputed tomography(CT) examinations

Computed tomography(CT) examinations prior to operation on the paranasal sinus with an endoscope are being carried out more frequently as CT has better spatial resolution. Since the patient dose from CT is higher than doses by conventional paranasal sinus imaging technique, it is worthwhile to compare the dose due to typical preoperative radiographic examinations.

The exposures of various organs or tissues using three types of sinography were measured, namely : (1) plain films with waters' view combined with lateral view in the direction of LR; (2) conventional tomography with twelve radiographic imaging from PA direction; (3) CT with 5mm slice thickness and with 3mm slice thickness, consisting of digital radiography for positioning prior to CT scanning and 16 CT scanning for the examination. The measurements were performed under conditions as close to clinical examinations as possible with an anthropomorphic phantom. Two different types of thermoluminescence dosimeters (TLDs), BeO and CaCO4:Tm, were used to determine the organ or tissue doses in the phantom experimentally. From the measured data, the effective dose were calculated according to the ICRP 60 recommendation.

The effective doses were 56, 94, 590 and 380 μSv for (1) simple radiography consisting of Waters' and lateral views, (2) conventional tomography, (3) CT with 5mm slice thickness and (4) CT with 3mm slice thickness, respectively. The brain received an equivalent dose in excess of the highest dose in any of the other organs for which a tissue weighting factor (WT) was specified, a WT of 0.025 applied to the brain following the footnote of the ICRP 60 Table 2. The contributions of the brain dose to the calculation results of effective doses were extremely high being 25% in the plain films, 16% in the conventional tomography, 60% in the CT with 5mm slice thickness and 74% in the CT with 3mm slice thickness.

The surface doses were about 2mSv and 9mSv for the back of the head from plain films and conventional tomography, respectively, and 17-22 mSv for the cheek from CT examinations. The doses to the eye lens from plain films were about 0.15mSv for the right eye and 0.8mSv for the left eye. From conventional tomography, eye lens dose was 0.3mSv. From CT examinations, the lens dose was 35mSv for 5mm slice thickness and 22mSv for 3mm slice thickness. According to the ICRP 60, the threshold of the detectable opacities in the eye lens and the cataract are 0.5-2.0 Sv and 5 Sv, respectively, in the case of a single brief exposure. The present measurements indicate that the eye lens dose from CT examinations was 35 mSv (5mm slice thickness) which was 7% or less of the threshold of the detectable opacities.

As the number of paranasal sinus treatments with an endoscope increases, there is a mounting need for accurate identification of the inflammation position, so paranasal sinus examinations with CT are increasing accordingly. While it is true that CT gives more information than conventional radiographic means, at the same time, it should be remembered that the dose of CT examinations are considerably higher than those of conventional radiography.

1.7Space Radiation Dosimetry by Combination of Radiophoto-luminescent Glass, Thermo-luminescent Dosimeter, and Plastic Nuclear Track Detector

Hiroshi Yasuda and Kazunobu Fujitaka

Keywords: space radiation, radiophoto-luminescent glass, thermo-luminescent dosimeter, plastic nuclear track detector, heavy ion, Mir, Spaceshuttle

Space radiation dosimetry was carried out in the Russian Space Station MIR and Shuttle/MIR Mission 8 (STS-89) using small solid dosimeters: radiophoto-luminescent dosimeters (RPLGs), thermo-luminescent dosimeters (TLDs), and plastic nuclear track detectors (PNTDs). Those dosimeters were exposed to heavy charged particles in HIMAC and NIRS-Cyclotron to examine their responses to high LET particles; their correction coefficients for high-energy heavy charged particles are little known. Specific radiophoto-luminescence intensities (RPLs) normalized by ^{137}Cs-γ ray are plotted versus the beam LETs in Fig.4. Clear decrease of specific RPL with LET is observed even at a very low LET region of the proton beam. Because RPLG has a large dynamic range, this tendency cannot be explained only by saturation of color centers; it might be due to a quasi-thermal effect appearing on the glass which has a non-crystal structure. From the regression curve shown in Fig. 4, it is judged that the geometric mean LET can be evaluated by RPLG for more than 0.5 keVμm^{-1} if the precise absorbed dose is known. For TLD-MSO, TL decreases with increasing LET, beginning at a high LET region as shown in Fig. 5. Because the degree of saturation of the color center should reflect increase of the ionization density, correction of the TLD-MSO value to the absorbed dose should be properly done according to the information on LET distribution of high LET components obtained by PNTD analysis.

These considerations were applied to estimation of the absorbed dose and the geometric mean LET in space. We had two opportunities for this in the Russian space station MIR from July 5 to August 14, 1997 (about 40 days) and the 8th Space Shuttle/Mir Mission from January 22 to January 31, 1998 (about 9 days). For each experiment, three packages of tissue-equivalent plate containing small solid dosimeters were used. The luminescence intensities of TLD-MSO and RPLG are shown in Figs. 6 and 7 for each experiment; these values are normalized by γ ray of mGy equivalent.

Estimated values for Mir mission:

Absorbed dose for 40 days:	10-21 mGy
Absorbed dose rate:	0.25-0.51 mGy d^{-1}
Geometric mean LET:	1.0-2.0 keVμm^{-1}

Estimated values for ShuttleMir Mission:

Absorbed dose for 9 days:	2.8-3.7 mGy
Absorbed dose rate:	0.31-0.41 mGy d^{-1}
Geometric mean LET:	4.6-8.0 keVμm^{-1}

In both cases, large variation are observed even in the same module. The values measured by this small, stable, and simple method seem to be reasonable based on comparison to previously reported values.

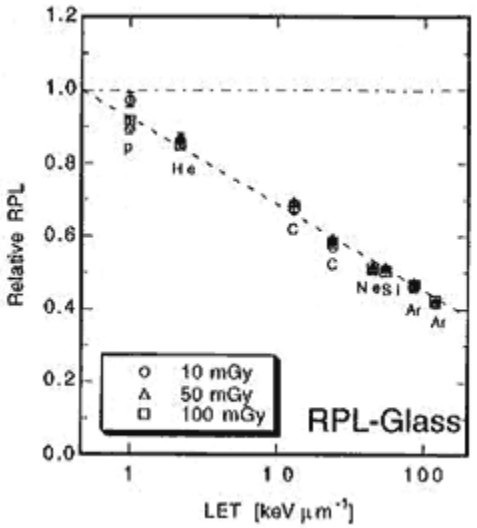

Fig.4 Plot of RPL normalized by ^{137}Cs-γ ray versus beam LET.

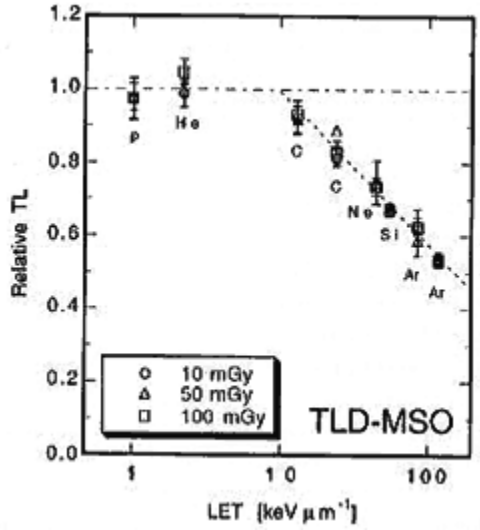

Fig.5 Plot of TL normalized by ^{137}Cs-γ ray versus beam LET for TLD-MSO.

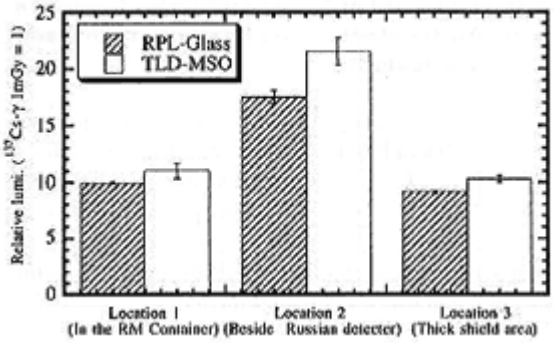

Fig.6 Normalized RPLG and TLD-MSO values measured in MIR core module.

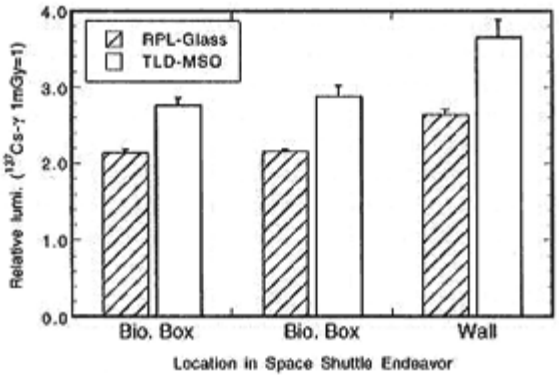

Fig.7 Normalized RPLG and TLD-MSO values measured in the Spacehab locker of Space Shuttle Endeavor.

1.8Theoretical Approach to the Relative Biological Effectiveness of High-Energy Heavy Ions

AYukio Sato and Fuminori Soga

Keywords: RBE, high-LET, quadratic dependence, mammalian cells

An expression has been developed to analyze the relative biological effectiveness (RBE) of accelerated heavy ions for the inactivation of mammalian cells. The RBE can be well explained by using the quadratic dependence on the LET of the cellular effect. For high-LET radiation in low-dose regions, the inactivation cross section (σ) can be expressed as σmax[1-exp{k $(LET/L1)^2$}]; here, k is the number of heavy ions traversing a cell nucleus and L1 is a geometrical parameter related to the DNA structure, which depends on the cell type.

Our consideration and interpretation are comprised of the following elements: 1) lethality is induced when the damage exceeds a critical level; 2) the endpoint damage leading to lethality is proportional to LET^2 in the high-LET region, and its characteristics were well studied using neutron data by Kellerer and Rossi; 3) the number of"hits" is given by k $(LET/L1)^2$, where L1 corresponds to the critical value for inducing lethal damage by a single track; 4) the Poisson fluctuation in energy deposition is introduced, since LET is an avenge quantity; 5) the lethal fraction with hit-number≧1 can be expressed as 1-exp{-k $(LET/L1)^2$}. A similar expression was used for spores by Powers 30 years ago, though his process was quite different from 3).

We used the expression in 3) and the Poisson distribution for the stochastic property of particle hitting to calculate the survival of cell populations and compared the results to the RBE-values of heavy ions recently obtained for Chinese hamster V79 cells. When S denotes the survival, our final expression is given as

$$S=\exp[-n(1-\exp\{-(L/L1)^2\}], \quad (1)$$

where n is the average number of heavy ions traversing per cell nucleus and L is the track-average LET[keV/μm]. By using the avenge dose (D), eq.(1) can be rewritten as

$$S=\exp[-A16L(l-\exp\{-(L/L1)^2\}D), \quad (2)$$

where A is the sensitive area of the cell, which is close to the projected area of the cell nucleus. Figure 8 compares the calculated D1 (i=1, 10, 37%) for different L1-values and the experimental results in which Chinese hamster V79 cells were irradiated with carbon beams having different LETs along the Bragg curve. Consequently, an L1 of 152keV/μm and an A of 50 μm^2 were found to give the best fit. For LET-values between 30 and 500keVμm, the calculated results using eq.(2) also agreed with other published data within an error of -15 to +8%.

As can be seen from Fig. 8 and eq.(1), when LET is very high (higher than 300keV/μm), saturation appearing in terms of LET and S is expressed as exp (-n) to a first order approximation; hence, those cells with a single traverse are always killed while other cells without a traverse are not killed. Under constant D, the number of such non-hit cells becomes large as LET increases. This suggests that RBE rapidly decreases in the very high-LET region, which is generally called "overkill". By contrast, when LET is

smaller than 30keV/μm, the value of LET^2 becomes very small. Therefore the lethal fraction also decreases, though indirect effects of radiation may appear in such low-LET regions. At around a LET of between 100 and 200keV/μm (about 150keV/μm in the case of V79 cells), the number of non-hit cells is not small and the LET^2 value of hit-cells is still large. As a result, the appropriate LET region shows efficient cell-killing, leading to a high-RBE.

Eqs.(1) and (2) can well explain the mechanism of a peaked curve of the RBE-LET relationship in the high-LET region.

Publication:

Sato, Y. and Saga, F.: J. Radiation Research, 103-1 10, 1997.

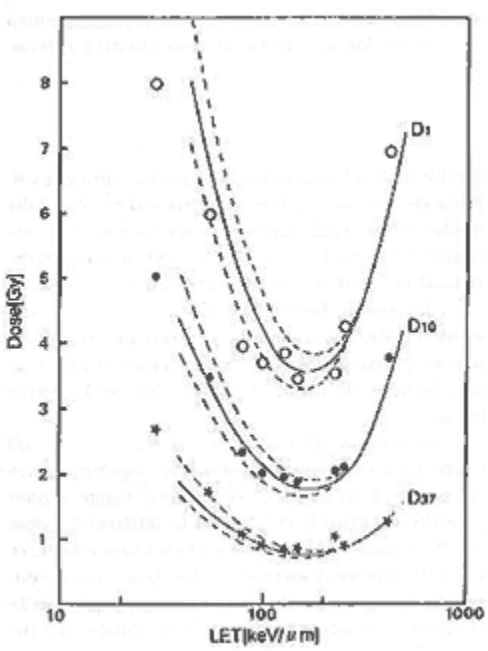

Fig.8 Solid lines show the calculated dose curves in 1,10 and 37% survival (D1,D10,D37)vs,track-averageLET when L1=152keV/μm.The two dotted lines are those at L1=174keV/μm(above) and 130keV/μm(below the solid lines).In Furusawa's experiment,V79 cells were irradiated with carbon beams having different LETs; the results are symbolized by ○for D1●for D10,and for D37.

1.9 Development of Secondary Beam Course in HIMAC for Medical Applications with Radioactive Isotopes

Atsushi Kitagawa, Mitsutaka Kanazawa, Sigeru Kouda, Takeshi Murakami, Koji Noda, Mitsuru Suda, Takehiro Tomitani and Masami Torikoshi

Key words: cancer therapy, dose distribution, radioactive isotope beam, positron camera, PET

As the relativistic high-energy heavyion beam has the characteristics of a good localized dose distribution and a large relative biological effectiveness, a ^{12}C beam with an energy higher than 290 MeV/u has been employed for cancer therapy at HIMAC (Heavy Ion Medical Accelerator in Chiba). In order to verify a particle range and to utilize its observation for more accurate treatment planning, a secondary beam course of a radioactive isotope beam has been constructed. The idea is that the stopping position of a short-lived positron emitting nuclei, such as 11C or ^{19}Ne, can be precisely detected by measuring annihilation gamma-rays with a positron camera or a PET.

Fig. 9 shows a schematic view of the beam course. A projectile fragmentation is used for the production of a radioactive isotope beam. Projectile particles of a primary beam produce various fragment particles through nuclear reactions in a target located at the focus point F0. As most of the fragment particles have the same velocity and the same angular distribution concentrated to the forward direction, it is possible to use them as the secondary beam. The on-line isotope separator is comprised of two dipole magnets, and it identifies and separates the required isotope from various fragments. The first magnet analyzes the fragment momentum on the basis of the rigidity analysis, where the particles of the desired charge-to-mass ratio, A/Z, are selected. Then the energy of the fragments of the selected A/Z is decreased in a thick energy degrader at the focus point F1. The energy loss depends on their charge, so that the momentum of different Z among particles of the same A/Z differs after passing through the energy degrader. The second analyzer magnet selects the particles of the desired Z by momentum selection. The purity of the secondary beam is analyzed by a particle identification system consisting of a time-of-flight (TOF) counter and an energy loss (ΔE) counter.

The ^{11}C isotope was effectively produced from the 12C primary beam. The production rate of ^{11}C was about 2×10^{-3} when employing a primary beam of ^{12}C with an energy of 400MeV/u, a Be target with a thickness of 51mm and an Al energy degrader with a thickness of 3.5mm. This result satisfied medical requirements. Development for a medical application apparatus, including the beam delivery system and beam monitor for precise range measurements is now

in progress.

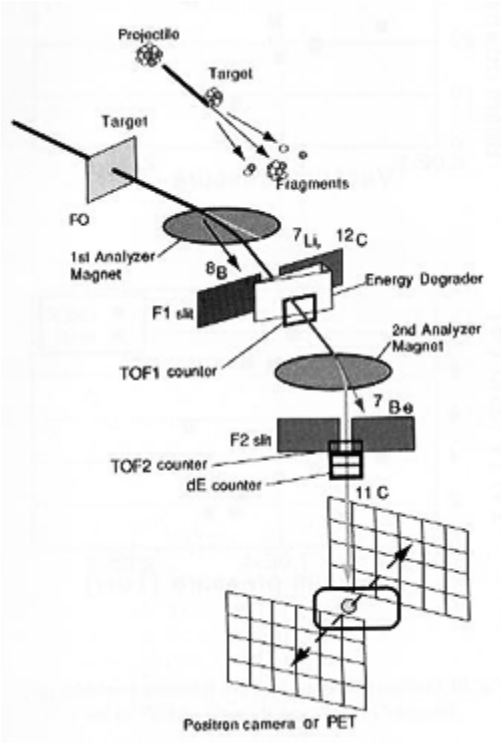

Fig. 9 Schematic view of the beam course

1.10 2.45 GHz Compact National Institute of Radiological Sciences Electron Cyclotron Resonance Ion Source

Masayuki MURAMATSU, Atsushi KITAGAWA, Shinji SHIBUYA[1], Toshiyuki HATTORI[2], Shinji SATO, Katsuto TASHIRO, and Sato YAMADA
([1]Sumitomo Heavy Industries, Ltd.; [2]Tokyo Institute of Technology)
Keywords: ECR ion source, microwave, extraction

A 2.45 GHz compact NIRS-ECR ion source has been developed for Heavy Ion Medical Accelerator in Chiba (HIMAC) at NIRS. This new ECR source is expected to produce C^{2+} ions of more than 160 eμA for high-energy heavy ion cancer treatment. This type source was adopted because of its excellent characteristics of long lifetime, casy operation and compact size (15cm in diameter, 20cm in length and about 20kg in weight). A set of permanent magnets was adopted to generate both the axial mirror and the radial sextupole fields. Several gas materials, He, CO2, CH4, N2, and Ne, have been tested. The present performance for C^{2+} ions, however, is 15 eμA and far below medical requirements. The estimated vacuum in the plasma chamber is around 5.0×10^{-5} Torr. A much better vacuum pressure is desired to produce C^{2+} ions of more than 100 eμA. The ECR plasma, however, can not be kept stable under such a good vacuum pressure. As another method to get the stable plasma, a different microwa method ve injection was tested with a microwave antenna.
One of the reasons why the plasma is not stable at a good vacuum pressure is that the injected microwave power is not effectively absorbed into the plasma. We therefore tested two different microwave injection methods, axial and radial. Microwave power is usually injected along the radial direction through an alumina window. In an axial power injection method, an rf antenna was attached at the left end of the plasma chamber. With the microwave antenna, both the 2+ intensity and 2+/1+ ratio are higher than those for radial microwave injection as shown in Fig. 10. Source parameters for these experiments are as follows: The microwave power for the radial injection ranges from 450 to 1300 W, depending on the vacuum pressure, whereas the microwave power varies from 340 to 1300 W for the axial injection. For both cases, the source is operated in the pulsed mode with a repetition frequency of 5 Hz and a duty factor of 5%. The extraction voltage is fixed at 15 kV. These results suggest that the radial injection has some problems to be solved, including the impedance mismatch, insufficient absorption efficiency, etc. The axial rf antenna has also one problem. Source operation with the antenna induces the surface contamination on the insulator of the feedthrough. We guess that the contamination tends to block the microwave injection.
After a systematic search of positions of the extraction slit and the extraction electrode, the distance between the extraction slit and the electrode (extraction gap) was optimized to be very small value of 4.5mm. Optimized distance is almost independent from the position of the extraction slit.
Since the extraction electrode is made of mild steel, the position of the electrode affects both the electric and the magnetic distributions around the extraction slit. The extraction slit should be positioned close to the peak position of the axial magnetic field to increase the extracted beam

intensity. The small values of the optimized extraction gap are effective to shorten the distance between the extraction slit and the peak of the magnetic field.

It is difficult to simulate the electric field between the extraction slit and the electrode, because the diameter of the extraction slit and the electrode is as large as 10mm compared to the extraction gap of 4.5mm. An appreciable amount of the extracted beam seems to be lost due to the such strong focusing effects of the electric field.

In our ECR source, two major reasons, which are concemed with the microwave absorption and the extraction system, did not allow us to realize the required intensities. It seems essential to change the material of the extraction electrode in order to improve the axial magnetic field configuration. Another important improvement is necessary in the feeding system of the microwave power to keep a stable ECR plasma in a good vacuum pressure.

Publications:

1) Shibuya, S., et al., Rev. Sci. Instrum., 67, 1171 (1996).

2) Muramatsu, M., et al., Rev. Sci. Instrum., 69, 1076 (1998)

3) Kitagawa, A., et al., Rev. Sci. Instrum., 69, 674 (1998)

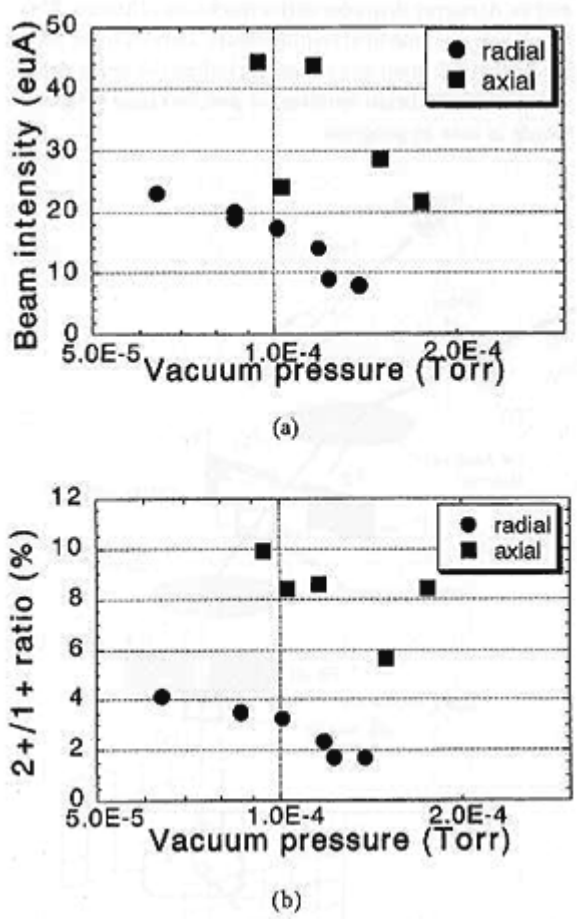

Fig. 10. Comparison of microwave injection methods; (a) intensity of Ne^{2+} and (b) ratio of Ne^{2+} to Ne^{+}.

1.11 Fundamental Study of Multi-port Irradiation System for Heavy Ion Radiation Therapy.

Haruo Yamashita, Tatsuaki Kanai, Yasuyuki Futami, Naruhiro Matsufuji, Munefumi Shimbo, Teiji Nishio, Akio Higashi* and Takashi Akagi*

(*Health Promotion Department, Hyogo Prefectral Government

Keywords: Cancer therapy, Heave ion, Multi-port irradiation

A clinical trial of a heavy ion cancer therapy was started in June 1994, at HIMAC (Heavy lon Medical Accelerator in Chiba). Heavy ion therapy can be expect to give better treatment results in comparison with usual X-ray treatments, because heavy ion therapy can provide uniform and maximum doses in deep positions of the human body. However, since the usual irradiation method (two-dimensional irradiation) cannot sufficiently decrease the irradiation dose to normal tissues, the development of new irradiation methods (three-dimensional irradiation, spot scanning, etc.) is being done. Multi-port irradiation with heavy ions improves the dose concentration inside of a tumor by adjusting the irradiation coefficients (number of ports, irradiation angle, beam weight, etc.) properly, while simultaneously decreasing any unnecessary dose to normal tissues.

In this report, we evaluated the clinical effectiveness of multi-port irradiation and the possibility of irradiation without the bolus. We proceed with our evaluation based on the assumption that the biological dose distribution for heavy ions can be added to the option. Fig. 11 plots the target radius and the 50% tolerance dose (TD50) of normal tissues. When the number of ports is increased, TD50 shows a tendency to increase. The change of TD50 is almost the same for any target radius. Therefore, we conclude that multi-port irradiation with heavy ions is significantly reduced the irradiated dose to normal tissues. Although it is only a guess at present, we think that similar conclusion s concerning multi-port irradiation with protons is possible, based on the assumption that the dose distributions for protons and heavy-ions have similar shapes. At present, we are developing a method (so-called "inverse treatment planning") which gives the optimal irradiation coefficients, which will minimize the dose to normal tissues.

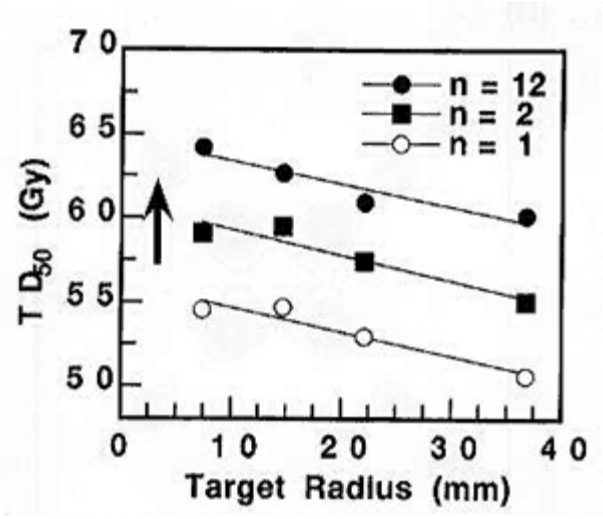

Fig.11 Relation between the target radius and the 50% tolerance dose (TD50). A dose calculation is performed on the following conditions: 1) bolus is used; 2) the irradiation angle is divided into equal intervals; 3) dose weight is divided into equal intervals; 4) target position is in the center of the human body; 5) the target margin is zero. The symbols show one-port (open circle), two-port (solid square) and twelve-port irradiation (solid circle). The rise (arrow) of TD50 suggests that the irradiated dose to normal tissues decreases.

1.12 A Depth Encoding Technique for Scintillation Detector Units

Hideo Murayama

Keywords: scintillation detector, positron emission tomography, nuclear medicine

A detector unit having a depth encoding (DOI) scheme was designed and an experimental study was performed to test the scheme for a positron camera detector. The detector unit consists of a multistage rectangular block of scintillation crystals optically coupled at the bottom face to four photomultiplier tubes (PMTs) in a 2x2 array or to a position sensitive photomultiplier tube. Each stage of the crystal block consists of four elements in a 2x2 array. Each scintillation event is mapped in a two dimensional (2D) distribution through the relative ratio of the output signals of the PMTs. Three-dimensional locations in the detector unit project onto the 2D map so that the four top crystals correspond to the four innermost regions in the map, and the four bottom crystals facing the PMTs correspond to the four outermost regions.

In all experiments, Gd2SiO5: Ce (GSO) crystals were used as elements of the detector unit and each 2D array of the elements was wrapped in a 0.2mm layer of PTFE (polytetrafluoroethylene, Teflon) tape except on the top and bottom surfaces. These 2D arrays were stacked to fabricate a 3D matrix detector unit which was wrapped in a 0.2mm layer of PTFE tape except on the bottom surface. Each crystal element of the bottom stage was optically coupled to each 9.8mm x 9.8mm square PMT (Hamamatsu Photonics R2248) by silicone oil (refractive index=1.4). A 0.1 mCi Cs-137 (662keV) point source was used for gamma ray irradiation. It was placed 15cm from the top face of the detector unit.

Three types of GSO arrays were designed for the detector module. The first was a 2x2 array of crystals, each 3.8mm (row) x 3.8mm (column) x 6mm (depth) and each optically separated from other elements by two 0.2mm layers of PTFE tape. The second was a 4mm slot array cut from a single 8mm (row) x 8mm (column) x 6mm (depth) block with two 0.4mm cuts of 4mm depth to form four equal squares. The third was a 2mm slot array cut from the same block as the second array was and with two 0.4mm cuts of 2mm depth. These 2D arrays were stacked to fabricate a 3D matrix detector unit. A three-stage detector unit (Fig. 12A) was assembled with the 2mm slot array for the top stage, and two 2x2 arrays for the other stages. These arrays were optically coupled to each other by air gaps. Output signals from the PMTs are used in Anger-type positioning logic for detector element identification. Depending on the distances from the elements to the individual PMTs, three peaks are obtained along each diagonal line in each quadrant of the 2D histogram image. The distance from the image center to each peak is a measure of the depth of interaction. In the 2D histogram image of the output signals (Fig. 12B), 12 peaks are recognized corresponding to individual crystal elements. The energy resolutions for the 3rd (top), 2nd, and lst (bottom) stages are 14.5, 14.2, and 13.0%, respectively. The experimental results represent a development towards DOI detector units for volume PET with high spatial resolution and high sensitivity. Our proposed detector is more reliable and simpler for volume PET devices because the proposed DOI scheme does not need additional photo-detectors or a combination of different type of scintillators.

Publication:

Murayama, H., et, al.. : IEEE Trans. Nucl. Sci., 45 , 1152-1157, 1998.

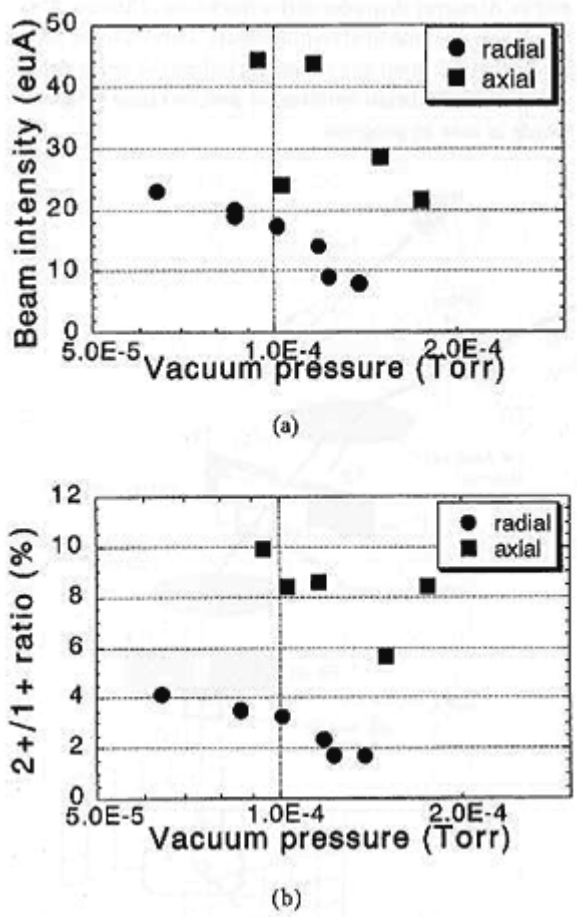

Fig. 12 (A) Schematic drawing of the three-stage detector unit. (B) Positioning contour image histogram for the three-stage detector unit.

2. CHEMISTRY

2.1 The Oxidation of Linoleic Acid by Copper (II) Complexes and Hydrogen Peroxide

Jun-ichi Ueda and Toshihiko Ozawa

Keywords: linoleic acid, copper (II) complexes, hydrogen peroxide, hydroxyl radical, lipid peroxidation, HPLC

The oxidation of lipid by active oxygen species such as hydroxyl radical (・OH) has been hypothesized to play a critical role in diverse biological processes including carcinogenesis and radiation damage. Then, we purposed to investigate how linoleic acid, one of the main constituents of lipid in membrane, is oxidized by ・OH generated from the reaction of Cu (II) complexes with H2O2. The following Cu (II) complexes were used: Cu (CyHH)2 (CyHH: cyclo (L-histidylhistidyl)); Cu (OP)2 (OP: phenanthroline); Cu (HGG) (HGG: histidylglycylglycine): and Cu (en)2 (en: ethylenediamine).

Lipid peroxidation proceeds through a chain reaction initiated by the abstraction of a hydrogen atom from polyunsaturated fatty acids containing unconjugated 1, 4-dienes to yield conjugated dienes with a characteristic UV absorption around 234 nm. Fig. 13 shows that the absorbance at 234 nm during the oxidation of linoleic acid by all Cu (II) complexes and H2O2 increased with the incubation time. The production of four isomers of linoleic acid hydroperoxide (LOOH) was confirmed by high performance liquid chromatography (HPLC)(data not shown).

These results indicated that ・ OH oxidized linoleic acid to generate LOOH. However, the absorbance at 234 nm observed in the reaction of linoleic acid with Cu (HGG) and Cu (en)2 decreased beyond 4 hr as shown in Fig. 13, suggesting that ・ OH decomposed LOOH to yield degradation products. Then, we investigated whether the decomposition of LOOH was caused by mixtures of these Cu (II) complexes and H2O2. The absorbance at 234 nm due to LOOH, which was separately synthesized from the reaction of linoleic acid with soybean lipoxygenase, decreased rapidly with incubation time in the presence of Cu (II) complexes and H2O2 (data not shown). HPLC also indicated the disappearance of LOOH and the appearance of unidentified degradation products (data not shown).

These results suggested that OH produced from the reaction of Cu (II) complexes with H2O2 could oxidize linoleic acid and furthermore decompose it.

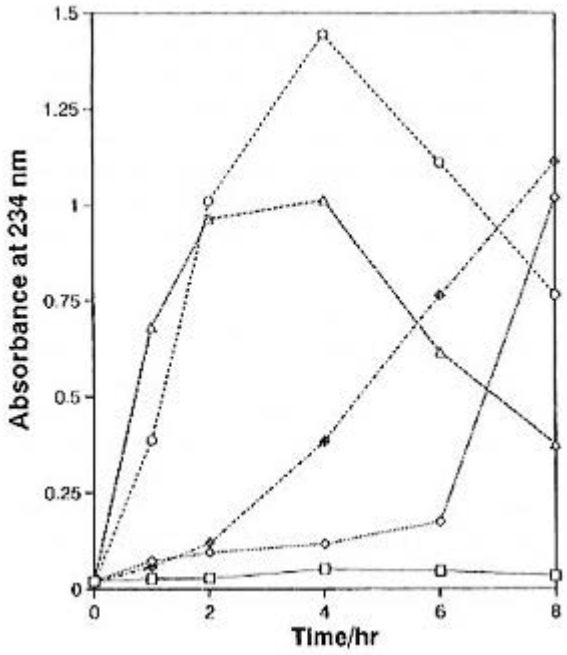
Absorbance at 234 nm
1.5
1.25
1
0.75
0.5
0.25
0
0
2
4
6
8
Time/hr

2.2 Synthesis of 1-Deoxynojirimycin from (S)- Pyroglutaminol

Nobuo Ikota, Hidehiko Nakagawa, and Hiroko Hama-Inaba

Keywords: polyhydroxylated piperidine, glyosidase inhibitor, (S)- pyroglutamic acid, diastereoselective dihydroxylation, chiral synthesis

1-Deoxynojirimycin and related polyhydroxylated piperidines show interesting biological activities such as glycosidase inhibitory activity and their synthesis has been a subject of recent research. In continuation of our synthetic studies of chiral polyhydroxylated amines, we describe here a synthesis of 1-deoxynojirimycin from (S)-pyroglutaminol (Fig.
14).

The dihydroxylation of 1 with potassium osmate (0.08 equiv.) using hydroquinidine 1,4-phthalazinediyl diether (0.20 equiv.) as a chiral ligand in the presence of $K3Fe(CN)^6$ (3 equiv.), K2CO3 (3 equiv.), and MeSO2NH2 (1 equiv.) in tert-BuOH-H2 (1:1) at 0℃ for 12 h gives the diol (2a) as a sole diastereomer in 84% yield. Complete diastereoselectivity for this dihydroxylation was confirmed by conversion of the crude diol into the corresponding diacetate, and no diacetate (3b) was detected in the ^1H NMR spectrum of the crude product. On the other hand, the double asymmetric induction for the dihydroxylation of (Z)-α,β- unsaturated ester (4) was not effective (up to 20% d.e. was observed using hydroquinidine 1,4-phthalazinediyl diether and hydroquinine 1,4- phthalazinediyl diether as chiral ligands, while 31% d.e.was obtained without chiral ligand).

The diol (2a) was converted into the corresponding di-MOM ether (2c) by the reaction with methoxymethyl methyl chloride and N,N- diethylaniline in methylenechloride. Then, the di-MOM ether (2c) was reduced with NaBH4 in EtOH to afford the primary alcohol (5). A high diastereoselectivity was also observed for the introduction of vinyl group to the aldehyde derived from 5 by Swern oxidation. Thus, the reaction of the aldehyde with the reagent prepared from vinylmagnesium bromide and copper bromide-dimethyl sulfide complex at -78℃ gave 6a and 6b in a ratio of 15:1 in 51% yield. The major diastereomer (6a) was converted into a corresponding MOM ether (7a) and was treated with ozone in methylene chloride followed by reductive work-up with NaBH4 to give the alcohol (7b) in 53% yield. Mesylation (methanesulfonyl chloride (MsCl), triethylamine (TEA), CH2Cl2) followed by cyclization with potassium tertbutoxide in THF gave the fully protected piperidine derivative (8) in 71% yield. Hydrolysis of 8 with MeOH-10% HCl (1:1) at 70℃ followed by treatment with Dowex 50W-X8 (H8176 form) gave 1-deoxynojirimycin (9) (mp 195-197℃, [α]8190 +46.5° (c=0.5, H2O), lit., mp 196℃, [α]8190 +47° (H2O)) in 80% yield.

Publications

1) Ikota, N., Hirano, J., Gamage, R., Nakagawa, H. and Hama-Inaba, H.: Heterocycles, 46, 637-643 (1997).

2) Ikota, N., Nakagawa, H., Ohno, S., Okumura, K., and Noguchi, K. : Tetrahedron, in press.

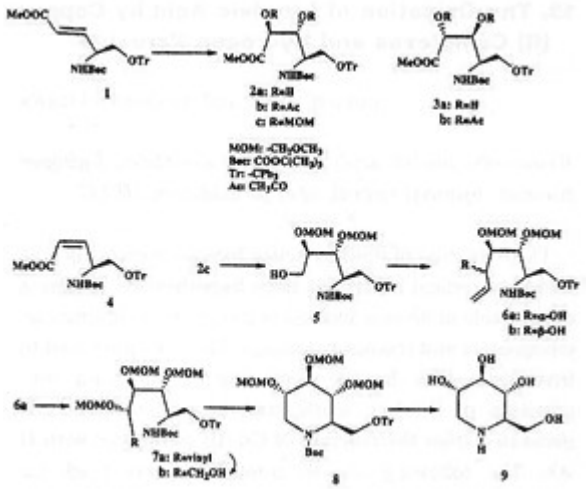

Fig. 14 Synthetic scheme for 1-deoxynojirimycin

2.3 Inhibitory Effect of Lipoic Acid, Melatonin Derivatives and Synthetic Antioxidants on Tyrosine Nitration and Oxidation by Peroxynitrite

H.Nakagawa, N.Ikota, T.Ozawa, E.Sumiki*, Y.Matsushima* (*Kyoritsu College of Pharmacy)

Keywords: peroxynitrite, tyrosine, melatonin, antioxidant, nitration, oxidation

Peroxynitrite (ONOO-) is one of the reactive oxygen species formed from nitric oxide and superoxide. It has been reported that peroxynitrite has a high activity for the oxidation of biological components, e.g., lipid peroxidation including LDL, thiol oxidation, and the oxidation of heme protein, and also that it has an activity for the nitration of free tyrosine and protein tyrosine residues. These oxidation and nitration reaction are assumed to be involved in oxidative damage of biological systems. In this study, the inhibitory activities of the endogenous and synthesized antioxidants for the oxidation and nitration of L-tyrosine by peroxynitrite were examined.

Peroxynitrite was synthesized from sodium azide and ozone in the alkaline solution, concentrated, and stored at -20℃ until use. The concentration of the synthesized peroxynitrite solution was determined from the absorbance at 302nm ($e=1670M^{-1}cm^{-1}$), and diluted to concentration used. Peroxynitrite was mixed with L-tyrosine in the presence or absence of inhibitory compounds at 37℃, and then the resulting mixture was analyzed. In the experiments, 2,2'-di-L-tyrosine as an oxidized product and 3-nitro-L-tyrosine as a nitration product of L-tyrosine were measured in the reaction mixture with the HPLC-UV- fluorescence detector system. Ascorbic acid and glutathione were shown to have inhibitory activity for the nitrotyrosine and dityrosine formation (IC50 value = 35uM and 40uM, respectively). Among the synthesized compounds (Fig. 15), dithiocarbamate (1) was effective (IC50=38uM and 32uM), but selen-containing compounds (2) was less effective for the formation of both dityrosine and nitrotyrosine (IC50=500uM and 1530uM). Lipoic acid (3), melatonin (4) and 5-methoxytryptamine (5) showed the inhibitory effect only on the nitrotyrosine formation (IC50=154uM, 289uM and 438uM, respectively), and dityrosine formation was increased somewhat by treatment with these reagents. DMPO, a typical radical trapping reagent, weakly inhibited the formation of both dityrosine and nitrotyrosine, andtyrosine radical was detected in the reaction mixture by using a spin trapping method. From these results, it was suggested that nitration by peroxynitrite proceeded through two different pathways, one is the radical reaction via two steps, that is the one electron subtraction from a tyrosine and addition of the nitrogen dioxide to the tyrosyl radical, and the other is the nucleophilic reaction, that is a nucleophilic addition to the deprotonated tyrosine.

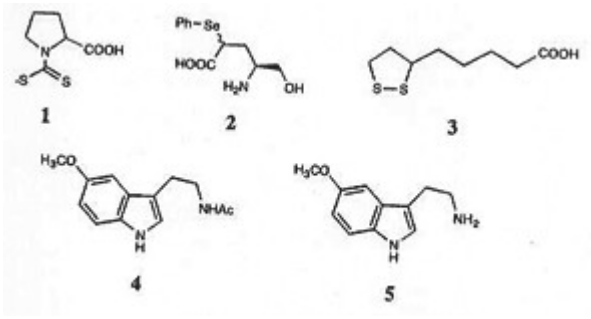

Fig. 15 Structures of antioxidants.

2.4 Spin Trapping of Nitric Oxide in Vivo with the Iron Complexes of New Dithiocarbamate Derivatives: Spin Trapping in Blood and Liver.

Hidehiko Nakagawa, Nobuo Ikota and Toshihiko Ozawa

Keywords: dithiocarbamate, iron complex, nitric oxide, ESR, spin trapping, L-proline

Nitric oxide (NO) is suggested to be an endogenous radical compound and to play important roles in inflammation, neurotransmission and vasodilation. Although there are a few iron complexes of the dithiocarbamate derivatives which have been used for the spin trapping of nitric oxide, their nitric oxide adducts were suggested to be accumulated in the liver in the septic shock model mouse. To improve the properties of these dithiocarbamate complexes, we synthesized a series of dithiocarbamate derivatives which have the L-proline or L- serine moiety. In this report, we investigated the spin trapping and detection of nitric oxide in the blood and liver in the septic shock model mouse using these synthesized complexes.

Three novel dithiocarbamate complexes were synthesized as reported previously. We synthesized an additional complex with N-methyl-L-serine moiety in this study. All the synthesized iron complexes were used for the spin trapping of nitric oxide in vivo. The structures of all the complexes synthesized are shown in Fig. 16.

In these experiments, the four synthesized complexes were shown to have almost the same affinity for nitric oxide. Septic shock model mice were obtained by a treatment of lipopolysaccharide (LPS, E.coli 026:B6) into the tail vein of ddY female mice. The complexes were injected into the septic shock model mice intravenously 5 hr after LPS treatment. The blood was collected into a heparinized capillary, and then the liver was rapidly removed and homogenized in Ar gas-bubbled phosphate buffered saline. The ESR spectra of the blood and the liver samples were measured with 9.4GHz ESR spectrometer.

The relative signal intensity of the NO-adducts of the complexes in the mouse blood and liver were measured 5.25 hr after LPS treatment.

Using Fe-DTCMP complex as a spin trap, NO-adduct was detected only in the LPS-treated mouse blood, but not in the liver. In the case of the other synthesized iron complexes, larger NO-adduct signals were detected in the liver the same as reported before for spin trapping reagents. Although these complexes had similar affinity for nitric oxide
in vitro, these complexes had different signal intensities for their NO- adducts in the blood and the liver for in vivo spin trapping. These results suggested that the complexes had different properties in the LPS- treated mouse body. In particular, Fe-DTCMP was shown to differ from the other complexes in regard to trapping ability in the liver. This result suggested that Fe-DTCMP complex had a unique property of forming its NO-adduct only in the blood. It was assumed that this complex may be used for spin trapping of nitric oxide produced in the blood.

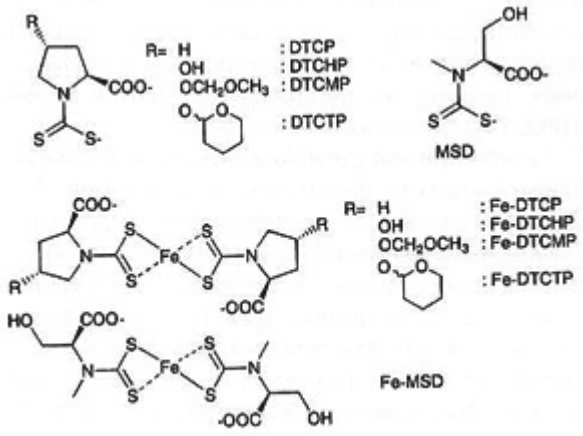

Fig. 16 Structures of dithocarbamate ligands and proposed structures of their iron complexes.

3.1.1 Antioxidative Characterization of Cultured Cells Resistant to Radiation and Hydrogen Peroxide

Osami Yukawa, Tetsuo Nakajima, Misao Hachiya and Makoto Akashi

Keywords: radioresistant cells, hydrogen peroxide, radical scavengers, glutathione reductase, GSH peroxidase, lipid peroxidation

Cultured HL60 cells derived from human leukemia cells and a mutant of HL60 cells, HP100 cells resistant to radiation and hydrogen peroxide, were used to analyze a mechanism of radiation sensitivity. The lipid peroxide level measured by TBARS in HP100 cells was only 20% of that of HL60 cells, suggesting the presence of effective free radical scavenging systems in radioresistant cells. The radical scavenging ability determined by the disappearance of diphenylpicrylhydrazyl, a stable free radical, in HP100 cells was 1.6 times higher than that in HL60 cells. This result indicates that HP100 cells have a greater abundance of intracellular low molecular antioxidants as compared with HL60 cells.

However, the total glutathione content was almost the same for HL60 and HP100 cells. On the other hand, glutathione reductase activity in HP100 was more than 2 times higher than that in HL60 cells, suggesting that the reduction rate of oxidized glutathione to produce reduced glutathione(GSH) that has a strong radical scavenging activity is higher in HP100 cells even if the total glutathione content is the same between these cells. Another importance of the higher GSH content is that GSH is also a cofactor of the antioxidative enzymes. GSH peroxidase activity in HL100 cells using hydrogen peroxide and cumine hydroperoxide as substrates was also higher than that in HL60 cells. This indicates that HP100 cells effectively scavenge not only H2O2 but also lipid hydroperoxides. These results suggest that one of the causes of the radioresistance is protection from radiation-induced cellular damages, including membrane lipid peroxidation, by maintaining higher level of various free radical scavengers for H2O2 or ・ OH produced by radiation. The present results provide a clue to the analysis of radiation sensitivity.

3.1.2 Characterization of Radiation-Induced Diacylglycerol Production in Cultured Rat Hepatocytes

Tetsuo Nakajima and Osami Yukawa

Keywords: rat hepatocytes, protein kinase C, diacylglycerol, hydroxyl radical, phospholipase C

We have already reported that radiation induces protein kinase C (PKC) translocation through membrane lipid peroxidation and, simultaneously, diacylglycerol (DAG) production in cultured rat hepatocytes. These observations imply that radiation-induced PKC translocation is mediated not only by lipid peroxidation, but also by DAG production. In the present study, we tried to characterize radiation-induced DAG production in cultured rat hepatocytes in detail. The DAG production after irradiation of the cells with 50 Gy was measured by converting DAG to [^{32}P] phosphatidic acid with [^{32}P-γ] ATP and DAG kinase. The DAG content increased 3 min after irradiation, decreased 15 min later and again increased 30 min after irradiation, showing a biphasic pattern. The biphasic production of DAG has also been reported to occur in the activation of signal transduction induced by H202, UV or by treatment with many stimulators like growth factors. Particularly, in the first phase of the production, phosphatidylinositol-specific phospholipase C (PI-PLC) is assumed to produce DAG.In previous experiments, we also demonstrated that hydroxyl radical, the main free radical produced by irradiation induced DAG production and the production could mimic the first production in the radiation-induced DAG production. Additionally, in the present study, neomycin sulfate, a PI-PLC specific inhibitor, effectively suppressed the hydroxyl radical-induced DAG production, which occurred 1 min after treatment with a hydroxyl radical generating system(the mixture of Cu (ethylenediamine)2 and H202). This result suggests that PI-PLC might participate in the first production of radiation-induced DAG production as well as hydroxyl radical-induced DAG production.

3.1.3 Secondary Structure within the Translated Region of mRNA and Discontinuous Translational Elongation of Polypeptides: Spider Silk Fibroin Spidroin 1

Mitsuo Zama

Keywords: mRNA secondary structure, discontinuous translation, spider silk fibroin

The production of discrete size nascent polypeptide chains through pauses during translational elongation has been observed for some proteins. In a series of studies for such proteins, silkworm fibroin, type I collagen, colicin A, chloroplast photosystem II reaction center protein D1 and globin, we have so far presented evidence to support the view that the pauses may be attributable to the mRNA secondary structure of the protein- coding region. As an extension of our previous work we have focused our attention on spider dragline silk fibroin in this study. Discontinuous translational elongation of polypeptides is observed during spider fibroin synthesis. The repeating segment of spider major ampullate (dragline) silk of the spider Nephila clavipes (Spidroin 1) consists of two regions, alanine-rich and glycine-rich, and specific codon usage patterns are observed within each region. We found that the free energy of the secondary structure of the mRNA per nucleotide for the alanine-rich region is always much lower than that of the successive glycine-rich region, although the sequence and the number of amino acids of the regions are not rigidly conserved. This alternate arrangement of the regions of high and low structural stability along the mRNA strand may explain the discontinuous translational elongation of spider fibroin.

Publication:

Zama, M.: Nucleic Acids Res. Symp. Ser.,39, 163-164, 1998.

3.1.4 Effects of Phospholipid Composition on Peroxidation of Unsaturated Fatty Acyl Chains of Phospholipids in Liposomes

Kazunori Anzai, Yumiko Senzaki*, Jun-ichi Ueda, Yuri Miura, and Toshihiko Ozawa

(*Kyoritsu College of Pharmacy)

Keywords: lipid peroxidation, liposome, hydroxyl radical, peroxyl radical

Reactive oxygen species (ROS) are considered to cause various diseases through reactions with constituents of a living body. It has been suggested that the formation of peroxidized lipids and their decomposed products plays an important role in the harmful effects of ROS, such as induction of atherosclerosis and increase in membrane permeability. In the present study, we have investigated the effects of phospholipid composition on lipid peroxidation of liposomes made of asolectin (soy bean phospholipid) or a mixture of egg phosphatidylcholine (PC) and phosphatidylethanolamine (PE).

A lipid peroxidation reaction was initiated by the peroxyl radical (ROO・) or hydroxyl radical (・OH) . Peroxyl radical (ROO ・) was generated by the decomposition of 2,2'-azobis(2-amidinopropane) dihydrochloride (AAPH) followed by the incorporation of O2. Hydroxyl radical (・OH) was generated by X-ray irradiation or by the reaction of hydrogen peroxide (H2O2) with a Cu^{2+} complex (Cu(en)2, en=ethylenediamine). The progress of the peroxidation reaction was estimated by the measurement of the absorbance at 234 nm, corresponding to the amount of conjugated diene, or by the measurement of thiobarbituric acid reactive substances (TBARS). Constant application of the radicals increased the lipid peroxide amount, but longer application induced the degradation of the lipid peroxide.

Asolectin liposomes were more sensitive to the peroxidation than egg PC/PE liposomes because of the presence of a larger amount of unsaturated fatty acyl chain in asolectin. When ・ OH was generated by the reaction of H2O2 with Cu(en), increase of PE content in the liposomes accelerated the peroxidation reaction, whereas the increase of PE content had no effect on the peroxidation initiated by ・ OH generated by X-ray irradiation. Peroxidation of the liposomes by ROO ・ was not dependent on the PE content of the liposomes. Since the PE-dependent peroxidation was observed under the condition where ・ OH was generated by the reaction of H2O2 with Cu(en)2, absorption of Cu(en)2
on the surface of the liposomes through the amino group of PE may be responsible for the acceleration of the peroxidation in PE containing liposomes.

3.1.5 Measurement of Radiation Effect in the Brain Using a Lipophilic Spin Probe of In Vivo ESR

Yuri Miura, Kazunori Anzai, and Toshihiko Ozawa

Keywords: in vivo ESR, radiation, nitroxyl radical, brain, reactive oxygen species

Oxidative stress such as radiation is known to generate active oxygen in living organisms, to vary the redox state significantly, and to cause various types of tissue damage. The brain may be especially susceptible to oxidative stress. Therefore, oxidative damage in the brain is particularly worthy of investigation. Stable nitroxyl radicals are often used for in vivo ESR as a probe. However, these conventionally used nitroxyl radicals are generally water-soluble and impermeable to the blood-brain barrier, so that oxidative damage on the brain physiology can not be studied by in vivo ESR.

In the present study, as a possible lipophilic spin probe for in vivo ESR, 3-methoxy carbonyl-2, 2, 5, 5-tetramethyl-pyrrolidine-1-yloxy (MCPROXYL) was examined. The permeability of the blood-brain barrier to this compound was evaluated with a brain uptake index and autoradiography; results showed this probe is well distributed in the brain. The in vivo ESR spectra were measured in the head and the abdomen of MCPROXYL-injected living mice. The rate of signal decay of MCPROXYL in the head measured at one hour after X-ray-irradiation was about 75% of that of the controls. The decrease in the head seems to be related to the early response of the brain to X-ray-irradiation. This is the first report that the behavior of free radicals such as MCPROXYL in the brain is influenced by X-ray-irradiation. MCPROXYL is thus useful as a novel spin probe for in vivo ESR to monitor radiation damage in the brain.

Publications:

1) Miura, Y., Anzai, K., Takahashi, S., and Ozawa, T.: FEBS Lett., 419, 99-102, 1997.

2) Miura, Y., Anzai, K., and Ozawa, T.: Magnetic Resonance in Medicine (in Japanese), (Utsumi, H. and Yoshikawa, T. eds.), Nihon Igakukan, Vol. 8, pp. 25-28, 1997.

3.1.6 Detection and Cloning of Integration Sites of Intracisternal A-particle Element in Genome of Murine Myeloid Leukemia Cells

Hiroshi Ishihara, Izumi Tanaka

Keywords: retrotransposon, intracisternal A-particle, myeloid leukemia, retrotransposition, gene rearrangement

Acute myeloid leukemia (AML) is induced in C3H/He inbred mice 1-2 years after whole-body irradiation by x-rays. It is believed that irreversible change including gene rearrangement in myeloid cells contributes to the tumorigenetic feature of the AML cells. We have previously found an example of rearrangement of the gene for interleukin-3 by integration of intracisternal A-particle (IAP) DNA element in the genome of the AML cells.

The IAP is one of the incomplete endogeneous retroviruses, and the DNA element exists in the genome of all the cells in mice. Similar to retroviruses, the IAP RNA is reverse-transcribed and the product is introduced into a novel locus of the genomic DNA. Although the retrotransposition efficiency is very low in normal cells, the copy number of the IAP element in mouse genome reaches 1000 copies per haploid by the accumulation of the event in the germ line cells from generation to generation.

It has been reported that integration of the IAP element activates adjacent genes in several mouse tumor cells. Rearrangement in IL-3 gene by IAP-mediated retrotransposition can award factor-independence in the leukemia cell, as was found previously. Similarly, the same event occurs during or after leukemogenesis in a myeloid cell which is the origin of a leukemia cell. If the retrotransposition commonly occurs in myeloid cells, genomes of leukemia cells prepared from different leukemia mice may possess a novel integration site of the IAP element. To examine the universality of the event in the C3H-derived leukemia, we analyzed the integration site in the genomes of leukemia cells isolated from different individuals. When IAP element-specific and short interspersed element (SINE)-B2-specific primers were used for the polymerase-chain reaction, IAP-integration sites that closely locate
SINE-B2 were specifically amplified (Fig. 17). Various insertion sites of the IAP element were detected in normal cells without any differences in the electrophoresis patterns among 15 individual mice (a part of the results are shown in lanes 1 and 2). In contrast, unique integration sites of the IAP element were found in the genomes of all the leukemia cells (lanes 3 to 7). Subsequent cloning and sequencing analyses showed that they were novel integration sites of the IAP element (data not shown). It was concluded that the gene rearrangement by the IAP-mediated retrotransposition is characteristic among the leukemia cells, even though they are generated separately with different processes.

Accumulation of the events irreversibly changes the genome of the myeloid cells and may contribute to leukemic features.

Publication:

Ishihara, H. and Tanaka, I.: FEBS Lett.418, 205-209, 1997.

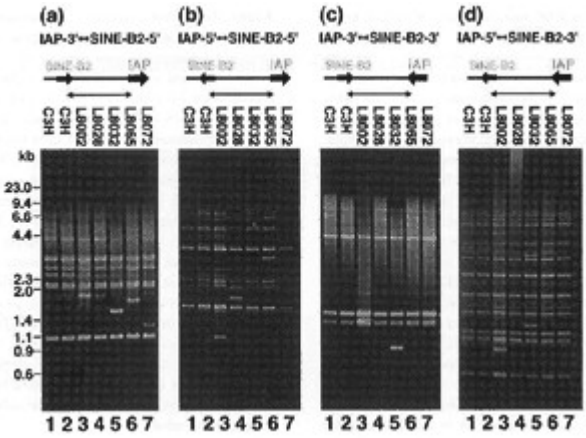

Fig. 17. PCR amplification of the IAP-integration sites in genome.

DNAs from normal livers of C3H/He mice (lanes 1 and 2) and from AML cells of different origins (lanes 3 to 7) were PCR-amplified using IAP-LTR primer and SINE-B2 primer. Four different combinations of the primer set were used to detect the IAP-integration sites closely located SINE-B2 as follows; Backward IAP-LTR plus forward SINE-B2 (a); Backward IAP- LTR plus backward SINE-B2 (b); Forward IAP-LTR plus forward SINE-B2 (c); Forward IAP-LTR plus backward SINE-B2 (d).

3.1.7 Essential Dynamics of DNA Containing a cis.syn Cyclobutane Thymine Dimer Lesion

Hiroshi Yamaguchi, Daan M. F. van Aalten[1], Miroslav Pinak[2], Akira Furukawa and Roman Osman[3]

([1]Keck Structural Biology Cold Spring Harbor Laboratory, NY, USA; [2]Comenius University, Bratislava, Slovakia; [3]Mount Sinai School of Medicine, NY, USA.)

Keywords: DNA, UV, thymine dimer, molecular dynamics, essential dynamics

Ultraviolet light produces cyclobutane-type pyrimidine dimers (PD) in DNA. Such lesions can cause mutations and they strongly correlate with UV-induced cancer. T4 endonuclease V (T4 Endo V) is a repair enzyme specific for PD. The enzyme scans nontarget DNA by an electrostatic unidimensional diffusion. The interaction becomes specific upon encountering the enzyme by the target PD. The enzyme catalyzes the excision of the damage by two distinct processes. First it hydrolyzes the glycosyl bond at the 5' side of the PD then the enzyme proceeds to incise the phosphodiester bond in the 3' position to the abasic site. Mutational studies of the enzyme established that the amino terminus acts as the nucleophile and Glu-23 is important in enzymatic activity. It appears that the enzymatic mechanism is reasonably well understood and it represents a rather general mechanism in base excision repair.

In contrast to the enzymatic mechanism the selectivity of damage recognition is still sketchy. Certain aspects of damage recognition can be inferred from the crystal structure of the enzyme and the enzyme-DNA complex. The determination of the crystal structure of the complex between endonuclease V and a damaged DNA provides an additional range of observations about the DNA-protein interaction. An important discovery in the complex is the flipped out adenine complementary to the 5' thymine of the PD. Also, the DNA has a substantial kink(60°) in the helical axis near the PD.

To explore the relationship between the kinked structure and base flipping we applied the essential dynamics (ED) for trajectories of the molecular dynamics (MD) of DNA to reveal dynamic motions that could be responsible for base flipping. The method identified several principal concerted motions among atoms of the damaged DNA.

Results from MD simulations of the damaged decamer DNA show a kink of about 21.7° at the PD damaged site and a disruption of H-bonding

between the 5'-thymine of the PD and its complementary adenine. However, no extrahelical flipping of the 3'-adenine complementary to the PD was observed. Comparison to two undamaged DNA decamers, one with the same sequence and the other with an AT replacing the TT sequence, indicates that these properties are specific to the damaged DNA. Results from ED analysis shows that the backbone phosphate between the two adenines complementary to the PD of the damaged DNA has considerably larger mobility than the rest of the molecule and occurs only in the damaged DNA (Fig. 18). As observed in the crystal structure of T4 Endo V in a complex with the damaged DNA, the interaction of the enzyme with the damaged DNA can lead to a larger bending (60°) along the flexible joint and to induction of adenine flipping into an extrahelical position. Such motions may play an important role in damage recognition by repair enzymes.

Publication:

Yamaguchi, H., van Aalten, D. M. F., Pinak, M., Furukawa, A., and Osman, R.: Nucleic. Acids Res., 26. 1939-1946, 1998.

3.2 BIO-MEDICAL SCIENCES Cell Biology

3.2.1 Non-fluorescent Chromosome Painting Using PeroxidaseDiaminobenzidine (DAB) Reaction

Reiko Kanda, Miyuki Suzuki, Masako Minamihisamatsu, Akira Furukawa, Takeko Odaka and Isamu Hayata

Keywords: chromosome painting, bright-field microscopy, human lymphocytes

FISH painting has been shown to be a valid and rapid method for detecting chromosome exchanges in human lymphocytes. However, it is difficult to analyze the painted chromosomes repeatedly because of photobleaching of fluorescent labels. A peroxidase/diaminobenzidine (DAB) reaction has been utilized for coloring mainly DNA segments in nuclei using repetitive DNA probes such as chromosome-specific centromeric probes. We have improved that method, and successfully applied it to the painting of chromosomes in metaphase cells.

By means of this`DAB painting' technique, we analyzed chromosome aberrations in the lymphocytes of uterine cancer patients who received heavyion radiotherapy at NIRS. Chromosome preparations were treated with RNase and pepsin, denatured mildly, hybridized with a biotinylated DNA probe specific for whole-chromosome 4, treated with horseradish peroxidase conjugated avidin repeatedly, and stained using the peroxidase/DAB reaction (Fig. 19). The quality of the slides was investigated using an atomic force microscope (AFM), a bright-field microscope and an automated system, NIRS-1000 KINETOSCORER. The topographical AFM image shows that the DAB signals equally and completely covered all the painted regions without losing the original shape of the chromosome. When chromosome 4 was painted, 11.5% of unstable aberrations were detected by DAB painting, while 10.8% of them were found by dual analysis of Giemsa staining and FISH painting. The detection of metaphases using the automated metaphase finding system shows that the false positive rate was 12.3% on a DAB painted slide, while that of Giemsa stained slides was 10.6%.

In conclusion, our study on DAB application as a chromosome painting method shows that it can effectively detect rearranged aberrations, and it has advantages over FISH painting. The advantages are a) the preparation can be analyzed by bright-field microscope, b) it can be preserved permanently, and c) it is suitable for an automated system.

Publication:

Kanda, R., Suzuki, M., Minamihisamatsu, M., Furukawa, A., Odaka, T. and Hayata. I.: Int. J. Radiat. Biol. 73, 529-533, 1998

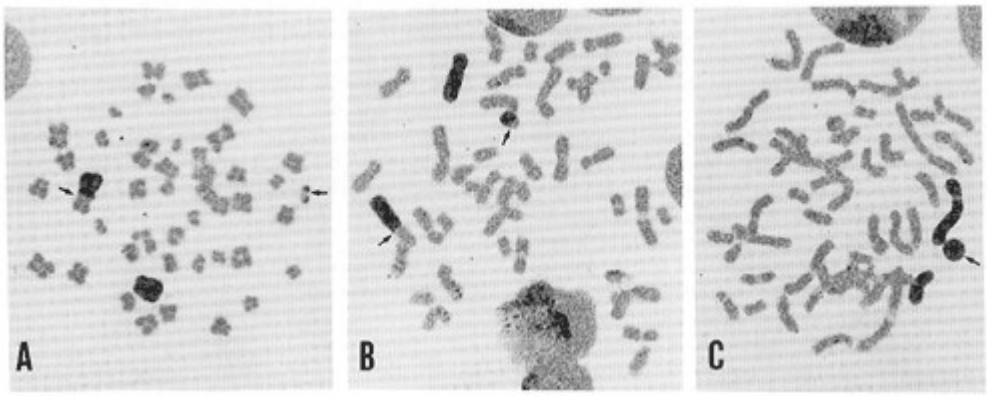

Fig 19 Human metaphases painted with probes for chromosome 4 and visualized by peroxidase/DAB reaction. (A) A dicentric and a fragment;
(B) translocated chromosomes; and (C) an acentric ring.

3.2.2 Effects of Genic Substitution at the Agouti, Brown, Albino, Dilute, and Pink-Eyed Dilution Loci on the Proliferation and Differentiation of Mouse Epidermal Melanocytes in Serum-Free Culture

Tomohisa Hirobe

Keywords: melanocyte, keratinocyte, proliferation, differentiation, coat- color gene

To examine the effects of coat-color genes on the proliferation and differentiation of mouse epidermal melanocytes, we cultured epidermal cell suspensions derived from neonatal skins of C57BL/10JHir (black) and its congenic mice carrying agouti, brown, albino, dilute, and pink- eyed dilution genes in serum-free medium supplemented with dibutyryl adenosine 3', 5'-cyclic monophosphate. The proliferative rates of agouti, brown, and dilute black melanocytes were similar to the rate of black melanocytes, while those of albino and pink-eyed black melanocytes were about one-third of that of black melanocytes. The morphology of albino and pink-eyed black melanocytes, though nonpigmented, was similar to black melanocytes; namely, dendritic, polygonal, or epithelioid. Dilute black melanocytes also possessed similar morphology, whereas their melanosomes were accumulated in the perinuclear region. Dopa- melanin depositions after the dopa reaction in brown and dilute black melanocytes were greater than in black and agouti melanocytes.

Although dopa-melanin depositions were not observed in albino melanocytes, about 8% of pink-eyed black melanocytes were positive to the dopa reaction. Silver depositions after the combined dopa-premelanin reaction in agouti, brown, and dilute black melanocytes were similar to those in black melanocytes. Although albino melanocytes were devoid of silver depositions, about 25% of pink-eyed black melanocytes were positive to the reaction. Pyrrole-2, 3, 5-tricarboxylic acid (PTCA, degradation product of eumelanin) contents in agouti and dilute black melanocytes were slightly lower than in black melanocytes, while the content in brown melanocytes was reduced to one-third. In contrast, PTCA contents in albino and pink-eyed black melanocytes were reduced to less than 0.5%. Aminohydroxyphenylalanine (AHP, degradation product of pheomelanin) contents did not differ among these melanocytes. These results suggest that coat-color genes exert their influences on the proliferation and differentiation of mouse epidermal melanocytes by affecting tyrosinase activity, melanosome maturation and transport, and eumelanin synthesis.

Publication:

Hirobe, T., Wakamatsu, K., and lto, S.: Eur. J. Cell Biol., 75, 184-191, 1998.

3.2.3 Cryopreservation of Medaka Spermatozoa

Kazuko Aoki, Masanori Okamoto, Kouichi Tatsumi and Yuji Ishikawa

Keywords: medaka, spermatozoa, cryopreservation, fish

In order to establish a reliable and reproducible method for cryopreservation of medaka spermatozoa, we tested several procedures. The vapor phase of liquid nitrogen (LN), the liquid phase of LN, and dry ice were used for freezing and dimethyl sulfoxide and N, N-dimethyl formamide (DMF) were used as cryoprotectants. The best results were obtained using the following method. Medaka spermatozoa were collected in a plastic tube containing 50μl of fetal bovine serum supplemented with 10% DMF by squeezing an isolated testis. The sperm suspension was frozen by holding the tube for 10 or 20 min in the vapor phase of LN at a depth of 9 or 10cm from the top of a container. The frozen sample was immersed and stored in LN. After more than one week of storage, the sample in the tube was rapidly thawed by being incubated in a waterbath for 0.5-1 min at 30℃, and then immediately diluted with 2 volumes of Iwamatsu's solution. Fertilization tests using fresh unfertilized eggs showed that the stored spermatozoa could fertilize 96-100% of the eggs. The hatchability of the fertilized eggs was 84-100%. Thus, this study provides, for the first time, a practical method for preserving medaka spermatozoa.

Publication:

Aoki K., Okamoto M., Tatsumi K. and Ishikawa Y.: Zool. Sci., 14, 641- 644, 1997.

3.2.4 Inhibition of bFGF Activity by Complement C1s: Covalent Binding of C1s with bFGF

Hisako Sakiyama, Kazuhiko Kaji*, Koichi Nakagawa and Ken Nagino (*Univ. of Shizuaka)

Keywords: bFGF, complement C1s, HUVEC, covalent binding, growth inhibition

The first component of complement C1s plays an important role in a defence mechanism by activating the classical complement cascade. We have shown that C1s degrades cartilage matrix components such as type II collagen and a small proteaglycan decorin and it activates pro- matrix metalloproteinase-9 (proMMP-9) which is also secreted by chondrocytes. In this report, we demonstrate that C1s covalently binds to basic fibroblast growth factor (bFGF, FGF-2), degrades it, and as a consequence, it inhibits the activity of bFGF. bFGF, the most potent mitogen for chondrocytes, is also mitogenic for various other types of cells. It is expressed in a variety of organs, including cartilage.

Chondrocytes in early stages synthesize bFGF, but the production decreases in accordance with chondracyte hypertrophy. bFGF stored in cartilage matrix inhibits final differentiation of chondrocytes. Cartilage consists of extracellular matrix and chondrocytes which differentiate from resting, to proliferating and maturing to hypertrophic cells. Hypertrophic chondrocytes undergo programmed cell death, then matrix and the lacunae, in which hypertrophic chondrocytes are present, are eventually replaced by bone marrow. We have shown that C1s is synthesized by chondrocytes and the synthesis increases in parallel with chondrocyte differentiation in vivo and in vitro. ln order to understand the biological significance of C1s production by chondrocytes we examined interaction of C1s with bFGF.

C1s formed large aggregates with bFGF when bFGF and C1s were incubated at 37℃ overnight. Under non-reducing conditions, a part of the aggregates did not penetrate into 5% polyacrylamide gel in the presence of SDS, and the rest penetrated into 5% gel but not into 12% gel. The aggregates were dissociated into monomers by reducing with

2-melcaptoethanol. Both active and inactive C1s formed aggregates with bFGF. In addition, a portion of the bFGF was degraded by active C1s but not by inactive C1s. Aggregates were not formed when 2-melcaptoethanol (2mM) was added to the incubation mixture. After the incubation with C1s the growth-stimulating activity of bFGF was measured by using human umbilical vein endothelial cells (HUVEC) as indicator cells. The aggregate formation between C1s and bFGF significantly reduced the activity of bFGF. Therefore, it is possible that C1s secreted to extra cellular matrix inhibits bFGF activity by covalent binding.

Publications:

1) Sakiyama, H., Nishida, M., Sakai, N., Nagino, K., Miyatake, S. and Imajo-Ohmi, S.: Intl. J. Cancer, 66, 768-771, 1996.
2) Toyoguchi, T., Yamaguchi, K., Nakagawa, K., Fukazawa, T., Moriya, H. and Sakiyama, H.: Cell Tissue Res. 285, 199-204, 1996.
3) Hidari, K.I.P.J., Ichikawa, S., Fujita, T., Sakiyama, H. and Hirabayashi, Y.: J. Biol. Chem. 271, 14636-14641 , 1996.
4) Ichikawa, s., Sakiyama, H., Suzuki, G., Hidari, K. I. P.J. and Hirabayashi, Y.: Proc. Natl. Acad. Sci. 93,

4638-4643, 1996.

5) Wada, E., Sakiyama, H., Nakamura, M. and Kanegasaki, S.: Cell Biochem. Func. 15, 19-26, 1997.

6) Sakiyama, H., Nakagawa, K., Kuriiwa, K., Imai, K., Okada. Y., Tsuchida, T. Moriya, H. and Imajoh-Ohmi, S.: Cell Tissue Res. 288, 557- 565, 1997.

7) Nakagawa, K., Sakiyama, H., Fukazawa, T., Matsumoto, M., Takigawa, M., Toyoguchi, T. and Moriya, H.: Cell Tissue Res . 289, 299-305, 1997.

8) Sakiyama, H., Kaji K., Nakagawa, K. and Nagino, K.: Cell Biochem. Func. in press.

9) Nakagawa, K., Sakiyama, H., Masuda, R., Toyoguchi, T., Yamaguchi,K. Tsuchida, T. and Moriya H.: Ann. Rheum. Diseases. in press

10) Inoue, N., Saito, T., Masuda, R., Suzuki, Y., Ohtomi, M. and Sakiyama, H.: Human Genet. in press.

3.2.5 Localization of Nitric Oxide Synthases and Nitric Oxide Production in the Rat Mammary Gland

Makoto Onoda and Hiroshi Inano

KeyWords: nitric oxide, nitric oxide synthase, mammary gland, organ culture, immunohistochemistry

Nitric oxide (NO) is an inorganic gaseous radical which is synthesized from L-arginine by nitric oxide synthase (NOS). NO is increasingly appreciated as a major regulator in the nervous, immune, and cardiovascular systems. Besides being a physiological mediator of homeostasis, NO has been shown to inflict detriment on important biomolecules and to be implicated in many pathological events including inflammation, arthritis, myositis and carcinogenesis. NOS has at least 3 distinct isoforms including the brain, inducible and endothelial types.
Although these were oniginally purified from the cerebellum, cytokine- induced macrophages, and the vascular endothelium and designated bNOS, iNOS and eNOS, respectively, the isoforms are now known to distribute across a wide spectrum of cell types and tissues. These include the adrenal gland, digestive organs, kidney, bladder, liver, pancreas, female reproductive organs, male reproductive and accessory organs, and other tissues and organs. In addition to these organs and tissues, NOS isoforms were identified in human breast cancer and cancer cell lines. The presence and distribution of NOS isoforms in the normal mammary gland, in contrast, are not yet known. The aim of the present study was to investigate the presence and distribution of NOS isoforms in the rat mammary gland by using an organ culture system and immunobiological and immunohistochemical means.
Mammary glands were excised from the inguinal parts of female Wistar-
MS rats primed by implantation with pellets of 17β-estradiol and progesterone, and diced into approximately 3mm cubes. Three of these cubes were cultured with 2ml of 10% FCS/DMEM plus carboxy-PTIO (a NO scavenger, 100μM) in the presence or absence of LPS (0.5μg/ml) for 2 days. The amount of NO produced spontaneously by the cultured mammary glands was relatively minute at the terminus of the 2-day culture period, and the NO production was significantly enhanced by the presence of LPS (Table 1). This enhancement of NO production was completely eliminated by the addition of hydrocortisone (3μM), an inhibitor of iNOS, to the incubation medium (Table 1). Immunoblot analyses with specific antisera against NOS isoforms such as iNOS, eNOS and bNOS showed immunoreactive bands of iNOS (122±2kDa, Fig. 20a) and eNOS (152±3kDa, Fig. 20b) in extracts prepared from the mammary glands in the culture without LPS. The immunoreactive band of iNOS was highly intense after the treatment of mammary glands with LPS, while, the corresponding eNOS immunoreactive band was faded (Fig. 20). These are suggestive of a basal expression of iNOS in the unstimulated rat mammary glands as well as of other constitutive NOS isoforms. Since there are precedents for the expression of iNOS isoform in normal rat kidney and guinea pig skeletal muscle, it is likely that the iNOS isoform is constitutively expressed to some extent in the normal rat mammary gland. In addition, it has been shown that LPS decreased the eNOS expression in cultured bovine coronary venular

endothelial cells at protein and mRNA levels in a dose- and time-dependent manner, and it was concluded that the reduction of eNOS by LPS treatment resulted from an increased degradation rate of its transcripts. Therefore, it is likely that similar downregulation mechanisms occur in a reciprocal modulation of the eNOS and iNOS expressions of the mammary gland after the LPS exposure.

The immunohistochemical study of anti-iNOS antiserum on frozen sections of the cultured mammary glands showed that an immunoreactive substance with the antiserum was localized to the basal layer (comprised of myoepithelial cells of alveoli and lactiferous ducts) of the mammary epithelia and to the endothelium of blood vessels which penetrated into the interstitium of the mammary glands. Similar observations were noted in the immunohistochemistry of eNOS. In contrast, the immunoreactive signal with the bNOS antiserum was barely detected in the epithelial parts of alveoli and lactiferous ducts of the mammary glands. These observations demonstrate that 3 isoforms of NOS are present not only in the endothelium of blood vessels but also in the parenchymal cells (the glandular epithelium) of the rat mammary gland such as epithelial cells and myoepithelial cells, and suggest that NO may have functional roles in the physiology of the mammary glands. It is known that the growth and differentiation of the mammary gland are essentially controlled by multiple interactions of several peptide and steroid hormones from endocrine organs, such as the pituitary gland, ovary and adrenal gland. Subsequently, development occurs in several phases, characterized by distinct morphological features. However, it was reported recently that those hormone releases from the endocrine organs are influenced by a NO-generating system. Therefore, it is likely that the development of the mammary gland is indirectly regulated through the NO-generating system by which hormone releases are controlled in the endocrine organs. Conversely, steroids have been shown to regulate the NO synthesis in diverse types of cells and organs. Taken together, these observations indicate that it is plausible that a NO- generating system may closely participate in the regulation of morphological and functional features of the mammary gland, since the growth and differentiation of the mammary gland are dependent upon the hormonal conditions which change with the developmental stages of this complicated gland. However, additional studies are needed to elucidate the precise roles of NO in the physiology and pathophysiology of the mammary gland.

Publication:

Onoda, M. and Inano, H.: J. Histochem. Cytochem., 46, 1269-1278,1998.

Table 1 Nitric Oxide Production by Cultured Rat Mammary Glands

Treatment	Produced NO_2 (nmol/ml)*1
Control	6.4±0.4
w/LPS (0.5μgml)	29.9±1.9*2
w/LPS, Hydrocortisone (3μM)	7.5±0.6

Three pieces of the mammary glands were cultured, and at the terminus of culture the conditioned media were collected for the determination of nitrite (NO_2^-) concentration. NO

produced and secreted by mammary glands into culture medium was estimated by measuring nitrite
converted from NO with Griess reagent.

*1: The values represent mean±S. E. obtained from three independent experiments. Each experiment contained 6 to 8 cultures per replicate.

*2: Significant difference from control:$p<0.001$.

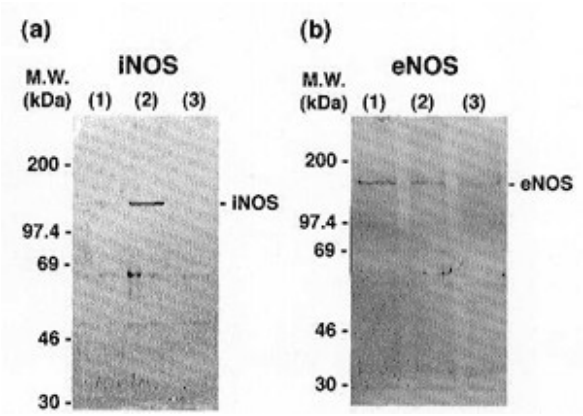

Fig. 20. Immunoblot analyses of iNOS (a) and eNOS (b) in extracts obtained from cultured rat mammary glands. The homogenates (a, 10μg/lane; b, 18μg/lane) were loaded onto the SDS-PAGE system and the immunoreactive substances were visualized by Western blot analysis with an alkaline phosphatase-conjugated secondary antibody.

Lane 1: Control, Lane 2: Control+LPS (0.5μg/ml), Lane 3: Control+LPS+hydrocortisone (3μM).

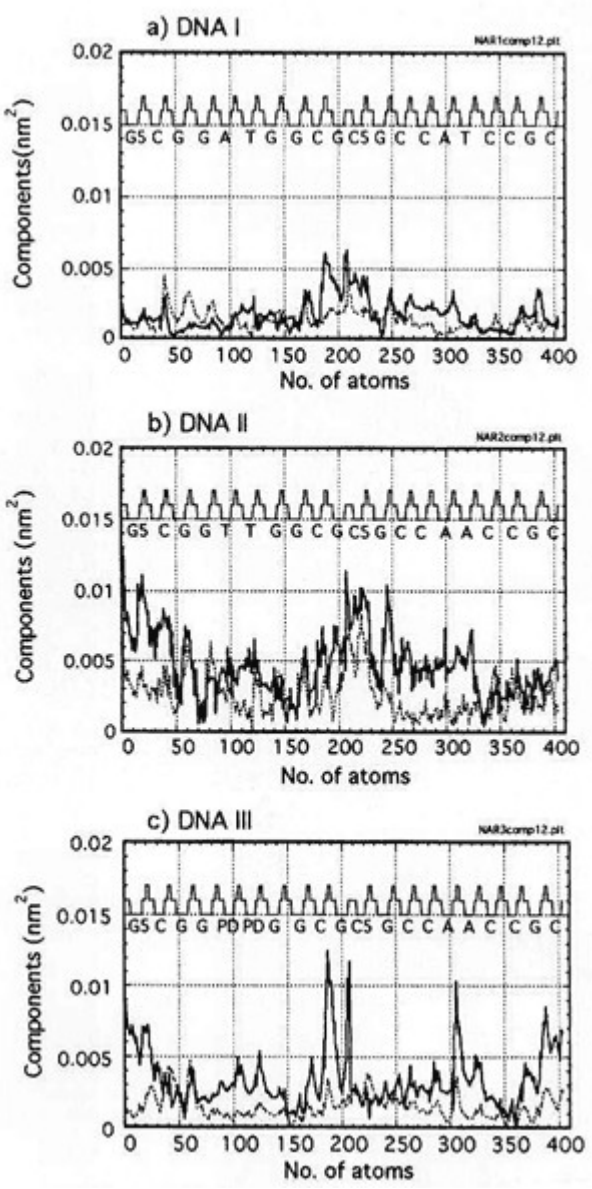

Fig. 18. Component (nm^2) of concerted motions of 404 atoms of a) DNA I, b) DNA II and c) DNA III along the directions of eigenvector 1 (solid line) and 2 (dotted line). The zipper pattern shows the position of phosphorus atom as a sharp peak, sugar as the next lower shoulder and base as the bottom line. Number 1-202 belong to the leading strand (in DNA III this strand contains the PD), and 203-404 belong to the complementary strand.

3.3.1 Effects of Fractionated Total Body Irradiation on Survival and Peripheral Blood Cell Counts in Mice

Kaoru Tanaka and Eiichi Kojima

Keywords: fractionated irradiation, total body irradiation, survival, peripheral blood cell, mice, X-ray irradiation

To minimize injury to nomal tissues, fractionation of irradiation is being used. But the relation between the effects of fractionated irradiation and fractionation intervals has not been well established. We have previously reported the effects of in vitro fractionated irradiation with various time intervals on hematopoietic progenitor cells in mice. In the present study, we investigated the effects of fractionation intervals upon the survival of the mice given two equal split doses of total body irradiation. Female BALB/c mice, 10-14 weeks old, were used for this study. The mice were housed in temperature-controlled rooms with a 12-h light and dark cycle. They were irradiated with two doses of 3.12Gy X-rays (200kVp, 20mA, 0.7Gy/min) with various time intervals (0-24h) and monitored for survival during a 30-day post-irradiation period. As shown in Fig. 21, the percentage of surviving mice increased with the increase of the intervals. When the time interval was 5h, 90% of the mice tested survive, that also being the maximal rate of survivat after 30 days. With a further increase in the interval, the fraction surviving decreased and then increased again. When 6.24Gy was given at a single dose, 99% of the mice died around 15 days after irradiation. The various time intervals of fractionated irradiation made some difference between the survival time of the animals that died. When the mice were irradiated with 5h intervals, the survival time was longer than that in the single dose irradiation. However, for the other time interval groups with low survival rates, the survival times were nearly the same as for sigle dose controls. Since 5h intervals showed a high percentage survival, we investigated peripheral blood cell counts for the intervals. Blood samples of the mice were collected from the outer iliac artery and vein. The numbers of leukocytes, erythrocytes and thrombocytes in the circulating blood were counted with a blood cell counter Sysmex K-1000. They were chased for 30 days after irradiation. Around 15 days after irradiation, leukocyte and thrombocyte counts showed little difference between groups having a single or a fractionated irradiation. However, erythrocytes counts in mice after the fractionated doses of irradiation continuously increased on day 10 and thereafter, compared with a single dose of irradiation.

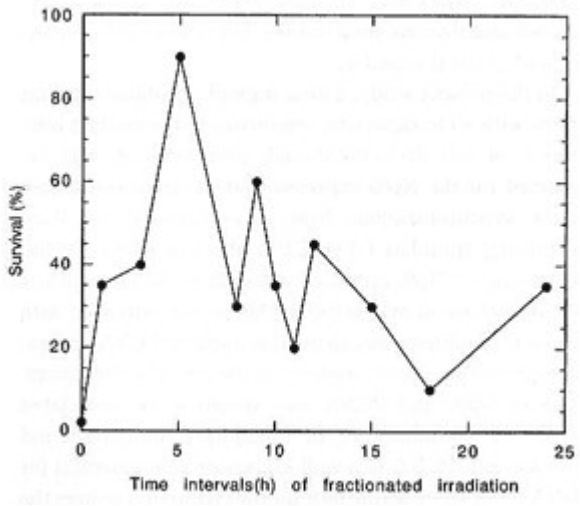

Fig. 21 Thirty-day survival of mice given two equal split doses (3.12Gy×2) of irradiation with various time intervals.

3.3.2 Temporal and Spatial Colocalization of Novel Nuclear Protein Np95 with Proliferating Cell Nuclear Antigen

AMasahiro Muto, Yoshihiro Takemoto*, Yasuyoshi Kanari, Eiko Kubo,Kouichi Tatsumi, and Akira Fujimori(Institute of Immunology, Syntex-Roche, Noda-shi, Chiba)

Keywords: novel nuclear protein Np95, PCNA, DNA replication, cell cycle

We previously produced a monoclonal antibody, Th-10a mAb, that recognizes a 95 kDa mouse nuclear protein (Np95). Np95 was stained with the Th10a mAb specifically in the S-phase of normal mouse thymocytes. In contrast, mouse T cell lymphoma cells showed a constantly high level for Np95 accumulation irrespective of cell stages during the cell cycle. To gain further insights into the physiological roles of Np95, we isolated the cDNA encoding Np95 by immunoscreening a λgt-11 cDNA expression library with the Th-10a mAb. Sequencing of the whole 3.5 kb cDNA revealed that Np95 is a novel nuclear protein with an open reading frame (ORF) consisting of 782 amino acids. The ORF contains a leucine zipper motif, a zinc finger motif, a potential ATP/GTP binding site, a putative cyclin A/E-cdk2 phosphorylation site and retinoblastoma protein (Rb)-binding motifs "LXCXE" and "IXCXE". Np95 was strongly expressed in the testis, spleen and thymus, lung tissues, but not in the brain, liver and skeletal muscles.

In the present study, a near-diploid fibroblast cell line, m5S, with a characteristic sensitivity to the contact inhibition of cell division, though immortalized, was examined for the Np95 expression at different cell stages after synchronization. Np95 was detected by flow-cytometry from late G1 to G2/M phase of m5S cells. Microscopically Np95 appeared as foci in nuclei through late G1 to S phase of m5S cells, and these foci coincided with those for proliferating cell nuclear antigen (PCNA) in double immunostaining studies. Moreover, the colocalization of Np95 and PCNA was shown to be associated with the chromosomes of metaphase, anaphase and cytokinesis. PCNA is a well known protein essential for DNA replication, acting as a sliding clamp that tethers the leading strand DNA polymerase δ to its template, enhancing the enzyme's processivity. Moreover, PCNA is required for nucleotide excision repair, and is also involved in DNA mismatch repair. In addition, PCNA is shown to bind DNA-(cytosine-5) methyltransferase. PCNA may be recruited to these different roles in replication, repair and methylation by interaction with proteins specific to each process.

In correlation with the amount of Np95 protein, Np95 mRNA was reduced when m5S cells reached confluence. Southern blot analyses of genomic DNA from different species using Np95 mouse cDNA probe suggested that the Np95 sequence was well conserved among mammals. These results collectively implicate this novel nuclear protein in cell cycle progression andor DNA replication.

Publications :

1) Muto, M., Chen, Y., Kubo, E. and Mita, K.: Jpn. J. Cancer Res., 87, 247-257, 1996.
2) Muto, M., Utsuyama, M., Horiguchi, T., Kubo, E., Sado, T. and Hirokawa, K.: Cell Prolif., 28, 645-657, 1995.
3) Fujimori, A., Matsuda, Y., Takemoto, Y., Hashimoto, Y., Kubo, E., Araki, R., Fukumura, R., Mita, K., Tatsumi, K., Muto, M.: Mammalian Genome, 9, 1032-1035 (1998).

3.3.3 Differential Cellular Basis for the Resistance of C3H and STS Strain Mice to Thymic Lymphomagenesis Following Fractionated Whole-body Irradiation

Hitoko Kamisaku and Shiro Aizawa

Keywords: fractionated radiation, bone marrow chimeras, thymic lymphoma

It has been known that B10 strain mice are extremely susceptible to induction of thymic lymphomas by fractionated whole-body irradiation (FIR), whereas C3H and STS mice are fairly resistant. In the present study, radiation bone marrow chimeras prepared in the combinations of susceptible and resistant mice were used to determine the influence of the host/thymic environment in strain-dependent thymic lymphomagenesis. B10→C3H and B10→STS bone marrow chimeras had a high incidence of thymic lymphomas after FIR-treatment as well as B10→B10 chimeras, whereas C3H→B10 and STS→B10 chimeras had a low incidence of thymic lymphoma as did C3H→C3H and STS→STS chimeras. Furthermore, FIR-treatment of [B10+C3H]→B10 mixed chimeras induced similar numbers of thymic lymphomas which originated from either B10 or C3H thymocytes, whereas FIR-treatment of [B10+STS]→B10 mixed chimeras preferentially induced thymic lymphomas of B10 origin. These results indicated that (1) the host environment of C3H and STS resistant mice is sufficient for the development of thymic lymphomas and (2) the resistance of STS mice to FIR-induced thymic lymphomagenesis is an intrinsic property of thymocytes as the precursors of thymic lymphoma, whereas bone marrow-derived thymic stroma cells play a role in the difference in sensitivity among B10 and C3H mice.

Publication:

Kamisaku, M., Aizawa, S., Kitagawa, M., Ikarashi Y., and Sado, T.: Int. J. Radiat. Biol. 72, 191-199, 1997.

3.3.4 Do Chemokines Control the Thymic Architecture?

Gen Suzuki, Hirofumi Sawa[1], Yukiko Nakata, Kenichi Nakagawa, Akiko Uzawa, Hisako Sakiyama, Kazuya Iwabuchi[2], Yoshiyasu Kobayashi[1] and Kazuo Nagashima[2]

([1]Hokkaido University School of Medicine; [2]Hokkaido University)

Key words: CXC chemokine, SDF-1, T cell development, chemoattractant, trafficking

Chemokine induces cell migration along the chemokine concentration gradient. It also activates integrin and induces cell adhesion. With these mechanisms chemokine controls T cell homing and trafficking. Here we propose a new role for chemokine in the thymus as a biological barrier that prevents forbidden clones from leaking from the cortex. A CXC chemokine, SDF-1, was originally defined as a pre-B cell stimulating factor. However, SDF-1 was a strong chemoattractant for mature and immature T cells and its mRNA was abundantly expressed in the thymus. In situ hybridization revealed that both mRNAs encoding SDF-1 and its receptor CXCR4 were expressed in the cortex but not in the medulla of the thymus. Expression of SDF-1R molecules on thymocytes was evaluated by SDF-1-Ig binding. Early immigrant cells, $CD44^{+}$ $CD25^{-}$ $NK1.1^{-}$ TN cells, were $SDF\text{-}1R^{-}$ while $CD44^{-}$ $CD25^{+}$ TN cells were $SDF\text{-}1R^{+}$. Thus, progenitor cells gained SDF-1 reactivity after immigration into the thymus. Interestingly, SDF-1R expression was down-modulated after positive selection; $CD69^{hi}$ $CD3^{int}$ DP cells started to lose SDF-1R and most SP cells were $SDF\text{-}1R^{-}$ (Fig.22). The results indicated that
SDF-1 controls the cell trafficking in cortex and prevents unselected DP cells from leaking from the cortex.

Publications:

1) Suzuki, G., Nakata, Y., Dan, Y., Uzawa, A., Nakagawa, K., Saito, T., Mita, K., and Shirasawa, T. : Int. Immunol. 10, 1049-1056, 1998.

2) Sawada, S., Gownrishankar, K., Kitamura, R., Suzuki, M., Suzuki, G., Tahara, S., and Koito, A. : J. Exp. Med. 187, 1439-1449, 1998.

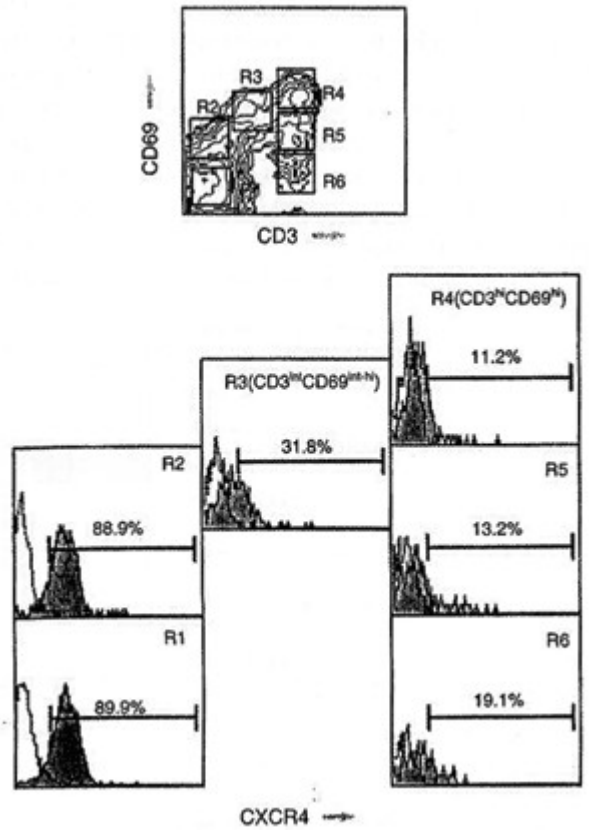

Fig. 22. SDF-1R (CXCR4) was down-modulated in positively selected thymocytes. Three color staining was performed to analyze the levels of SDF-1R (FITC), CD69 (PE), and CD3 (Cy Chrome). Electrical gates (R1 - R6) were set on the basis of CD69 and CD3 expression, and the SDF-1R profile of each sub-population was depicted.

3.3.5 Control of Endotoxin Shock by the Dried Preparation of Low Virulent Streptococcus pyogenes OK-432

Masako Nose, Akiko Uzawa, Masayuki Nomura, Yoshinori Ikarashi, Yukiko Nakata, Makoto Akashi and Gen Suzuki

Key words: OK-432, NO, IL-10, LPS tolerance, TNF-a

Bacterial endotoxin, lipopolysaccharide (LPS), is a causative agent of Gram-negative septic shock. However, if pre-administered at low dose, LPS makes mice resistant to subsequent endotoxin challenge, the phenomenon known as LPS tolerance. Here we demonstrated that pharmaceutical preparation of Gram-positive Streptococcus pyogenes, OK-432, also induced a state analogous to LPS tolerance if administered 6 - 48 h prior to LPS challenge. The pre-administration of OK-432 increased the lethal dose of LPS threefold in BDF1 mice, and this was accompanied by the reduced gene expression of IL-6, IFN-γ, inducible nitric oxide synthase (iNOS), and IL-10 in spleen and peritoneal cells.
Serum concentrations of IL-6 and IFN-γ were also suppressed by the pre-administration of OK-432. In contrast to the LPS tolerance, the levels of TNF-α mRNA were not suppressed in OK-432-administered mice, and their peritoneal cells produced high levels of TNF-α and soluble TNF receptor (sTNFR) p75 in response to LPS in vitro. Peritoneal cells from OK-432-administered mice, but not LPS-administered ones were hyporesponsive to IFN-γ in terms of nitric oxide (NO) synthesis, and this hyporesponsiveness to IFN-γ was abrogated by anti-IL-10 antibody (Fig. 23). Likewise, peritoneal cells from both OK-432- and LPS-administered mice were hyporesponsive to LPS, serum, TNF-α, IFN- γ, and PMA in terms of IL-6 production. Anti-IL-10 antibody increased IL- 6 production eight-fold in cells from OK-432-administered mice, but marginally in cells from LPS-administered mice.Even in peritoneal cells from OK-432-administered mice, anti-IL-10 antibody failed to fully restored the IL-6 production. Thus, the hyporesponsive state of peritoneal cells was mediated by both IL-10-dependent and - independent mechanisms. These results demonstrated that OK-432 controlled endotoxin shock by blocking the cytokine cascade from TNF- α.

Publication:

Nose, M., Uzawa, A., Nomura, M., Ikarashi, Y., Nakata, Y., Akashi, M.,and Suzuki, G.: Cell. Immunol., 188: 97-104, 1998.

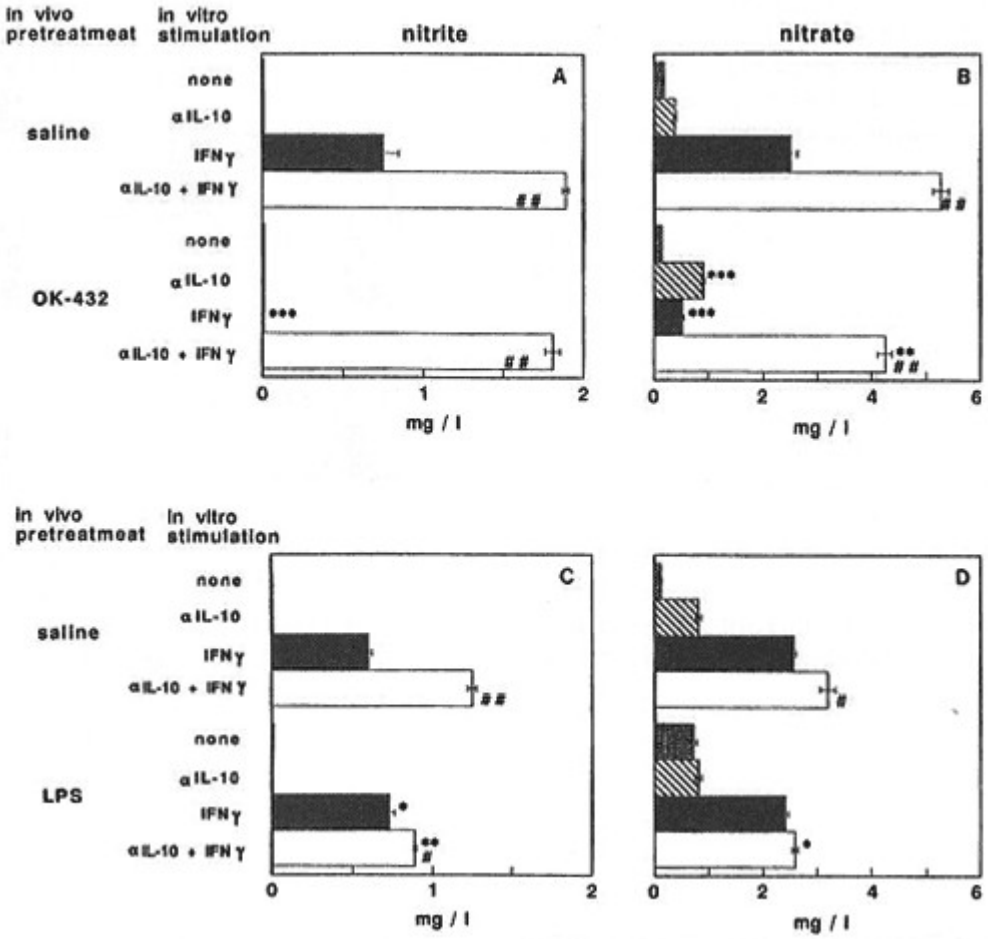

Fig. 23. IL-10 is one of the factors mediating the hyporesponsiveness of peritoneal cells. BDF1 mice received physiological saline, OK-432 (5KE), or LPS (50μg) i.p. On the next day, peritoneal cells were harvested and cultured with IFN-γ (100U/ml) for 24 h in the presence or the absence of anti-IL-10 antibody. In order to measure NO synthesis, nitrite and nitrate in the culture supernatants were measured by ELISA. Representative results of two (LPS pretreatment) and three (OK-432 pretreatment) independent experiments was shown. OK-432 PEC produced less NO, and anti-IL-10 antibody in the culture significantly restored the NO synthesis (saline vs. OK-432, $^{*}p<0.05$, $^{**}p<0.01$, $^{***}p<0.001$; with anti-IL-10 antibody vs. without the antibody, #p<0.05, ##p<0,001 by Student's t-test.)

3.4 BIO-MEDICAL SCIENCES Pathology and Physiology

3.4.1 Possible Application of PIXE Method to Intestinal Permeability Measurements

Keitaro Nakao* , Yasuo Suzuki*, Ryoichi Sato*, Yasushi Saito*, Itsuro Tamanoi, Shinji Matsumoto, Hisamasa Joshima, and Hitoshi Imazeki (*School of Medicine, Chiba Univ.)

keywords: PIXE, Rb, Mn, intestinal permeability, C57BL/6J mouse, oral administration

We measured intestinal permeability of C57BL/6J mice by the PIXE method. A mixture of a rubidium chloride solution and a manganese chloride solution was administered orally to the mice. Their blood was sampled successively after the administration, and its element contents were measured by the PIXE method. The Rb content in the plasma of the Rb+Mn administered group reaches a maximum 5 min after the administration and decreases subsequently. The value in the whole blood of this group increases slightly for the first 30 min after the administration and then remarkably from 3 hrs. This increase continues for 48 hrs. The Rb content in the control group is very small. Rb is probably transferred into plasma from intestinal mucosa at first, and subsequently moves into blood cells. The Mn content in the control group is small. The values in the whole blood and the plasma of the Rb+Mn administered group reach a maximum 5 min after the administration and then decrease, reaching the level of the control group at 24 hrs. Mn is probably transferred into the blood from intestinal mucosa, and washed out more rapidly than Rb.

The Rb and Mn contents in the plasma of Rb+Mn administered mice are found to increase to the peak level 5 min after the administration. Rb and Mn are useful as a tracer to study intestinal disease with PIXE measurements. By the PIXE method, intestinal permeability can be measured more quickly than by other existing methods. In order to assess intestinal permeability, an indicator is proposed which is obtained by comparing the element amounts of Rb and/or Mn in blood sampled just after the administration.

3.4.2 Association of CAR bacillus with Natural Chronic Tracheitis in Goats

Satoru Matsushita[1], Akihiro Kawano, Jorge Oros[2], Antonio Fernandez[2],Jose L. Rodriguez[2], C.L. Franklin[2] and Tsuneya Matsumoto

([1]Institute for Environmental Sciences, Rokkasho, Aomori; [2]Faculty of Veterinary Sciences, University of Las Palmas de Gran Canaria, Spain)

Keywords: CAR bacillus, goats, chronic respiratory disease

Cilia-associated respiratory (CAR) bacillus, causing chronic respiratory disease, is a descriptive term for an unclassified, gram-negative, motile, filamentous bacterium that colonizes the respiratory epithelium of laboratory and domestic animals. The infection has been reported in rats, mice, rabbits, guinea pigs, hamsters, cattle and pigs.

In the present paper, we describe the infection of the CAR bacillus in 83 slaughtered goats (33 aged 3-4 months and 50 aged>12 months) from a farm with a history of caprine pleuropneumonia caused by mycoplasmas of the Mycoplasma mycoides cluster.

Histologically, the CAR bacilli were detected by the means of the Warthin Starry (WS) method in the tracheal epithelium of seven (21.2%) of the kids and 16 (32%) of the adults goats. Chronic diffuse tracheitis characterized by mixed lymphocyte and plasma-cell infiltration was found in the same seven kids and in 17 adults, including the 16 infected with the CAR bacillus. Although not proved, it is possible that the CAR bacillus caused the chronic tracheitis in the goats.

Ultrastructural examination of WS-positive tracheal and bronchial samples revealed filamebntous bacteria. The morphology of these bacilli, and the associated tracheal lesions, were in general accord with earlier reports of CAR bacillary infections in other animal species.

In the immunohistological study, an immunoperoxidase technique, based on the labeled strep-tavidin biotin (LSAB) method with 3-amino- 9-ethylcarbazole (AEC) as substrate was used. The examination with guinea pig anti-rabbit CAR bacillus serum revealed a positive reaction in the ciliated respiratory epithelium of all WS-positive animals. However, no positive immune reaction was observed in any of the goats with the mouse anti-rat CAR bacillus serum.

In recent molecular biological studies, it has been shown that the rabbit CAR bacillus is closely related to the genus Helicobacter, while the rat CAR bacillus is more closely related to the genus Flavobacterium. Our results suggest that the goat CAR bacillus found is more closely related to the rabbit CAR bacillus than to the rat CAR bacillus.

Publication:

Oros, J., Fernandez, A., Rodriguez, J.L., Franklin, C.L., Matsushita, S., Poveda, J.B.: J. Comp. Path., 117, 289-294, 1997.

3.4.3 Effects of Clinostat-microgravity Alone and in Combination with Irradiation on Bone Metabolism in Rats

Satoshi Fukuda and Haruzo Iida

Keywords: clinostat, simulated microgravity, radiation, bone metabolism, rat

To clarify the changes in bone metabolism caused by space flight, a 3D- clinostat developed for small animals was used to examine the effects of simulated microgravity both alone and in combination with irradiation on bone metabolism in rats. The clinostat is an apparatus which rotates five rats (put in capsules) equally toward all directions, giving a simulated microgravity on earth (Fig. 24). Male rats, 3 months of age, were divided into thirteen groups based on loading time and velocity of rotation, a fixed method of putting the rat into the clinostat capsule, and whole-body X-ray irradiation at a single dose of 5 Gy before the experiment. The experimental period was for 42 days. In the microgravity alone experiment, with prolongation of loading time and increasing velocity of the clinostat, the following were observed: decreased calcium content and increased fragility of femur; and increased trabecular separation and decreased osteoid volume in the proximal metaphysis of the tibia. With a combination of microgravity and irradiation, decreased calcium content of the femur and lumbar vertebra, increased trabecular separation and decreased osteoid volume were observed, but these effects were not consistently seen (Fig. 25).

These results indicate that the clinostat might be useful for studying changes in bone metabolism caused by microgravity in space, because the mineral loss and fragility in bones of the lower limbs were similar to reported observations in astronauts. These effects are probably induced by the inhibition of bone formation and acceleration of bone resorption because of simulated microgravity, and might be enhanced by the severer inhibition of bone formation in combination with radiation.

Publication:

Fukuda, S. and Iida, H.: J. Jpn. Soc. Bone Morphom., 7, 175-182, 1997.

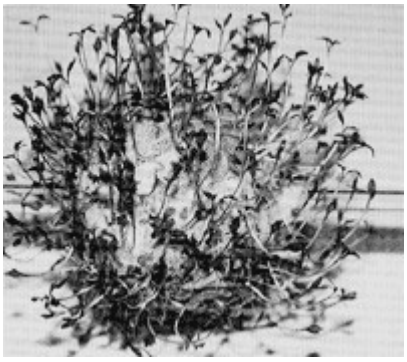

Fig. 24 Plant seeds grew towards all directions after being sowed on the surface of the sphere which was rotated continuously, indicating that the simulated microgravity was produced due to equal dispersion of gravity. In the control (norotation), plant seeds put forth buds toward only one direction of the sphere.

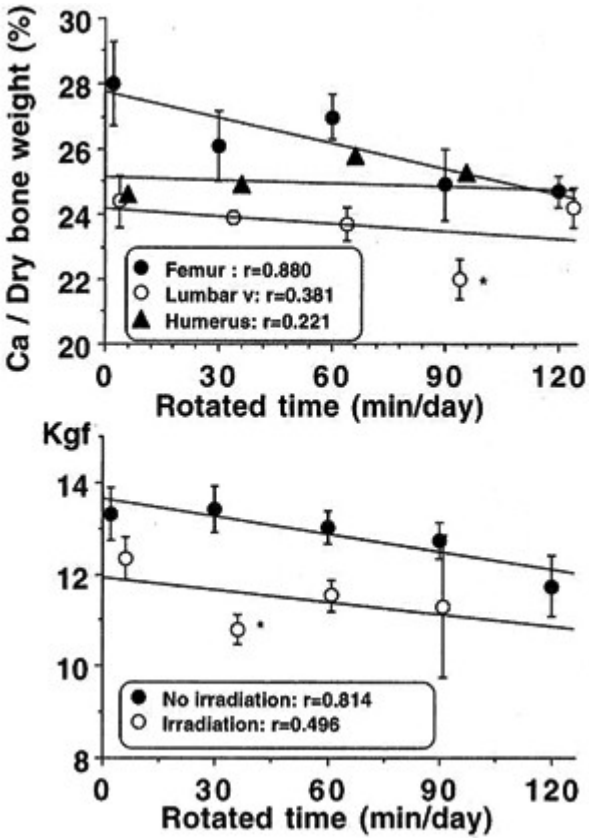

Fig. 25 Calcium content of the femur decreased with prolongation of loading rotation time of the clinostat compared to the lumbar vertebra and humerus in the no-irradiation group (upper), because the femur, being in the hind limb, always received a stronger load than the other bones. Bone strength of the femur in the combination group, clinostat- loading and irradiation, decreased compared to clinostat-loading alone (lower).

3.4.4 Dose-Response Relationship for InducA059tion of Bone Tumors in Mice Irradiated Neonatally with Gamma Rays

Shunsaku Sasaki

Keywords: bone tumors, gamma rays, dose-response, neonatal mice

In our previous experiment using female B6C3F$_1$ mice we showed that infant mice are susceptible to induction of bone tumors. Incidence of bone tumors increased significantly after irradiation with gamma rays at 17 days of the prenatal age or 0, 7 or 35 days of the postnatal age; whereas, bone tumors did not develop in excess when mice were irradiated at 105, 240 or 365 days of age. The present study examined the dose-response relationship for inducA059tion of bone tumors in female B6C3F$_1$ mice irradiated at 0 day of age with gamma rays from ^{137}Cs. Because the incidence of bone tumors had not been so high in the previous study, we designed an experiment using a larger sample size in order to obtain more precise data. Number of mice in experimental group irradiated with 0, 0.48, 0.95, 1.43, 1.90, 2.38, 2.85, 3.80 or 5.70 Gy was 885, 453, 338, 338, 331, 332, 205, 272, 81 and 91, respectively. All the mice were allowed to live out their entire life span under a specific pathogen-free condition. Findings of autopsy and histoA059logical examinations were recorded as electric images.

Dose-response curve for induction of bone tumors is shown in Fig. 26. Initial slope of the dose-response curve was upward concave and the highest incidence was observed in group irradiated with 3.80 Gy.

Incidence in the group irradiated with 5.70 Gy was lower than that of the 3.80 Gy group. Dose-response relationship was analyzed using a model that tumor incidence is determined by an inducing effect, sterilization of the potentially tumoriA059genic cells and competing risks. The inducing effect of gamma rays seemed to be proportional to the square of the dose. Dose-response relationship for incidence of bone tumors was adequately described by the following equation:

$$I(D)=I(0)\cdot(1-0.1504D-0.0016D^2)\cdot(1+1.487D^2)$$

Where, I (D) and I (0) represent incidence in a group irradiated with dose D and incidence in the control group, respectively.

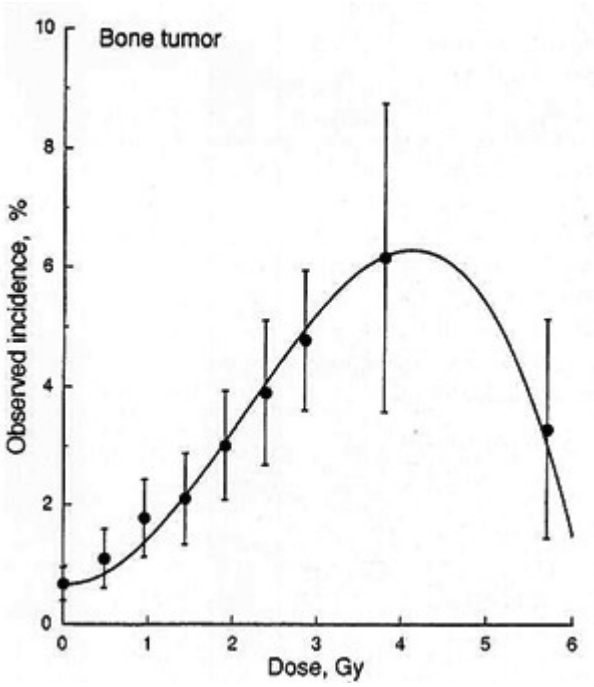

Fig. 26. Incidence of bone tumors as a function of dose of gumma rays from ^{137}Cs in female $B6C3F_1$ mice.

Vertical bars indicate standard errors.

3.5.1 Cryopreservation of Spermatozoa for Strain Maintenance of Gene Disrupted Mice

Masanori Okamoto, Naomi Nakagata[1], Otoya Ueda[2], Nobuo Kamada[2] and Hiroshi Suzuki[2]

([1]Kumamoto Univ.; [2]Chugai Pharmaceutical Co., Ltd.)

Keywords: cryopreservation, gene disrupted mouse, spermatozoa, in vitro fertilization

We developed a strain maintenance system using the embryo cryopreservation method on inbred mice which were produced in our facilities, which includes cleaning of HVJ infected mice and producing germfree mouse using an embryo transfer technique. We carried out the embryo cryopreservation for strain maintenance of inbred mice by a slow freezing method with a programmable electrical cooling freezer.

Cryopreservation was done for a total of 6,640 embryos of 25 inbred mouse strains which were produced in our facilities and 4 lines of transgenic and gene disrupted mice introduced from outside laboratories. For strain maintenance of transgenic and gene disrupted mice, it is possible to cryopreserve in the spermatozoa. There is no necessity for always cryopreserving as the embryo, because the manipulated gene may be transmitted in the next generation.

Spermatoza use is superior to embryo use, and many samples can be collected easily at once. Cryopreservation of mouse spermatoza has recently become available for use.

In this study, we attempted to apply this technique to the maintenance of 2 gene disrupted mice lines.

Cauda epididymides that were taken from Et^{tm1Csk} and Gk^{tm1Csk} mice were minced in 100 µl of a cryopreservation solution which consisted of 18% raffinose and 3% skim milk. Sperm suspensions were put into plastic straws and cooled rather rapidly by being placed in the gas phase above liquid nitrogen, before being then were stored at -196℃. By immersion of the frozen straws in a water bath at 30℃, the sperm were thawed rapidly. For in vitro fertilization, 1µl of frozen-thawed sperm suspensions from each mouse strain was added directly to oocytes contained in 200µl of medium.

Following pre-incubation of the frozen-thawed spermatozoa, ICR oocytes were introduced into the medium containing the frozen-thawed spermatozoa. The fertilization rates of the oocytes inseminated with Et^{tm1Csk} and Gk^{tm1Csk} frozen-thawed spermatozoa were 71% and 77% respectively (Table 2). The development rates into young after embryo

transfer ranged from 32-65%. Progeny tests revealed that the mutated locus/loci were transmitted to the next generation according to the Mendelian law of the inheritance of characteristics. These results indicate that cryopreservation of spermatozoa provides an effective alternative to embryo freezing for maintenance of gene disrupted mouse strains.

Publications:

1) Aoki, K., Okamoto, M., Tatsumi, K. and Ishikawa, Y.: Zoological Science, 14, 641-644, 1997.

2) Nakagata, N., Okamoto, M., Ueda, O. and Suzuki, H.: Biol. Reprod., 57, 1050-1055, 1997.

3) Okamoto, M., Nakagata, N., Ueda, O., Kamada, N. and Suzuki, H.: J. Mamm. Ova Res., 15, 77-80, 1998.

Table 2. In vitro fertlization with frozen-thawed gene disrupted mice spermatozoa and subsequent embryos transfer.

Gene disrupted mouse strain	Spermatozoa	No. of oocytes inseminated	No.(%) of oocytes fertilized and developed to 2-cell stage	No. of parturitions/no. of recipients	No. of live young/no. of embryos transferred(%)
$Et1^{tm1Csk}$	Frozen-thawed	136	90(71)$_a$	3/5	29/90(32)$_a$
	Fresh	130	98(75)$_a$	-	-
Gk^{tm1Csk}	Frozen-thawed	137	106(77)$_{a,c}$	5/5	66/102(65)$_a$
	Fresh	440	380(86)$_{a,c}$	-	-

ICR oocytes were inseminated with spermatozoa from heterozygous mice. Values with the same superscripts are not significantly defferent in the same column at $p>0.05$.

3.5.2 Genomic Evolution Mediating the Duplication of Short Motif Sequences

Sachiko lchimura and Mitsuru Nenoi

Keywords: molecular evolution, tandem repeat, mismatch repair, RAD27, histone H1 gene

Evolution of genomes is based on the genetic flexibility, lt is significant that fidelity of the genome in the normal cell cycle requires various repair systems corresponding to different type of mutations. Namely, DNA flexibility is under the control of some rearrangement rules that are regulated by the repair systems. For example, the defect in a mismatch repair system confers an increase in expansion mutations of di or tri- nucleotide repeating sequences. Another type of duplications of short sequences (>5bp) frequently occurs in a rad 27 mutant of S. cerevisiae. Quantitative mutational spectrum analysis of p53 shows that 10-15% of somatic and germ line mutations are small, intragenic deletions or insertions. Almost all deletions and insertions can be explained by one or more of the following DNA sequence features: monotonic base runs, adjacent or nonadjacent repeats of short tandem sequences, palindromes, and runs of purine or pyrimidines (homocopolymer runs). We found that tandem duplication of short motif sequences would be an important pattern in the evolution of DNA sequences. In this report we analyzed the histone HI subtype sequences to better understand the role of duplication in sequence rearrangement producing subtypes. Five H1 histone subtype genes in the human genome were characterized by highly conserved core sequence and variable 3'and 5'tailes. The alignment of the nucleotide sequences at variable regions showed that the highly varied parts were clustered but not uniformly dispersed. The detailed analysis of the parts of low homology suggested that the short elements were duplicated or deleted in addition to the base substitution in the evolution process.

3.5.3 Genome Sequencing of Schizosaccharomyces pombe Chromosome III by Use of cDNA

Mitsuoki Morimyo, Kazuei Mita, Etsuko Hongo, Tomoyasu Higashi, Kimihiko Sugaya, Masahiro Ajimura, Shunichi Sasanuma, Junko Nohata, Terumi Kimura, Hiromi Inoue, Yoshie Ishihara and Shizuko Koike

Keywords: S. pombe, cDNA, DNA sequencing

In a study of the structure and function of the housekeeping genes of eukaryotic cells, we chose Schizosaccharomyces pombe (S. pombe) as a model organism. It is assumed to have 6,000 genes and the genome size of 14 megabases (Mb) compared to 100,000 genes and 3,000 Mb for humans. In spite of the greater numbers for humans, S. pombe can be used as a model organism for humans, because its genes are similar to human genes which can be normally expressed in yeast, its housekeeping genes are considered to be conserved through eukaryotic evolution and many of its genes have introns which make cDNA sequences essential to determine physical organization of genes from the genomic DNA sequence. Moreover, the functions of S. pombe genes are easily identified by disrupting the genes with homologous recombination.

We have analyzed 12,000 cDNA clones made by mRNA prepared from late log phase cells of S. pombe and identified over 2,500 genes (900 similar clones with known genes and 1800 newly found clones). Among the cDNA clones, 8,118 were deposited with the DDBJ and put on the WWW homepage of NIRS (http://www.nirs.go.jp). By using these cDNA clones mapped on the chromosome III of S. pombe, we started genome sequencing by a bottom-up strategy. We selected 300 corresponding genomic clones from the S. pombe genomic library generated by a lambda phage vector. The insert yeast DNA was amplified by LA-PCR, partially digested by an endonuclease followed by sedimentation in a sucrose gradient and DNA fragments ranging from 1 to 3 kb were recovered for a shotgun-sequencing. The DNA sequence determined was confirmed to be more than 99.9 % accurate by the fact that the DNA size determined by an agarose gel electrophoresis after restriction enzyme digestion was a good agreement with the DNA size deduced by the DNA sequence determined. We identified an ORF found in an assembled DNA sequence as a gene by a homology search in public databases and our S. pombe cDNA database. To date, we have sequenced over 60 clones covering about 800 kb DNA region at a redundancy of 6. Over 200 genes were identified to have no introns and about 100 genes were predicted to have them. A systematic disruption of genes related to radiation sensitivity is in progress to identify their functions.

Publications

1) Morimyo, M., Mita, K., Hongo, E., Higashi, T., Sugaya, K., Ajimura, M., Yamauchi, M., Tsuji, S., Park, W-Y., Sasanuma, S., Nohata, J., Kimura, T., Inoue, H., Ishihara, Y.: Yeast 13, S258, 1997.

2) Morimyo, M., Mita, K., Hongo, E., Higashi, T., Sugaya, K., Ajimura, M., Yamauchi, M., Tsuji, S., Park, W-Y., Sasanuma, S., Nohata, J., Kimura, T., Inoue, H., Ishihara, Y.: 8203Biodefence Mechanisms against Environmental Stress", p115-123. Kodansha and Springer-Verlag, Tokyo and Heidelberg, 1998.

3.5.4 Construction of cDNA Sequence Libraries of Major Tissues of the Silkworm, Bombyx mori

Kazuei Mita, Mitsuoki Morimyo, Kazuhiro Okano[1], Susumu Maeda[1] and Toru Shimada[2]

([1]RIKEN; [2]Univ. of Tokyo)

Keywords: cDNA library, Bombyx mori, EST database, multi-cellular organism

Aiming at the genome analysis of Bombyx mori, we have started to construct the EST database through the analysis of cDNA libraries. The gene expression patterns significantly depend on tissues as well as developmental stages in multi-cellular organisms, unlike the case of umi-cellular organisms such as yeast. The cDNAs from which the ESTs are derived are present in libraries in proportion to the level of mRNA in the tissues from which the library was prepared. Thus, ESTs are subject
to `expression bias' for multi-cellular organisms. Therefore, we took the following strategy: cDNA libraries of various tissues (and different stages) were constructed by the directional cloning method. 1000 cDNA clones were chosen at random from each library and around 700 nucleotide sequences from the 5' end of the cDNA were determined, followed by gene identification with a protein homology search in public protein databases. 1000 cDNA clones are enough to configure the abundantly expressed genes in the tissue from which the cDNA library is constructed, and the analyses of various tissues (and different stages) will provide a sufficient amount of ESTs for genome analysis. In addition, this approach explicitly represents the gene expression patterns of all genes identified. Another advantage of the cDNA catalog is to configure all members of related genes and display the whole pathway that the cells (or tissues) employ.
So far, we have performed the analyses of cDNA libraries of a culture cell (as a control), male and female fat bodies at the 5th instar, the 5th instar midgut, the wing disc at the beginning of spinning and 2 days after spinning, and the embryo at 40 hrs and 96 hrs after fertilization.
By a comparison of the cDNA sequences and their deduced protein sequences with those in private and public databases, the cDNA libraries were classified into two groups of more than 1000 newly identified clones and more than 500 homologous clones with known genes.
Various tissue-specific and developmental stage-specific genes were found as well as many housekeeping genes, in which interesting genes
related to apoptosis, differentiation of tissues, hormone regulation, formation of nerve system and behavior were involved. Now studies on the cDNA libraries of the posterior silk glands at the 5th instar and 4th molt, testis, pheromone gland, brain and baculovirus infected tissues are being carried out to expand the EST database.

3.5.5 All of the Three Clusters of Basic Amino Acids in the Carboxyl Terminus of NPAT Are Required to Localize the Protein in the Nucleus

Takasi Imai, Eri Takeda, Harumi Ohyama, Yoshiro Toyama[1], Shigeki Yuasa[1] and Shunsaku Utsumi[2]

([1]Dept, of medicine, Chiba Univ., [2]Dept. of Education, Chiba Univ.)

Keywords: GFP, nuclear localization signal, NPAT

NPAT is a gene closely linked to the ATM gene. The two genes are transcribed in opposite directions and share a 0.5-kb 5' upstrem sequence. Our previous sequence analysis of NPAT suggested that this gene product could be transported into the nucleus because it contains sequences matching nuclear localization signlas consisting of four continuous basic amino acids, ^{1368}KKRK^{1371}, ^{1397}KKKK^{1400}, and ^{1402}KKKK^{1405}. To investigate whether the NPAT product is transported into the nucleus, we constructed a green fluorescent protein (GFP)-NPAT fusion (GF-NP). After transfection into cultured mammalian cells, GF-NP was directly detected in the nucleus using fluorescence microscopy.

When three basic amino acid clusters were mutated to ^{1368}KELK^{1371}, ^{1397}KELK^{1400}, and ^{1402}KLKK^{1405}, respectively, all of the mutants were observed in both the cytoplasm and the nucleus. A truncated fusion protein which lacked the NPAT carboxyl terminus containing all of the three basic amino acid clusters, and ^{1368}KKRstop^{1371} were also distributed throughout the cytoplasm and nucleus. These data suggest that NPAT is a nuclear protein and that all of the basic amino acid clusters in the carboxyl terminus of the NPAT are essential for transporting the protein into the nucleus.

3.5.6 Analysis of Bi-directional Promoter Activity between NPAT and ATM Genes

Masashi Sagara, Yasuharu Ninomiya, Eri Takeda[1], Akiyo Nishiyama, Hiroko Ito, Masatake Yamauchi, Naohiko Seki[2], Takahiro Nagase[2], Tada- aki Hori and Takashi Imai

([1]Dept. of Education, Chiba Univ., [2]Kazusa DNA Research Institute)

Keywords: NPAT, ATM, bi-directional promoter, transcription

NPAT is identified as a gene closely linked to the ATM gene. Because these two genes are transcribed in opposite directions and share a 0.5- kb 5' upstream sequence, we have investigated the possibility that each gene influences the expression of the other. The present study was conducted to determine the essential DNA sequences required for the transcription of the human NPAT and ATM genes.

To investigate the mechanism regulating the expression of each gene, we analysed the 0.5 kb nucleotide sequence flanked by the two genes. We tentatively predict four GC boxes, two CCAAT boxes, one CRE-like site and two E2F-like sites in the region. Some of the promoter elements and regulatory sequences work in either orientation. Therefore, this NPAT and ATM upstream region may regulate the transcription of both genes.

First, the 5' flanking sequence of the NPAT gene was amplified with genomic DNA. Then the fragment was sequentially deleted and fused with the coding region of the luciferase gene. These new constructs contained NPAT promoter fragments with different 5' ends residing at 2752, 1838, 1240, 605, 350, 147 and +10, and a common 3' end at position +23. Besides, a similar deletion series of ATM promoter was constructed. These new constructs contained ATM promoter fragments with different 5' ends residing at 2210, 1500, 713, 506, 107, 65, 15 and

+47, and a common 3' end at position +116. Each of these recombinant DNAs were then used for transient gene expression studies by transfection into various cell lines. The results showed that DNA sequences between -350 to +10 for NPAT and -107 to -15 for ATM, particularly those in the upstream region, were responsible for the full promoter activities.

Next, when the mutant whose E2F-like sites were disrupted was transfected into the HepG2 cells, the NPAT promoter activity decreased from 100% to 82% (E2F-like I), 57% (E2F-like II), 37% (E2F-like I&E2F-like II) and the ATM promoter activity also decreased from 100% to 57% (E2F-like I), 75% (E2F-like II). 40% (E2F-like I&E2F-like II). When the mutant whose CRE-like site was disrupted was transfected into the HepG2 cells, the NPAT promoter activity decreased from 100% to 10% and ATM promoter activity also decreased from 100% to 24%. These results suggested that the CRE-like and the E2F-like sites were essential for the NPAT and ATM transcriptions.

In the present study we found that the positive regulatory cis-acting DNA elements were involved in the regulation of the bi-directional promoter activity of the NPAT and ATM genes.

3.5.7 Analysis of the Expression Pattern of the NPAT Gene in Cell Cycle Stages Using Human Fibroblast Cells

Yasuharu Ninomiya, Masasi Sagara, Masahiro Muto, Kiyomi Kasai, Hiroko Ito, Tada-aki Hori and Takashi Imai

Keywords: NPAT, ATM, cell cycle

We identified a housekeeping gene, the NPAT gene which is located 0.5kb from the 5' end of the ATM gene. As these two genes share the same promoter, there is a possibility that the NPAT gene is also related to genome stability, cellular responses to DNA damage or cell cycle control. At first, to investigate the relationship between NPAT function and cell cycle control, we studied the mRNA expression pattern of the NPAT gene in each stage of the cell cycle in human fibroblast cells.

Our quantitative RT-PCR assay (Taqman system: Perkin-Elmer), using synchronized-cultured cells with serum starvation, indicated that a peak of the mRNA expression was at the G1/S stage. The NPAT mRNA level at the G1/S stage was approximately three times that at other stages.

We confirmed that NPAT was a substrate of cyclin E-CDK2 and suggested NPAT played a role in S-phase entry. The protein level of NPAT peaked at the G1/S stage. It was approximately 10 times the protein level of NPAT at other stages. Expression pattern of NPAT protein was similar to that of NPAT mRNA throughout the cell cycle. The amount of NPAT protein at the G1/S stage increased approximately 10 times that at other stages, while the amount of the mRNA at the G1/S stage increased approximately three times that at other stages. Therefore, the range of the increase of NPAT protein was approximately 3-fold that of NPAT mRNA. These results suggested that the expression of NPAT protein was regulated by both transcriptional and post-transcriptional steps. We concluded that NPAT gene was related to cell cycle control.

Reference:

Zhao, J., Dynlacht, B., Imai, T., Hori, T. and Harlow, E.: Genes&Development, 12, 456-461, 1998.

3.5.8 Molecular Analysis of the Germ-line Mutation Induced by Ionizing Radiation.

Masatake Yamauchi, Satsuki Tsuji, Toshiyuki Saito, Tada-aki Hori, Yoshiya Shimada, Yoko Ishii, Mayumi Nishimura, Toshiaki Ogiu, Masanori Okamoto, Tsuneya Matsumoto

Keywords: radiation, germ-line mutation, mouse, Scid, genetic instability

Germ-line mutation induced by ionizing radiation is suspected as a cause for the increased risk of developing cancers in successive generations.
However, no increased risk has been observed among children born to atomic bomb survivors exposed at Hiroshima or Nagasaki.
Our three year project aims at investigating the germ-line mutation induced by ionizing radiation using experimental mouse strains, with or without a genetic background that affects radiosensitivity. The Pc-1 locus is known as a hypervariable minisatellite, and we analyzed it to detect the germ-line mutation (genetic instability). Molecular analysis of the Pc- 1 locus in the offspring of CB17 revealed that the spontaneous mutation rate was about 5% under the ordinary breeding condition used in our institute. However, the offspring between CB17 and Scid showed higher genetic instability compared to the parental strain, CB17, suggesting the Scid mutation affects the genetic instability of the Pc-1 locus.

3.5.9 Growth Properties of Cells from xpg-deficient Mice

Tadahiro Shiomi, Naoko Shiomi, Yoshinobu Harada and Manabu Koike

Keywords: xeroderma pigmentosum, xpg mouse model, replication senescence, immortalization

We have generated a mouse model (xpg-deficient mice) for the nucleotide excision repair deficient human disorder, xeroderma pigmentosum (XP). The mice showed post-natal growth failure and had a short life span. We carried out studies to find out the cause of their post-natal growth failure and premature death. The body size of the mutant homozygotes (-/-) at birth appeared to be almost identical to those of the normal littermates, i.e. the wild type (+/+) and heterozygote (+/-) pups. However, at 5 days post partum, the mutant homozygotes were easily distinguished from the normal littermates because of their smaller body sizes. After around 13 days post partum, most mutant homozygotes became thin, were apparently emaciated and weak, and their activity was relatively low.

To characterize the growth failure further we examined growth properties of embryonic primary fibroblasts derived from xpg -deficient mice. When cultured continuously in vitro, cells from -/- embryos ceased growing by 4-5 weeks after the start of in vitro culture. On the other hand, cells from +/+ or +/- embryo kept their growth capability 3-4 weeks longer than -/- cells did, indicating that -/- cells underwent premature replication senescence. After 3-4 weeks of non-growing periods, -/- cells which had gained an immortal phenotype started to grow again. Normal (+/+ or +/-) cells were restored to their growth capability after somewhat longer latent periods (5 weeks) than for -/- cells. Furthermore, xpg-deficient cells started to accumulate p53 which is stabilized by mutation faster than +/+ or +/- cells. Accumulation of p53 is strongly associated with gaining malignant phenotypes, such as fast growing property, escape from contact inhibition, and changes in cellular morphology. These phenotypes were observed in -/- cells that accumulated p53. These results indicate that cells from xpg-deficient mice have a short replication life span and are apt to gain immortal and malignant phenotypes, suggesting that the -/- cells are genetically unstable since some genetic changes are needed to acquire these phenotypes.

3.5.10 Protein-protein Interaction and Transcriptional Activation Regions within the Ku Proteins

Manabu Koike, Yoshi-nobu Harada, Naoko Shiomi and Tadahiro Shiomi

Keywords: heterodimer, Ku70, Ku80, one-hybrid system, subcellular localization, two-hybrid system

DNA damages induced by ionizing radiation result in measurable endpoints such as cell death, mutation and cell transformation. In particular, double-strand breaks can induce the lethal effect. The DNA-dependent protein kinase (DNA-PK) complex is a nuclear serine/threanine protein kinase composed of at least three components, Ku70, Ku80, and a catalytic subunit (DNA-PKcs). Though a large body of evidence suggests that DNA-PK is involved in DNA double-strand break repair and V (D) J recombination, its physiological function is still unclear.

Ku protein is a complex of Ku70 and Ku80 subunits, and it has been suggested that Ku functions as a heterodimer to bind DNA double-strand breaks and activate DNA-dependent protein kinase. Ku is also capable of binding sequence-specific promoter elements, but it remains unclear whether Ku is involved in transcriptional regulation. To determine whether Ku contains the transcriptional activation domain, we examined N- and C-termininal deletion mutants of Ku for their ability to activate transcription in the GAL4-based one-hybrid system. We found that the N-terminus peptide fragment of Ku70 (amino acid residues 1-81) was capable of activating the transcription of the HIS3 and lacZ reporter genes in yeast cells. In addition, the N-terminal acidic domain within this region of Ku70 was evolutionally conserved, suggesting that the domain is important for the activation of transcription. No region involved in transcriptionai activation was detected in Ku80. To help define the role of Ku in transcription, we next examined the subceilular localization and determined the interacting regions of the Kus using two-hybrid system. Our results indicated that heteradimers of Ku70 and Ku80 were localized in the nuclei, and that the stretches from as 378 to 482 of Ku70 and from aa 374 to 502 of Ku80 were necessary for heterodimerization. These observations suggested that the Ku proteins play a role in transcriptional activation in nuclei in the heteradimeric form.

Publications:

1) Koike, M., Miyasaka, T., Mimori, T., and Shiomi, T.: Biochem. Biophys. Res. Commun., 252, 679-685, 1998.

3.6.1 Radiation-Induced Apoptosis Responsible for Limb Teratogenesis in Embryonic Mice

Bing Wang, Harumi Ohyama, Takeko Odaka, Masahiko Mori, Kaoru Tanaka, Eiichi Kojima, Kazuko Fujita[1], Chisa Ohhira[1], Keiko Watanabe[1], Takeshi Yamada[1], Hiroshi Mitani[2], Akihiro Shima[2] and Isamu Hayata ([1]Toho Univ.; [2]Univ. of Tokyo)

Keywords: radiation, apoptosis, teratogenesis, limb buds, mouse

Exposure to radiation in utero at the pre-implantation period induced a high incidence of prenatal death but a low incidence of abnormalities, and at the organogenesis period it induced high incidences of both abnormalities and neonatal death. Radiation-induced apoptosis has been intensively studied in organs and established cell lines, but how apoptosis functions in the radiation-induced malformation is almost unknown. Recently, it was reported that at the early period of organogenesis, radiation-induced apoptosis aborted damaged embryos, which resulted in a low incidence of congenital malformations. Although cell death is believed to be responsible for radiation-induced malformations late in organogenesis, no direct evidence has been reported so far.

Our previous results that pre-digital cells were more radiosensitive than pre-interdigital cells in limbs indicated that radiation-induced apoptotic cell death may play an important role in loss of proliferating and differentiating cells to cause digital malformations of embryonic mice. In this study, we investigated limb malformations on E19 by external gross observation and whole mount skeleton examination. Most malformations were ectrodactyly when embryos were irradiated on E11 or E11.5 with 5 Gy of x-rays. Referring to literature data that radiation-induced prenatal death through induction of apoptosis in the embryos cut the incidence of congenital malformations, the present study showed paradoxically a relationship between radiation-induced apoptosis and radiation teratogenesis: i.e. a preventive function against incidence of congenital malformations at the preimplantation period or early in organogenesis and a causative effect for malformations late in organogenesis. These results should provide clues to further understanding the mechanisms of radiation teratogenesis.

3.6.2 Frequency of p53 Mutations in the Rat Lung Carcinomas after Inhalation of $^{239}PuO_2$ Aerosols

Yoichi Oghiso and Yutaka Yamada

Keywords: p53, mutation, alpha particles, inhalation, rat, pulmonary carcinogenesis

Tumor malignancies after the initiation and promotion by chemical or radioactive compounds could be closely associated with an activation of certain protooncogenes and an inactivation of tumor suppressor genes which resulted from mutations. The mutations of p53, an important tumor-suppressor gene, are frequently detectable in human lung cancers with variable malignant phenotypes from radon-exposed uranium miners. The experimental models for radiation carcinogenesis, however, have revealed much less evidence on the relevance of p53 mutations to variable stages and phenotypic expression of tumors. We have found differential dose responses of pulmonary tumor types in lifespan studies of rats after inhalation of $^{239}PuO_2$ aerosols as shown by the appearance of benign adenomas at doses less than 1.0 Gy, adenocarcinomas at 1.5 Gy or higher, and adenosquamous and squamous carcinomas at 5.0-8.0 Gy. Such dose-dependent and differential pulmonary carcinogenesis would be based on cellular and molecular events from the mutations of tumor-related genes leading to sequential appearance and expansion of preneoplastic and malignant tumor cells.

To screen the alteration of p53 in a total of 241 epithelial types of lung tumors induced by inhalation exposures of rats to $^{239}PuO_2$, immunohistochemistry of intranuclear protein accumulation was performed with either polyclonal or monoclonal antibodies specific to mutant and wild type human p53 protein. Almost 80% of the tumors, including all adenomas, were negative, whereas about 16% were slightly positive, and only 3% were mildly or severely positive. All the positive tumors were shown to be carcinoma types, particularly adenosquamous or squamous carcinomas. For molecular analysis of p53 mutations, PCR-SSCP amplification of the rat p53 gene (exon 5-8) from the extracted DNA was applied on the sites of 82 epithelial types of tumors in deparafinized sections. Depite the differences in tumor types and intranuclear protein accumulation, the p53 mutations were detectable in 23 tumors (28%), while the remaining 59 tumors (72%) were wild types. In addition, the p53 mutations were most frequently detectable in exons 5 and 6, and occasionally in either exon 7 or 8, but no correlation between tumor types and exons distribution of mutations was noted. Molecular sequences of these p53 mutants are now being performed to elucidate the reality of mutation frequency and its significance specific to alpha particles-induced pulmonary carcinogenesis.

Publication:

Oghiso, Y., Yamada, Y., Iida, H. and Inaba, J.: J. Radiat. Res., 39, 61-72, 1998.

3.6.3 Effects of DTPA Therapy on Removal of Inhaled High-fired Plutonium in Rats

Satoshi Fukuda, Haruzo Iida, Yuji Yamada, Akira Koizumi and Nobuto Ishigure

Keywords: chelation therapy, Ca-DTPA, Zn-DTPA, high-fired plutonium oxide, rat

In chelation therapy, DTPA (diethylenetriaminepentaacetic acid) is generally considered useful in reducing the risk of cancer in patients contamined with plutonium. Although it is recommended that DTPA therapy be initiated immediately whenever an intake of plutonium into the body is suspected, regardless of the chemical form of the contaminant, the effects of DTPA chelation to plutonium oxide are often variable. Delayed chelation therapy has the effect of increasing plutonium excretion into the urine in humans, probably because insoluble plutonium forms do not begin to dissolve in a short period after inhalation. The effects of chelation therapy by combined administration of Ca-DTPA and Zn-DTPA on the removal of inhaled "high-fired" plutonium oxide initiated at different times after exposure were examined in rats. After inhalation of plutonium oxide, the rats were divided into four groups of five. Chelation therapy was initiated 1 day after the inhalation in the first group, 7 days after in the second group, and 14 days after in the third group. The fourth group was a control (no DTPA treatment). A daily dose of 150μmol/kg of Ca-DTPA was administered by peritoneal injection for the first four days and subsequently, the same dose of Zn- DTPA was given orally for 26 days. In order to examine the effects of chelation therapy, lung retention of plutonium was measured with a phoswich detector along with the amount of plutonium in excreta after Ca-DTPA injection and the plutonium contents in various organs at the end of the experiment.
The results indicate that DTPA therapy is not effective in removing
"high-fired" plutonium oxide from the body. Therefore, chelation therapy should be considered as one part of a long term treatment and the behavior of plutonium in the body should be carefully monitored.

Publication:

Fukuda, S. and Iida, H.: J. Health Physics., 32, 382-386, 1997.

4 CLINICAL RESEARCH

4.1 Clinical Study for Proton Beam Therapy

Takashi Nakano, Sinroku Morita, Shigeo Furukawa, Tatsuaki Kanai, Kouichi Shibayama, Takayoshi Ishii, Takeshi Hiraoka, Atsuko Abe,Tatsuya Ohono and Hirohiko Tsujii

Keywords: proton beam therapy, ocular melanoma

Proton beam therapy for ocular melanoma has been undertaken since 1985. The NIRS cyclotron generates 70MeV protons, which penetrate tissue to a maximum of approximately 37mm. In 1988, a new vertical beam port was installed and patients were treated while in a sitting posture. In addition, a CT image-based, computerized treatment planning system was developed for the proton beam treatment. In order to get sharp beam quality and accurate treatment setting with quite good responsibility and reproducibility, the proton beam port was specialized for ocular melanoma and rather small lesions at superficial sites of the body, and treatment systems including patient head setting, eye gazing system, and x-ray verification system have been developed. By 1996, 55 ocular melanomas had been treated with protons. In 1996, the treatment protocol was changed. The patients were treated with 5 fractions over 1.5 weeks with a total dose of 60 Gy for small tumors and 70 Gy for medium and large tumors. A new version of the treatment system was developed and utilized for the treatment planning, which substantially decreased the planning burden.

This year, the treatment planning systems was modified in order to use MRI images for treatment planning. Additionally, a titanium ring was introduced as the marker instead of a tantalum ring in order not to disturb the CT images. After these modifications, a bolus was created and used for treatment. With bolus application, dose distribution was improved and the dose distribution of the retina could be displayed. This new version of treatment substantially decreased the planning burden. By March 1998, 63 patients with ocular melanoma had been treated with protons. Of these 62 were treated with radical intent. 15 patients had small to medium tumors and 47 had large tumors. In particular, 60% of them were located contiguous to or involved in the optic disk or macula which are critical organs and relating to complications. The 5 and 10 year survival rates were 95% and 89%, respectively. Both 5 and 10 year local control rates were 88%. The 5 year cumulative retention rate of the involved eye after treatment was 70%. These results suggested that proton beam therapy for ocular melanoma is one of the better treatment modalities.

References

Nakano, T., Morita, S., Furukawa, S., Kanai, T., Miyahara, N., Shibayama, K., Hiraoka, T., Abe, A., Ohono, T., Tusii, H.: Proton beam therapy for ocular melanoma. J. JASTRO, 9, 42-45, 1998

4.2 Clinical Assessment of Tumor/Tissue Responses of Heavy Ions by Radiobiological Basis and Volume Effect for Treatment Optimization

Takashi Nakano, Atsuko Abe, Tatsuya Ohono, Atsuro Terahara, Shinitiro Sato and Suho Sakata

keywords: heavy ion therapy, treatment, cervical cancer

Heavy ion beams have advantages for controlling radiation resistant cancers due to the high LET beam character which gives them superior dose distribution and a 2 to 3 times stronger biological effect of cell killing than conventional x-rays. However, the assessment of a biological effect with incorporation of a volume effect, which is very important for estimation of the effects in inhomogeneously irradiated tissues, remains to be investigated.

Twenty-five patients with advance cervical cancers (stages 3B and 4A) were treated with carbon beam therapy. They were followed for 6 months to 3 years. Tumor volume was evaluated 3-dimensionally with T2 weighted MRI images before, during, and after treatment. Fifteen patients achieved local control and 10 had recurrence. There was no correlation between local control and tumor volume.

The local control was analyzed for total treatment time. Four patients were treated at the time of long holidays of more than 1 week which resulted in prolonged treatment. All these patients had recurrens even though their tumors were not so large. Prolonged treatment was a strong adverse factor for local control, but tumor volume was not a significant prognostic factor.

Acute response of abdominal organs of the patients with very advanced cervical cancer occurred when they were treated with carbon ion beam therapy. The degree and frequency of diarrhea and bowel movements were compared to those of conventional photon treatment.

Diarrhea developed significantly 3-4 weeks after initiation of radiation, and disappeared with medication. The incidence and degree of the diarrhea was significantly smaller in carbon beam therapy than the conventional photon therapy. Fig. 27 shows acute reaction score by RTOG according to fraction doses. Fraction doses of less than 2.8 GyE for the carbon beam showed significantly less acute response than for photons therapy. However, fraction dose of 3.0 GyE for the carbon beam showed a similar intensity for acute reaction as photon therapy. Bowel movements showed similar results to the acute reaction, mainly diarrhea.

DVH analysis of abdominal organs demonstrated that the dose sparing advantage for the small intestine area in carbon beam treatment was substantial. Therefore, the superior dose distribution may be the main reason for the weaker acute bowel reaction.

References

Tsujii, H., Morita, S., Myamoto, T., Mizoe, J., Mukai M., Nakano, T., Kato, H., Kamada, T., Ishikawa, A. and Matsuoka Y.: 1997, Preliminary results of phase I/II carbon-ion therapy at the National Institute of Radiological Sciences. J. of Brachytherapy International, 13, 1-8.

Nakano, T., Suzuki, M., Abe, A., Morita, S., Mizoe, J., Sato, S., Miyamoto, T., Kamada, T., Kato, H. and Tsujii, H.: The phase I&II clinical study of carbon ion therapy for cancer of the uterine cervix. High LET carbon beam irradiation may overcome hypoxic tumor but could not overcome tumors with faster cell cycle speed

in cervical squamous cell carcinoma.. Submission to Cancer, 1998
Terahara, A., Nakano, T., Ishikawa, A., Morita, S. and Tsujii, H.: Dose- volume histogram analysis of high dose rate intracavitary brachytherapy for uterine cervix cancer. Int. J. Radiato. Oncol Biol Phys. 35, 549-554, 1996

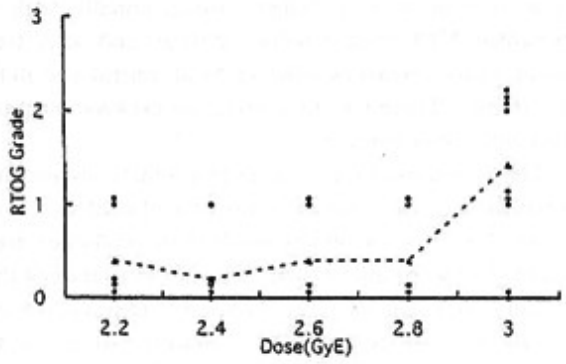

Correlation between Dose and Early Reaction

4.3 Clinico-pathological and Molecular Biological Analyses of Heavy Ion Radiation Effect

Takashi Nakano, Tatsuya Ohono, Yuzuru Niibe, Atsuko Abe, Nobuyuki Miyahara, Hideo Niibe, Kuniyuki Oka

Keywords: heavy ion therapy, cervical cancer, biological effect

Pathological and molecular biological analyses of the heavy ion radiation effect on cervical cancer were continued with larger numbers of patients. Assessment of the biological effect remains to be investigated, but the beams are considered to have a 2 to 3 times stronger biological effect of cell killing than conventional x-rays. In order to estimate biological characteristics of carbon beams, we have established a radiobiological scale which is essential for comparison of the radiobiological effects between carbon and photon treatments. To date, the following subjects have been studied.

The purpose of this study was to define biological parameters predictive of local control after carbon beam therapy for cervical cancer. Twenty- five patients who had been irradiated by carbon beams in phases I/II of study were examined. Seventeen patients had stage 3B diseases and 8 had stage 4A diseases.

After follow-up of more than 6 months, 15 patients atained local contol and 10 patients had recurrence. We investigated the following factors:

(1) reduction of the tumor size as calculated with a CT image; (2) histological response; (3) the frequency of radiation-induced apoptosis detected by the TUNEL method; (4) growth fraction by Ki-67 (expression stained immunohistochemically); (5) pMI (mitotic index of proliferating cell population); (6) tissue oxygen tension measured by pology graphy.

All parameters were statistically analyzed by multiple regression methods. Table 3 shows results of multiregression analysis for various prognostic parameters. Clinical stage was not a local control predictor. Of various parameters before treatment, pMI was a statistically significant local control predictor. Among parameters at 1 week during treatment, tissue oxygen tension was a weak predictor of local control. The prognostic power of pMI was analyzed with over all treatment time. Tumors of pMI more than 4% had a local control rate of 33%, significantly poorer than the 11/13 of pMI less than 4%. All 4 patients with over all treatment time of more than 50 days had recurrence. The present study demonstrated that pMI was the strongest prognostic parameter for local control after carbon beam therapy. These analyses demonstrated that prolongation of treatment time was risky for local control. Additionally, even when treated in a regular treatment time, for tumors having faster cell proliferation it was difficult to attaining local control. Tumor cell repopulation during carbon beam therapy is very important to take into consideration in terms of attain local control of tumors.

References

Ohno, T., Nakano, T., Niibe. Y., Tsujii. H. and Oka, K.: Bax Protein Expression Correlates with Radiation-induced Apoptosis in Radiation Therapy for Cervical Cancer. Cancer, 83, 103-110, 1998.

Oka, K., Nakano, T and Arai, T.: Expression of cathepsin D and epidermal growth factor receptor in stage III cervical carcinomas. Int J. Gynecol Cancer 1997, 7, 122-126.

Nakano, T., Oka, K., Ishikawa, A. and Morita, S.: Correlation between c- erbB-2 oncogene and cell proliferation parameters in radiation therapy for cervical cancer. Cancer 1997; 79: 513-20.

Nakano, T., Oka K., Taniguchi, Y.: Manganese superoxide dismutase expression correlates with p53 status and local recurrence of cervical carcinoma treated with radiation therapy. Cancer Res. 56, 2771-2775, 1996.

Oka, K., Nakano, T. and Hoshi, T.: Analysis of response to radiation therapy of patients with cervical adenocarcinoma compared with squamous cell carcinoma. MIB-1 and PC10 Laveling indices. Cancer 77, 2280-2285, 1996.

Nakano T., Oka, K., Ishikawa, A. and Morita, S.: Immunohistochemical prediction of radiation response and local control in radiation therapy for cervical cancer. Predict Prevent Oncol, 21, 1997.

4.4 Metabolic Mapping with PET of Glia Cell Activity in Brain

Osamu Inoue[1], Kaoru. Kobayashi[1], Rie Hosoi[1], Koichi Ando,

Yoshiya Furusawa, Juniichi Ishida[2] and Antony Gee[3]

([1]Osaka Univ.; [2]Fukuoka Univ.; [3]Arhus Univ. Hospital, Denmark)

Keywards: ammonia, brain, glia, cooperativity

The mechanism for uptakes of ^{13}N-ammonia into the brain and heart has been thought to be the metabolic trapping in tissue by converting to labeled amino acid through an enzyme reaction. The conversion rate of ammonia to glutamine (k3) has been reported to be much faster than the rates of transport of ammonia through cell membrane (k1 and k2) and it has been used as a blood flow marker. However, the brain uptake of ammonia was significantly smaller as compared with the heart uptake, although the glutamine synthetase (GS) activity in the brain was higher than that in the heart. These results indicated a diffusion boundary or other rate limitting factor might exist in the brain. As GS has been used as a marker for glia cells in the brain, ^{13}N-ammonia has a potential use as a selective radiotracer for metabolic mapping of glia cell activity. In order to understand the mechanism for brain uptake process of ammonia, an autoradiographic study using a unilateral lesioned rat brain was performed. Rats were unilaterally lesioned with ibotenic acid, and ^{13}N-ammonia or ^{3}H-SCH23390, a dopamine D1 antagonist, was intravenously injected 2 weeks after the lesion was made. Rats were decapitated after 1min for ^{13}N-ammonia uptake or after 60min for ^{3}H- SCH23390 binding, and brain slices were prepared. The slices were put on imaging plates, and autoradiograms were obtained. A significant decrease in ^{3}H-SCH23390 binding in legioned striatum was observed probably due to neural cell loss. On the other hand, a slight increase in uptake of ^{13}N-ammonia in lesioned striatum was observed. These experiments indicated that uptake of ammonia was dependent upon the number of glia cells in addition to the blood flow. By the combined use of ^{13}N-ammonia and ^{15}O-water, the metabolic rate image of ammonia to glutamine in glia cells might be obtained. We performed double tracer experiments using ^{13}N-ammonia and ^{3}H-water. The brain uptake of ^{13}N- ammonia was significantly altered by modifications of dopaminergic system, whereas no significant change in the brain uptake of ^{3}H-water was observed. These results supported our hypothesis. It is of interest that the brain uptake of ammonia (% injected dose/gram) was significantly increased by increasing injected dose, although the heart uptake was decreased. This apparent positive cooperativity of the brain uptake seemed to be related to the regulation of ammonia in brain. The brain uptake of carrier added ^{13}N-ammonia was also significantly reduced by pretreatment with benzodiazepine agonist, indicating an important role of GABAnergic system on the regulation of metabolism of ammonia in the brain.

4.5 Distributions of HL91, Deoxyglucose, and GLUT1 in Tumor

Tsunehiko Nishimura[1], Kenji Yutani[1], Takayuki Nakano[1], Mitsuaki Tatsumi[1], Osamu Inoue[2], Kyosan Yoshikawa

([1]Osaka Univ. Medical School; [2]School of Allied Health Sciences, Osaka Univ.)

Keywords: hypoxia, tumor, HL91, GLUT1

Biodistribution of HL91, a putative hypoxic tracer, after intravenous injection was studied in C3H mice bearing NFSa fibrosarcoma by determining blood and tissue levels of radioactivity from 15 min to 6 hr after injection. The uptake of [^{99m}Tc]HL91 in tumor peaked at 60 min post-injection (4.61 ± 0.33% injected dose/g tissue). The uptake of HL91 in the liver and kideny were higher than that in the tumor at all sampling points. The radioactivity in the heart, lung, muscle, and blood was lower than that in the tumor at 60 min or later. The tumor/muscle ratio peaked at 240 min (4.51, n=2) after the intravenous injection of HL91. In Walker-256 tumor which was subcutaneously transplanted in Wistar rat, a dual ex vivo autoradiographic study was performed on sections of the tumor using HL91 (74 MBq) and [^{14}C] deoxy glucose (185 kBq). Tumor tissue was histologically divided into viable cancer cell area, necrotic area, and granulation tissue. A number of focal necrotic areas were scattered in the viable cancer cell area. The focal necrotic area was composed of small necrotic foci and surrounding viable cancer cells. The viable cancer cell layers bordering the necrotic area and surrounding the small necrotic foci was defined as the hypoxic area. The viable cancer cell area other than the hypoxic area was defined as the normoxic area. The uptake of HL91 in the histologically defined hypoxic area was significantly higher than the other areas in tumor tissue ($p<0.0001$). The uptake off DG and the expression of glucose transporter type 1 (GLUT 1) in the hypoxic area were also significantly higher than those in the non oxic area ($p<0.0001$). There was a strong correlation between the uptake of HL91 and the expression of GLUT1 ($r=0.624$-0.868, mean $r=0.743$, $p<0.0001$), whereas a weak correlation was observed between the uptake of DG and the expression of GLUT1 ($r=0.328$-0.669, meanr=505, $p<0.0001$). In conclusion, these results indicate that HL91 has a great potential for detecting tumor hypoxia and that hypoxia induces GLUT1 expression.

4.6 Clinical Application of Autoactivation PET Imaging

Kyosan Yoshikawa, Takehiro Tomitani, Mitsutaka Kanazawa, Tastuaki Kanai, Katsumi Tamura, Masahisa Koga, Masakuni Kanai, Susumu Kandatsu, Hirohiko Tsujii, Tetsuya Suhara, Katsuya Yoshida, Furmio Shishido[1], and Hiroshi Fukuda[2]

([1]Fukushima Medical Univ.; [2]Tohoku Univ.)

Keywords: PET, autoactivation, C-12 ion radiotherapy

Clinical application of PET imaging of autoactivation derived from C-12 ion radiotherapy was studied. Quality of the image of autoactivation in each region from the brain to lower pelvis was checked. Images were fairly good in all regions. There was a strong RI distribution at the beam entrance area compared to deep areas from the body surface. Bone showed especially strong RI activity. We think that is because bone has very low blood flow. The RI derived from C-12 ion radiotherapy is washed out from regions with high blood flow. So, regional blood flow affects the quality of the antoactivation PET image. We got fine PET images for brain cancer, lung cancer, esophageal cancer and liver cancer. There was an RI distribution at the vertebra which is on the opposite side from the beam entrance point in the case of lung cancer. The RI was distributed in a wide area in the case of uterine cervical cancer, but no RI activity in the cervical tumor was detected due to the high regional blood flow for the uterine cervical cancer. We found that regional metabolism such as blood flow of the tumor was very important factor which affects the autoactivation PET image quality. There might be some possibility that a high RI distribution in the tumor means low metabolism of the tumor. The activity of RI derived from autoactivation might correlate with the level of damage of the tumor by C-12 ion radiotherapy.

4.7 The Cancer Functional Diagnosis and the Evaluation of Therapeutic Effects Using Magnetic Resonance Imaging and Spectroscopy

Masahisa Koga, Kyosan Yoshikawa, Takayuki Obata, Hirotoshi Kato, Susumu Kandatsu, Masanori Kanai, Junetsu Mizoe, Hirohiko Tsujii,Katsuya Yoshida, Tetsuya Suhara, Kazutoshi Suzuki and Hiroshi Yoshioka

Keywords: brain neoplasm, magnetic resonance spectroscopy, positron emission tomography, heavy ion therapy, choline

Differential diagnosis of brain necrosis and irradiation with regrowth of brain tumor is difficult with MRI and CT. We studied ^{1}H-CSI and PET (^{11}C-methionine and ^{18}F-Deoxyglucose) in 23 cases of gliomas before and after heavy ion radiotherapy. We compared each pattern of MRS signal (NAA, choline, creatinine and lactate) and PET images before and after heavy ion radiation therapy. In cases of brain necrosis, loss of choline signal was observed in most cases, but slight accumulation of methionine was seen in PET study. In cases of regrowth tumor, elevation of choline signal was significant. Choline signal elevation in brain neoplasm is thought to be associated with increased cellular proliferation.

4.8 Functional Diagnosis Using PET and Evaluation of Therapeutic Effects of Cancer

Kyosan Yoshikawa, Katsumi Tamura, Yasunori Imai, Noriyo Matsuno, Masahisa Koga, Masakuni Kanai, Susumu Kandatsu, Hirohiko Tsujii, Tetsuya Suhara, Katsuya Yoshida, Kazutoshi Suzuki, Osamu Inoue[1],Fumio Shishido[2] and Hiroshi Fukuda[3]

([1]Osaka Univ.; [2]Fukushima Medical.; [3]Tohok University)

Keywords: C-11 methionine, PET, head and neck cancer, diagnosis, therapeutic effects

The role of PET in clinical diagnosis of cancer and the evaluation of therapeutic effects were studied. The change of C-11 methionine uptake in tumor between pretreatment and post-treatment using HIMAC was compared with clinical prognosis. Fifteen patients with head and neck cancer were treated by HIMAC and then followed for more than 12 months. The maximum observation period was 24.9 months. PET findings at pretreatment and post-treatment were compared with results of clinical observation of patients. We divided our cases into three groups according to the level of methionine accumulation in the tumor at the time of the pretreatment PET study. The first group was cases showing excessive high accumulation, the second group was cases showing high accumulation, and the third group was cases showing moderate or less accumulation. All patients in the first group died of metastasis. One case whose methionine accumulation at post-treatment did not decrease so much was found as disease progressed. The other cases were well controlled in the tumor lesion and showed high reduction rates in accumulation of methionine at post-treatment. Cases in the second group were well controlled in the tumor lesion, but had one case whose methionine accumulation of tumor did not decrease at post-treatment. In the third group showing moderate or low accumulation at pretreatment, no specific tendency between methionine accumulation and clinical prognosis was seen. We think that the level of accumulation in the tumor at pretreatment might correlate to the risk of metastasis and the reduction rate might correlate to local control level.

If methionine does not accumulate at high levels in the tumor at pretreatment, methionine PET might not be a good indicator of patient prognosis, and we should use other indexes to evaluate patients prognosis after treatment in such cases.

4.9 Quantitative Measurement of Acetylcholinesterase Activity in Living Human Brain Using a Radioactive Acetylcholine Analog and Dynamic PET

Kiyoshi Fukushi, Shin-ichiro Nagatsuka, A05A Hiroki Namba, Masaomi Iyo, Hitoshi Shinotoh, Tetsuya Suhara, Yasuhiko Sudo,Kazutoshi Suzuki and Toshiaki Irie

Acetylcholinesterase (AChE) activity in living brains has been measured using radiolabeled N-methylpiperidyl esters in rodents and primates in our earlier studies. In the present study, the hydrolysis rate constant of[^{11}C]methyl-4-piperidyl acetate (MP4A) by AChE (k3) was quantitatively estimated in the human brain using a three-compartment model analysis of plasma[^{11}C]MP4A and time-radioactivity curves of the brain tissues obtained from dynamic PET.

Twelve healthy subjects (24-80 years old) participated in the study. Serial PET scans and timed arterial blood sampling were performed for 40 min following the 60s intravenous injection of[^{11}C]MP4A. Plasma radioA059activity of[^{11}C]MP4A and its metabolite was determined to obtain the input function. Intravascular radioA059activity was corrected using a fixed value of blood volume fraction, 4%. A three-compartment model and a non-linear least squares analysis were employed to yield estimates of K1 (transport from blood to brain), k2 (transport back to blood), and k3 (hydrolysis by AChE) from the time-radioactivity curves generated from the dynamic PET data. The exchange of the radioactive metabolite between blood and brain compartments was assumed not to occur based on previous results.

The mean k3 values were 0.077±0.009 min^{-1} (±sd) in the frontal, 0.084±0.010 min^{-1} in the temporal, 0.071±0.011 min^{-1} in the parietal, 0.065±0.010 min^{-1} in the occipital cortices; 0.321±0.093 min^{-1} in the thalamus; and 1.022±0.289 min^{-1} in the cerebellum. The ratios of k3 for the cerebral cortex: thalamus: cerebellum were 1: 4: 11, corresponding well with the AChE activity ratios in the postmortem brain (1: 3: 8).

Relative sample sd values of k3 were 13% in the cerebral cortex, 29% in the thalamus and 28% in the cerebellum. The reliability of estimated k3 decreased in regions with higher AChE activity, where tracer uptake was more flow-dependent rather than reflecting metabolic activity.

The present study indicates applicability of PET using[^{11}C]MP4A for in vivo detection of regional brain AChE activity. Cerebral cortical AChE activity can be reliably evaluated and distribution of k3 values in the normal human brain agreed with reported postmortem AchE distribution. The method will be useful in evaluating cortical AChE activity, which has been shown to decrease in patients with Alzheimer's disease.

Publications:

1) Irie, T. et al.: Nucl. Med. Biol., 21, 801-808, 1994.

2) Namba, H., Irie, T.,Fukushi, K. and Iyo, M.: Brain Res., 667, 278- 282,1994.

3) Irie, T., et al.: J. Nucl. Med., 37, 649-655, 1996.

4) Iyo, M., et al.: Lancet, 349, 1805-1809, 1997.

4.10 The Lung as Reservoir for Antidepressants in Pharmacokinetic Drug Interactions

Tetsuya Suhara, Yasuhiko Sudo, Katsuya Yoshida, Yoshiro Okubo, Hiroshi Fukuda, Takayuki Obata, Kazutoshi Suzuki, Kyosan

Yoshikawa, Yasuhito Sasaki

Keywords:[^{3}H]imipramine, Lung, antidepressants

Although high affinity[^{3}H]imipramine binding sites have been reported in both rat and human lungs, the role of the lung in the pharmacokinetics of antidepressants has not received much attention. It seems that the lung plays an important role in drug interaction between tricyclic antidepressants and selective serotonin reuptake inhibitors (SSRIs), since significant accumulation of SSRIs in the lung has been reported.

Carbon-11 labelled imipramine derivative cyanoimipramine was used to measure, uptake in the lung and brain of normal volunteers by positron emission tomography. Clomipramine was administered to measure the effect of antidepressants with high affinity to serotonin transporter on lung and brain uptake. A large proportion of the injected[11C]cyanoimipramine (68-86%) was extracted by the lung.

Clomipramine decreased the lung uptake, whereas whole brain uptake and plasma radioactivity were significantly increased. The lung may function as a reservoir for antidepressants with high affinity to serotonin transporter. The accumulated antidepressants might be displaced by other antidepressants, and this may produce signifincant elevation in plasma concentration and thus induce toxicological effects.

Publication:

Suhara, T., et al.: Lancet, 351, 332-335, 1998

5 ENVIRONMENTAL SCIENCE

5.1 Correlation between Indoor Radon Concentration and Dose Rate in Air from Terrestrial Gamma Radiation in Japan

Kenzo Fujimoto

Keywords: surveys, radon, gamma radiation, screening measurement

A nationwide indoor radon survey was performed in Japan at more than 7,000 houses using passive radon detectors and annual average radon concentrations were obtained at 5,717 houses. The annual concentration varied from 2 Bq m^{-3} to 313 Bq m^{-3} with median, arithmetic mean and standard deviation of 16.0, 20.8 and 18.8 Bq m^{-3}, respectively. Our group also conducted a nationwide external exposure survey at 1,115 sites throughout Japan. The mean and its standard deviation of exposure rate was 79治酌 18nGy h^{-1} (9.0治酌2.1示捨R h^{-1}).

Minimum and maximum city average exposure rates were 34nGy h^{-1} (3.9 示 捨 R h^{-1}) and 148nGy h^{-1} (16.9 示 捨 R h^{-1}). It is believed that the indoor radon concentration has a coarse correlation with the dose rate in air from terrestrial gamma radiation at the area. Therefore, a correlation between the indoor radon concentration and dose rate in air from terrestrial gamma radiation was studied using the results of nationwide indoor radon and external exposure surveys, although the surveys were not conducted at the same time nor at the same location. The radon concentration showed a log-normal-like distribution, whereas the terrestrial gamma radiation dose rate in air had a normal-like distribution. A log-linear scatter plot for each pair of the indoor radon concentration and gamma-ray dose rate in air in each city revealed a clearer relationship than the linear-linear scatter plot (Fig.28). The correlation explained only a small part of the variation observed between the two variables. However, the average, maximum and minimum as well as regression line of radon concentration were found to increase with the gamma-ray dose rate in air. The group in a higher quantile of the radon concentration showed larger dependence on the gamma-ray dose rate. The rate of increase of radon concentration with the gamma-ray dose rate in air depended on the house structure.

Prefabricated and steel frame houses showed the lowest indoor radon concentration for all air dose ranges. Wooden houses had a larger rate of increase than concrete houses, and the regression lines crossed at high air dose rate. Based on the present findings a criterion for air dose rate level could be established and used for an effective survey to identify houses which might require remedial action, while taking into account such items as geological character of the house site, year of construction, etc. The criterion of air dose rate level might be more effective if it is set for each house structure since the rate of increase of radon concentration depends on this.

Publication:

Fujimoto, K.: Health Phys., 75, 1-7, 1998.

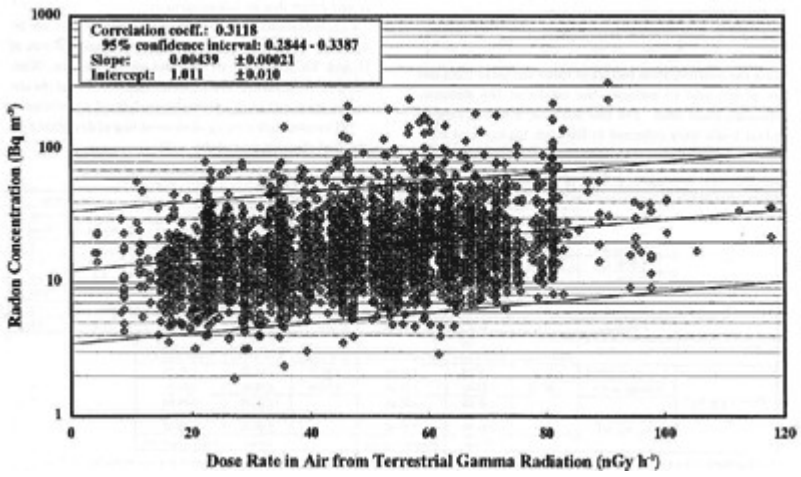

Fig. 28: Scatter plot in log-linear scale for each pair of indoor radon concentration and gamma-ray dose rate in air.

5.2 Determination of U and Th Concentrations in Soil and Plants, and the Transfer to Humans in a High Background Radiation Area of China

Masae Yukawa, Yoshito Watanabe, Yoshikazu Nishimura, Atsuko Shinohara[1], Guo Yicao[2], Zha Yongru[2], Lu Huimin[3], Zhang Wei[3], Wei Luxin[3] and Tao Zufan[3]

([1]Jyutendo Univ. School of Medicine; [2]Guangdong Institute of Radiation Hygiene and Protection, China; [3]Laboratory of Industrial Hygiene, Beijing)

Keywords: U, Th, natural radiation, intake, transfer, soil, plants

In a high natural radiation area in China, an epidemiological study on the effect of the radiation to human health has been carried out for more than 10 years. This high natural radiation is mainly due to ^{238}U and ^{232}Th, and their decay products being present in the soil in higher contents compared to the other areas. The contribution of internal radiation from radionuclides taken into the human body has not been sufficiently evaluated. We tried to determine U and Th in soil and plants to obtain the concentration factors of these elements from soil to plants and to estimate the intake of the elements through plant food. For this purpose, soil and various plant foods were collected in the high background radiation area (HBRA) and a control area (CA) in Guangdong Province, China, in 1997 and 1998.Three hamlets from HBRA and one hamlet from CA were selected, with three families from each hamlet being chosen. We sampled soil from a paddy field and a dry field for each family. The major crop, rice, and the second one, sweet potato, were obtained from each family's field. Other potatoes, leafy vegetables, fruit vegetables and stored beans were also collected.U and Th in soil samples were determined using two analytical methods, γ counting and Inductively Coupled Plasma Mass Spectrometry (ICP-MS) to examine the feasibility of ICP-MS to the analysis of U and Th in environmental samples. In the plant samples, these elements could be determined by only ICP-MS, since the concentrations of the elements are too low to determine them γ counting without any chemical treatment.The concentrations of U and Th in soil determined by γ counting and ICP-MS agreed well with each other generally, and the results of ICP-MS on the standard reference soil coincided well with the certified values.However, the results by ICP-MS on the actual soil collected in HBRA and CA showed larger variations than γ counting when the analyses were repeated several times with different portions of one sample. This was thought to be due to inhomogeneity of the soil sample. ICP-MS method is so sensitive that a very small amount, about 20mg, is enough to detect those elements. As 30-50g of the soil are used in the case of γ counting, the results have hardly any effect due to inhomogeneity.Concentrations of U and Th in soil and plants are indicated in Table 4. We calculated the transfer factors of U and Th from soil to rice and water spinach (Kunshingzai in Chinese). The concentration factors of the elements from soil to the plants were defined as follows:

Transfer factor=(μg of element in g of dry plant)/(μg of element in g of dry soil).

The results are also shown in Table 4 with the literature values. Though the obtained concentration factors for rice and water spinach from each family varied widely, the factors in HBRA were about 10 times higher than those in CA. No specific difference between rice and water spinach was observed in this study.

Table 4. Th and U concentrations in soil and the transfer factors from soil tp plants.

Concentrations(μg/g-dry)		High background radiation area						Control area	
		Madi hamlet		Liuzuitang hamelt		Yangdiang hamelt		Hengpizai hamelt	
		Paddy filed	Field	Paddy filed	Field	Paddy filed	Field	Paddy filed	Field
Th	Family-1	59.6	42.8	46.5	48.7	51.0	46.2	1.1	1.1
	Family-2	59.2	60.3	58.6	59.8	48.4		2.8	7.7
	Family-3	66.7	66.4	73.3	54.5	40.5	33.1	5.2	4.6
U	Family-1	9.1	6.1	24.3	17.6	21.0	23.7	0.71	0.69
	Family-2	8.9	18.2	18.9	23.2	19.2		0.65	1.2
	Family-3	7.5	11.2	17.6	20.5	24.6	15.3	2.2	0.8

Transfer factors from soil to plant		Th			U		
		Rice Grain	Rice leaves	Water spinach	Rice Grain	Rice leaves	Water spinach
Plant(μg/g-dry) / Soil(μg/g-dry)	Average in HBRA	1.5E-05	2.1E-03	1.5E-04	2.2E-05	1.5E-03	5.3E-03
	Average in CA	1.8E-03	1.7E-02	2.6E-03	1.1E-04	1.9E-02	2.8E-03
	Literature values *1, *2, *3	1.5E-04	1.1E-03 ~ 1.1E-01	4.5E-05 ~ 7.2E-02	1.9E-04	2.3E-03 ~ 2.3E-01	5.0E-04 ~ 9.0E-03
			Grass	Mixed Green Veg.		Grass	Leafy Vegetable

*1: Handbook of Parameter Values for the Prediction of Radionuclide Tranfer in Template Environments, IAEA Technical Reports Series No.364 (1994).
*2: Radioactive Waste Management Center, Japan: Transfer Factors of Radionuclides from Soils to Agricultural Products, Environmental Parameter Series 1 (1998).
*3: Misako Komamura and Akiko Tsumura: The Transfer Factors of Long-lived Radionuclides from Soil to Polished Rice Measured by ICP-MS, Radioisotopes, 48, p.1-8 (1999).

5.3 Daily Intakes of ^{134}Cs, ^{137}Cs, ^{40}K, ^{232}Th, and ^{238}U in Ukrainian Adult Males

Kunio Shiraishi, Keiko Tagami, Tadaaki Ban-nai, Masayoshi Yamamoto[1], Yasuyuki Muramatsu, Ivan P. Los[2], Galina V. Phedosenko[2], Vitary. N. Korzun[2], Nikolay Y. Tsigankov[2], and Ilya I. Segeda[2]

([1]Kanazawa Univ., [2]Ukrainian Scientific Centre of Radiation Medicine)

Keywords: radionuclide, dietary intake, Th, U, Cs, K, Chernobyl, Global contamination by radionuclides was likely caused by the

Chernobyl accident in April 1986. Contamination in the environment has
been studied during the more than ten years since the accident. Now, information on dietary nuclide intakes for a background level in a typical Ukrainian has become important.

In this report, diet samples were collected to establish reference values of daily intakes of ^{232}Th, ^{238}U, and ^{40}K by using duplicate portion studies. Dietary intakes of man-made radionuclides (^{134}Cs and ^{137}Cs) for Ukrainian males were also estimated as related to the Chernobyl accident. Twenty-three total diet samples were collected from the Kiev, Rovno, and Volynsky regions between September and October 1994.

Each sample consisted of the total daily whole meal collected for an adult male. The samples were dried and dry-ashed at <450℃. Analyses of ^{134}Cs, ^{137}Cs and ^{40}K were done with a Ge-detector coupled to a multichannel analyzer. Thorium-232 and ^{238}U were determined by inductively coupled plasma mass spectrometry (ICP-MS). The analytical procedure employed has been described in detail elsewhere.

Estimated daily intakes of the nuclides studied are shown in Table 5. The total geometric mean and its standard deviation (S.D.) of dietary ^{137}Cs intake were found to be 4.05 and 4.97 Bq d^{-1} per person (/d/p) from 23 whole diet samples. Intake covered a wide range from 0.53 and 315
Bq/d/p. The daily intake for Ukrainian adult males, 4.05 Bq/d/p was equal to or slightly higher than that of neighboring countries. Daily intakes of the Rovno and Volynsky regions were compared with those of the Kiev region. There was a statistically significant difference in ^{137}Cs intake ($p<0.01$) in a non-parametric test
(Mann-Whitney test): the Rovno and Volynsky regions were more highly contaminated than the Kiev region. For ^{134}Cs, daily intake ranged between<0.1 (non-detectable; N.D.) and 10.3 Bq/d/p. Except for one sample (10.3 Bq/d/p) collected from Ljubeshiv, almost all other samples were approximately below 1 Bq/d/p.

The geometric mean and S.D. of dietary ^{40}K intake for Ukrainian males were 85.1 and 1.58 Bq/d/p. The range was 25.4 to 169 Bq/d/p. The intake level of ^{40}K for Ukrainian males was equivalent to that of a West European.

The geometric mean and S.D. of dietary ^{232}Th intake were found to be 1.98 and 2.42 Bq/d/p from 23 whole diet samples. The range of 0.37-10.5 mBq/d/p was relatively large. The intake values of ^{232}Th are limited, but this Ukrainian dietary intake, 2.0 mBq/d/p was relatively lower than that of other countries, global mean 5.5 mBq/p/d (UNSCEAR 1988). For ^{238}U, the geometric mean and S.D. were 7.52 and 2.13 mBq/d/p. It was in the range of 1.74 and 34.6 mBq/d/p. The highest value (34.6 mBq/d/p) was found in Kamin-Kashirsky, the Volynsky region. The daily intake of U for a Ukrainian was not higher than average global intake values except for four high values (18.7, 19.0, 21.0, and 34.6 mBq/d/p). Uranium isotopes may possibly result from the Chernobyl accident although they are natural radionuclides. Therefore, ratios of U in the four diet samples were analyzed by ICP-MS. The mean ratios of $^{234}U/^{238}U$ and $^{235}U/^{238}U$ in the four diet samples were found to be $6.2 \times 10^{-5} \pm 2.3 \times 10^{-5}$ and 0.00728 ± 0.00006, respectively. The ratio of $^{235}U/^{238}U$ was very similar to the natural abundance (0.00720). The ratio of $^{234}U/^{238}U$ was also in the range observed for natural U. The high dietary intakes were thus probably due to the presence of naturally occurring radionuclides, and not due to effects from the Chernobyl accident. The mean daily intake, 7.5 mBq/d/p for Ukrainian males was almost equal to or lower than intakes in other countries, 7-33 mBq and global mean 16 mBq/d/p (UNSCEAR 1988).

The annual effective doses of ^{137}Cs, ^{134}Cs, ^{232}Th, and ^{238}U through ingestion were estimated to be 0.019, 2.0×10^{-3}, 1.6×10^{-4}, and 1.2×10^{-4} mSv y^{-1}, respectively.

Publication:

Shiraishi, K., Tagami, K., Ban-nai, T., Yamamoto, M., Muramatsu, Y., Los, P., Phedosenko, G. V., Korzun, V. N. Tsigankov, N. Y., and Segeda, I. I.: Health Phys. 73, 814-819,1997.

Table 5 Daily intakes of ^{134}Cs, ^{137}Cs, ^{40}K, ^{232}Th, and ^{238}U for Ukrainian adult males.

Kiev	Kiev	Sep 1994	0.53 ± 0.04[a]	<0.1	54.6 ± 1.0[b]	0.50 ± 0.08[b]	7.36 ± 0.06[b]
Kiev	Kiev	Sep 1994	1.09 ± 0.04	<0.1	40.5 ± 0.9	0.48 ± 0.03	3.92 ± 0.07
Kiev	Kiev	Sep 1994	10.1 ± 0.10	0.35 ± 0.04[a]	64.0 ± 1.1	0.66 ± 0.02	10.7 ± 0.1
Kiev	Kiev	Sep 1994	2.78 ± 0.06	0.16 ± 0.04	74.8 ± 1.3	3.10 ± 0.27	19.0 ± 0.1
Kiev	Kiev	Sep 1994	0.98 ± 0.05	<0.1	123 ± 1.6	1.59 ± 0.27	6.83 ± 0.20
Kiev	Kiev	Sep 1994	0.53 ± 0.04	<0.1	83.6 ± 1.3	2.36 ± 0.30	8.15 ± 0.03
Kiev	Kiev	Sep 1994	0.73 ± 0.05	<0.2	158 ± 2	1.85 ± 0.15	7.18 ± 0.11
Kiev	Kiev	Sep 1994	2.58 ± 0.05	<0.1	92.8 ± 1.5	10.5 ± 1.15	21.0 ± 1.9
Kiev	Kiev	Sep 1994	5.76 ± 0.08	0.14 ± 0.05	79.3 ± 1.4	6.83 ± 0.16	12.5 ± 0.1
Kiev	Kiev	Sep 1994	15.6 ± 0.13	0.49 ± 0.06	70.2 ± 1.5	2.55 ± 0.26	18.7 ± 1.8
Kiev	Kiev	Sep 1994	1.28 ± 0.06	<0.2	105 ± 2	8.06 ± 0.09	9.96 ± 0.18
Kiev	Kiev	Sep 1994	1.50 ± 0.08	<0.2	134 ± 2	1.24 ± 0.14	1.74 ± 0.08
Kiev	Kiev	Sep 1994	0.64 ± 0.04	<0.1	81.9 ± 1.4	2.51 ± 0.54	8.44 ± 0.15
Mean of Kiev region[c]			1.77 (3.06)	<0.2	83.2 (1.44)	2.10 (2.71)	8.73 (1.97)
Rovno	St. Selo	Sep 1994	9.62 ± 0.13	0.34 ± 0.06	55.8 ± 1.4	3.41 ± 0.63	3.13 ± 0.56
Volynsky	Ljubeshiv	Oct 1994	1.75 ± 0.05	<0.1	97.3 ± 1.2	1.17 ± 0.19	4.14 ± 0.23
Volynsky	Kamin-Kashirsky	Oct 1994	10.3 ± 0.14	0.25 ± 0.08	161 ± 2	2.67 ± 0.33	34.6 ± 1.5
Volynsky	Ljubeshiv	Oct 1994	37.4 ± 0.35	1.23 ± 0.09	67.6 ± 2.0	1.34 ± 0.01	11.2 ± 0.3
Volynsky	Kamin-Kashirsky	Oct 1994	8.65 ± 0.09	0.23 ± 0.04	63.6 ± 1.1	2.28 ± 0.19	5.28 ± 0.52
Volynsky	Kamin-Kashirsky	Oct 1994	1.43 ± 0.05	<0.1	122 ± 2	5.90 ± 0.38	14.6 ± 0.9
Volynsky	Manevychi	Oct 1994	7.82 ± 0.09	0.23 ± 0.04	103 ± 1	1.35 ± 0.18	7.78 ± 0.24
Volynsky	Ljubeshiv	Oct 1994	315 ± 0.87	10.3 ± 0.2	169 ± 3	1.72 ± 0.10	2.35 ± 0.05
Volynsky	Ljubeshiv	Oct 1994	28.7 ± 0.45	1.15 ± 0.16	25.4 ± 2.7	0.37 ± 0.05	2.94 ± 0.37
Volynsky	Ljubeshiv	Oct 1994	9.10 ± 0.08	0.26 ± 0.05	95.9 ± 1.4	2.65 ± 0.43	4.04 ± 0.27
Mean of Rovno & Volynsky resions[c]			11.7 (4.67)	<0.4	85.1 (1.74)	1.84 (2.11)	6.19 (2.32)
Total mean[c]			4.05 (4.97)	<0.3	85.1 (1.58)	1.98 (2.42)	7.52 (2.13)

[a]Counting errors, 1 sigma.
[b]Mean ± 1 s.d. of triplicate determinations.
[c]Geometric mean and geometric standard deviation in parentheses.

5.4 Precise Determination of Lithium Isotopic Composition by Thermal Ionization Mass Spectrometry in Natural Samples such as Seawater

Sarata Kumar Sahoo and Akimasa Masuda* (*Univ. of Electra-Communications, Chofu)

Keywords: lithium, isotope ratios, seawater, thermal ionization mass spectrometry

Precise determination of isotopic composition of lithium is of great interest in various fields of science and technology, such as geochemistry, astrophysics, nuclear power industry and biomedicine. Lithium is comprised of two stable isotopes, ^{6}Li and ^{7}Li. An important caveat is generally omitted in compilation that variations of the concentration of ^{6}Li have been observed in minerals from a low of 6.77% to a high of 9.28%. For example, in the nuclear power industry, ^{6}Li is used as a tritium breeder in fusion reactor blankets because of its high cross section for the n, α reaction if its natural abundance only∼7.5%, enrichment would be desirable for tritium generation. In a single crystal like lithium niobate, used in electro-optic devices, the isotopic composition of Li has an effect on the radiation resistance, this is another example where precise determination is desired.

In general thermal ionization mass spectrometry (TIMS) is a method of choice for the determination of isotopic composition of Li because of its high analytical accuracy. However, isotopic fractionation is one among many possible parameters that restricts the accuracy of the isotopic analysis of Li by TIMS. In addition, such a mass fractionation cannot be eliminated by the internally-derived correction as lithium has only two stable isotopes. In order to minimize isotopic fractionation, we have developed a new technique which uses lithium phosphate as the loading material and employs a triple filament. The method produces a stable, high intensity Li^{+} ion beam that allows measurement of nanogram quantities of lithium for several hours (Fig-29). Lithium was separated from the sample matrix and further converted to LiOH for the synthesis of Li3PO4 by employing a two-column ion exchange process. The mass ratio of LiOH to phosphoric acid was nearly stoichiometric in relation to Li3PO4. Lithium isotopes ratio in a reference material supplied by NIST L-SVEC Li2CO3 was measured to check the reproducibility of the method for comparison with other researchers (Table 6). A comparison was made between two TIMS units equipped with different types of detectors, such as a Faraday cup and a secondary electron multiplier. The difference in results of isotope ratios is about 0.35% in spite of the different geometry of the detectors and of the different physical effects for measurements. The isotope ratios of lithium ($^{6}Li^{+}/^{7}Li^{+}$) in a SRM924 Li2COLi3PO3 and in seawater yielded an average value of 0.049277±0.00002 and 0.080231±0.0002, respectively whereas the ($^{7}Li^{+}/^{6}Li^{+}$) ratio for an isotopically enriched 6Li2CO3 supplied by ORNL yielded 0.047396±0.00018. The uncertainty values are expressed as two standard deviations of the mean. The high precision and sensitivity of measuring Li isotopes offers significant improvement for measuring isotopically enriched commercial products. The Li isotopic analysis method can be used successfully to measure Li concentrations in ocean water by isotope dilution.

Publication:

Saboo, S.K. and Masuda, A.: Anal. Chim. Acta, 370, 215-220, 1998.

Table 6 Comparison of lithium isotopic composition of NIST L-SVEC standard.

Researche (Year)	Measured Ion	Loadedas (Chemical form)	$^6Li/^7Li$ ratio
Flesch et al.(1973)	Li^+	LiI	0.0832 ± 0.0002
Chan (1987)	$Li_2BO_2^+$)	$Li_2B_4O_7$	0.082 ± 0.0001
Green et al.(1988)	Li_2F^+	LiF	0.08201 ± 0.0001
Xiao & Beary (1989)	Li^+	$Li_2B_4O_7$	0.082212 ± 0.00002
Sahoo & Masuda (1996)	$Li_2BO_2^+$	$Li_2B_4O_7$	0.082289 ± 0.00004
Moriguti & Makamura (1998)	Li^+	Li_3PO_4	0.082543 ± 0.0002
Qi et al.(1997)	Li^+	$Li+H_3BO_3$	0.08215 ± 0.0002
This study	Li^+	Li_3PO_4	0.082606 ± 0.00009

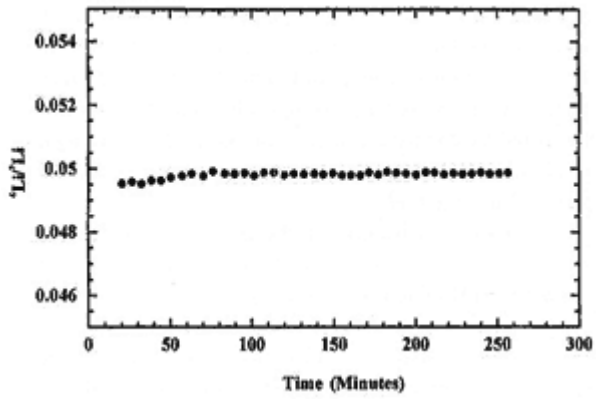

Fig. 29. Variation of $^6Li/^7Li$ ratio with time.

5.5 Effect of Acidification on the Population of Aquatic Microcosm

Kiriko Tanaka-Miyamoto, Hiroshi Takeda, Shoichi Fuma, Kei Yanagisawa, Yoshikazu Inoue, Naoe Sato, Mayumi Hirano and Zen-ichiro Kawabata* (*Ehime University)

Keywords: acidification effect, aquatic microcosm, ecological assessment, Escherichia coli, Euglena gracilis, model ecosystem, Tetrahymena thermophila

It is necessary to establish a reasonable method to evaluate the ecological effect of acidification, if human beings intend to have a sustainable development. In this study an aquatic microcosm was adopted as a model ecosystem for ecological assessment of acidification effect. This microcosm is one of the simplest biological communities, which can demonstrate an indirect effect on species caused by an ecological stress. The aquatic microcosm consists of three species of microorganisms in a small container like a test tube or a small plastic bottle. This system was set forth by Kawabata et al. [J. Protozool. Res., 5, 23-26, 1995], and the interaction among the three species has been well investigated. It consists of flagellate algae Euglena gracilis Z as a producer which has chloroplast for photosynthesis, ciliated protozoa Tetrahymena thermophila B as a consumer which grazes bacteria, and bacteria Escherichia coli DH5α as a decomposer which decomposes metabolites and dead bodies of the other two species. The three species can survive by exchanging materials with each other in the closed container with limited nutrients when the microcosm is first started and their population densities can be kept in a steady-state for a long time, usually for more than a year.

Last year the authors reported the acidification effect on the population of the aquatic microcosm in the growth stage just after inoculation. It was found that the population of E. coli and pH in an acidified microcosm increased to the same order as the control on the tenth day after inoculation. This is because Eu. gracilis elevated the pH of the microcosm medium by the process of photosynthesis. In the present paper, the acidification effects on the population of the aquatic microcosm in the late and the early steady-state were investigated and compared with those in the growth stage.

An experiment was carried out as follows: Each microorganism was preincubated following the method of Kawabata et al. Then the three species were inoculated into a culture medium (0.05 % proteose peptone in a half strength of modified Taub and Dollar's solution) in plastic bottles and incubated under 2500 lx and 12-12 hr. LD light regime at 25 ℃. The culture medium was acidified to pH 4.0 on the 67 th day or 128 th day after inoculation by adding a volume of equivalently mixed solution of nitric acid and sulfuric acid; the control medium was originally pH 7.0 - 8.0. Population densities of each organism were determined at various time intervals after acidification. The population density of T. thermophila was counted microscopically, that of E. coli was measured by counting colonies formed in the broth- agar medium, and that of Eu. gracilis was measured by the plate culture method.

Fig. 30 shows variation of the population density of three species in the microcosm. When the microcosm was acidified to pH 4.0 in the late steady-state (128 th day), the population density of E. coli decreased quickly, while that of T. thermophila decreased following the change of the E. coli population density; then both species disappeared. This is because T. thermophila relies on E. coli as food. When the microcosm

was acidified to pH 4.0 in the early steady-state (67 th day), population density of E. coli temporarily decreased to 10^4 cellsml order and soon started to increase, while that of the control kept 10^5 cells/ml order. The change of population density of T. thermophila followed that of E. coli with a four-day lag. It was also found that the pH of acidified microcosm recovered to the same order as the control, because Eu. gracilis elevated the pH of the microcosm medium by the process of photosynthesis.

The present study showed that acidification did not always affect the microcosm system itself. Although some species were directly or indirectly affected, other species acted as remediators. This self- remedying ability of the ecosystem depends on the time length after inoculation.

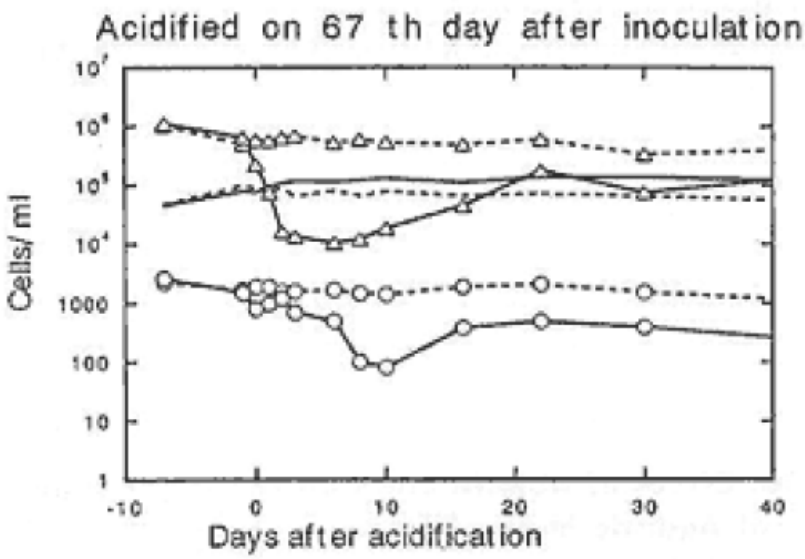

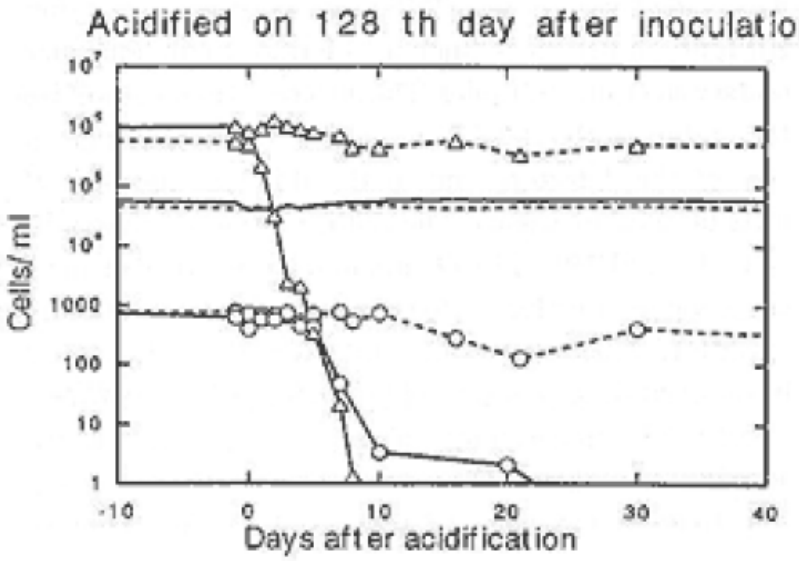

5.6 Specific Accumulation of Iodine by the Operculum of the Strawberry Conch Strombus luhuanus

Toshiaki Ishii, Motokazu Nakahara, Ryouichi Nakamura, Taeko Miyazaki and Teruhisa Watabe

Keywords: iodine, accumulators, indicator, neutron activation analysis

Accumulators having a special ability to concentrate a specific element at a high level have been discovered in the animal kingdom. They are regarded as very effective indicator organisms for monitoring marine pollution by heavy metals and radionuclides. Since little data on the concentrations of iodine in marine gastropods were reported, a screening study for finding iodine accumulators was focused on gastropods.

Thirty species of gastropods belonging to Strombidae, Trochidae, Potamididae, Muricidae, Conidae and Turbinidae were collected from August 1994 to September 1995 in the shallow water off the coast of Japan. They were dissected into several organs such as the operculum, foot, gills and intestine.

Determinations of iodine in specimens were carried out by neutron activation analysis. Specimens and a standard were irradiated with thermal neutrons (5.5×10^{13} n・cm^{-2}・s^{-1}) in the JRR-3M at the Japan Atomic Energy Research Institute. The Leco model 932 CHNS analyzer was used to measure the concentrations of C, H, N, O, and S in the operculum of Strombus luhuanus. Point (beam size=10μm) analyses by JEOL JXA-8900R electron probe X-ray microanalyzer (EPMA) were carried out for ten targets in the operculum of S . luhuanus to obtain the average concentrations of Br, Ca, and Cl.

The BIO-RAD Digilab FTS-60A/896 Fourier transform infrared (FT-IR) spectrometer was used to identify the major component in the operculum of four species of conch.

The concentrations of iodine in various organs of thirty species, except the operculum of the conch, ranged from 0. 20 to 35.3μg/g on a dry weight basis. In contrast, the operculum of the conch had very high concentrations of iodine, as shown in Table 7. In particular, S. luhuanus showed the highest concentration (mean±SD=22,800±5,200μg/g dry wt, n=10) of iodine among four species of Strombidae. The specific accumulation of iodine was thought to be common and limited to Strombidae since gastropods belonging to other families showed low concentrations (22-980μg/g dry wt) of iodine in their operculum.

Quantitative analyses by neutron activation analysis or with the CHNS analyzer and EPMA revealed that the major elements in the operculum of S . luhuanus were : Br (1.7%), C (47.7%), Ca (0.30%), Cl (1.5%), H (6.2%), I (2.3%), N (15.6%), O (16.0%), and S (0.30%). The large percentages (85.5%) of C, H, N, and O indicated that the operculum was made of organic materials. The operculum of the conch was mainly composed of protein since three characteristic absorption bands (amide I band at 1638 cm-1, amide II band at 1517 cm^{-1}, and amide III band at 1236 cm^{-1}) indicating the presence of protein were observed by FT- IR. In fact, most of the operculum of S. luhuanus could be digested (experimental conditions; 37℃, 72 hr) by a continuous treatment of an acid protease from Aspergillus niger, an alkaline protease from Bacillus subtilis and carboxylpeptidase from a bovine pancreas.

Secondly, the VG Plasma Quad PQ-2 inductively coupled plasma mass spectrometer was used to select only the iodine-containing fraction from many peaks which were obtained by the application of HPLC, equipped with a silica- ODS column, to the protease-digested solution. Eleven kinds of amino acids were present in the iodine-containing fraction. In contrast, no aminosugar, saccharides and lipids were detected in it. LC-MS revealed that iodine was not bonded to valine, although only valine existed as a free amino acid. It was also found from X-ray absorption fine structure analysis by synchrotron radiation that iodine atoms were covalently bonded to carbon atoms and iodine did not exist as I2, I^- and $IO3^-$. From these results, it was concluded that iodine atoms were covalently bonded to carbon atoms of certain amino acids in the operculum of S. luhuanus.

Table 7. Concentrations (μg/g dry wt) of iodine in the operculum of four species of the family Strombidae

Species	Concentration	Composition	No.of samples
Strombus luhuanus	22,800 ± 5,200	Protein	10
Lambis truncata	5,760 ± 1,580	Protein	5
Lambis lambis	3,680 ± 1,200	Protein	5
Harpargo harpargo	3,630 ± 1,000	Protein	5

6 APPENDIX

6.1 PUBLICATIONS

> Annual Report 2002-2003

The list includes publications by the staff members issued during the period from April 1, 1997 to March 31, 1998

Division of Education and Sientific Services

Oros, J., Fernandez. A., Rodriguez, J. L., Franklin, C. L., Matsushita, S.and Poveda, J. B: Association of cilia-associated respiratory (CAR) bacillus with natural chronic tracheitis in goats. J. Comp. Path., 117, 289-294, 1997.

Okamoto, M. and Matsumoto, T.: Production of germfree mice by embryo transfer. Germfree Life and its Ramifications. Hashimoto, K., Sakakibara, B., Tazume, S. and Shimizu, K. eds., XII ISG Publishing Committee, 21-24, 1996.

Nakagata, N., Okamoto, M., Ueda, O. and Suzuki, H.: Positive effect of partial zona-pellucida dissection on the in vitro fertilizing capacity of cryo-preserved C57BL/6J transgenic mouse spermatozoa of low motility. Biol. Reprod., 57, 1050-1055, 1997.

Aoki, K., Okamoto, M., Tatsumi, K. and lshikawa, Y.: Cryopreservation of medaka spermatozoa. Zoological Science , 14, 641-644, 1997.

Okamoto, M.,Nakagata, N., Ueda, O., Kamada, N. and Suzuki, H.: Cryopreservation of gene disrupted mice spermatozoa. J. Mamm. Ova Res., 15, 77-80, 1998.

Division of Radiation Research

Tomitani, T.: Analysis of potential distribution in a gaseous counter of rectangular cross-section, Selected papers on Photon-Counting Detectors, SPIE Milestone Series, Vol. MS 143, pp31-43, 1997. Elsevier, Amsterdam. Reproduction of Nucl. Instr. & Meth. Vol. 100, pp. 179-191, 1972.

Yamamoto, M.,Yasuda N, Kaizuka [*1], Yamagishi M[*2], Kanai T, Ishigure N, Furukawa A, Kurano M, Miyahara N, Nakazawa M[*1], Doke T[*3], Ogura K[*4]: Cr-39 sensitivity analysis on heavy ion beam with atomic force microscope. Rad Meas, 28: 227-230, 1997 ([*1]Quantum Engin. And Systems Sci., Univ. of Tokyo, [*2]Physics,Toho Univ. [*3]Waseda Univ. [*4]Coll. Ind. Tech., Nihon Univ.)

Shiragai, A., Saitou, M.,* Kudo, I.,** Kanaiwa-Kudo, S.,*** Matsumoto, T., Furuse, T., Yanai, T.,* Ichinohe, K.,* Sato, F.,* and Ohmomo, Y.*: Estimation of the Absorbed Dose to mice in prolonged Irradiation by Low Dose Rate γ-Rays from ^{137}Cs Sources. Radioisotopes 46, 904-911, 1997 (*Institute for Environmental Sciences, **Nuclear Fuel Environment Co., Ltd., ***Tohoku Nuclear Co., Ltd.)

Division of Biology and Oncology

Sakiyama, H., Nakagawa, K., Kuriiwa, K., Imai, K., Okada, Y., Tsuchida, T., Moriya, H. and Imajoho-Ohmi, S: Cell Yissue Res., 288, 557-565, 1997.

Fushiki, S., Hyodo-Taguchi, Y., kinoshita, C., Ishikawa, Y. and Hirobe, T.: Short-and long-term effects of low-dose prenatal X-irradiation in mouse cerebral cortex, with special reference to neuronal migration. Acta Neuropathol., 93, 443-449, 1997.

Hyodo-Taguchi, Y., Fushiki, S., kinoshita, C., Ishikawa, Y. and Hirobe, T.: Effects of continuous low-dose prenatal irradiation on neuronal migration in mouse cerebral cortex. J. Radiat. Res. 38, 87-94, 1997.

Kamisaku, H., Aizawa, S., Kitagawa, M., Ikarashi, Y. and Sado, T.: Limiting dilution analysis of T-cellprogenitors in the bone marrow of thymic lymphoma-susceptible B10 and resistant C3H mice after fractionated whole-body X-irradiation, Int. J. Radiat. Biol. 72, 191-199, 1997

Nakagawa, K., Sakiyama, H., Fukazawa, T., Matsumoto, M., Takigawa, M., Toyoguchi, T., Moriya, H.: Coordinated change between complement Cls producion and chondrocyte differentiation in vitro, Cell Tissue Res., 289, 299-305, 1997

Ichimura, S., Mita, K. and Sugaya, K.: A major non-LTR retrotransposon of Bombyx mori, L1Bm., J. Mol. Evol., 45, 253-264, 1997

Akira Fujimori, Ryoko Araki, Ryutaro Fukumura, Toshiyuki Saito, Masahiko Mori, Kazuei Mita, Kouichi Tatsumi, Masumi Abe: The murine DNA-PKcs gene consists of 86 exons dispersed in more than 250 kb. Genomics, 45, 194-199, 1997

Shuji Ohzeki, Akira Tachibana, Kouichi Tatsumi and Takesi Kato: Spectra of spontaneous mutations at the hart locus in colorectal carcinoma cell lines defective in mismatch repair, Cancinogenesis, 18(6), 1127-1133, 1997

Ishikawa, Y. and Hyodo-Taguchi, Y.: Heritable malformation in the progeny of the male medaka (Oryzias latipes) irradiated with X-rays. Mutation Res., 389, 149-155, 1997

Aoki, K., Okamoto, M., Tatsumi, K. and Ishikawa, Y.: Cryopreservaiton of medaka spermatozoa. Zool. Sci., 14, 641-644, 1997

Zama, M.: Translational pauses during the synthesis of proteins and mRNA structure. Nucleic Acids Res. Symp. Ser., 37, 179-180, 1997

Kawai, H., Kitamura, Y., Nikaido, O., Tatsuka, M., Hama-Inaba., Muto, M., Ohyama, H., Suzuki, F.: Isolation and characterization of apoptosis- resistant mutants from a radiosensitive mouse lyphoma cell line. Radiat. Res., 149, 41-51, 1997

Hirobe, T., Wakamatsu, K.* and Ito, S.*: Effects of genic substitution at the agouti, brown, albino, dilute, and pink-eyed dilution loci on the proliferation and differentiation of mouse epidermal melanocytes in serum-free culture. Eur. J. Cell Biol., 75, 184-191, 1998 *Fujita Health University, Chemistry.

Hyodo-Taguchi, Y., Fushiki, S., Kinoshita, C., Ishikawa, Y. and Hirobe, T.: Effects of low-dose X-irradiation on the development of the mouse cerebellar cortex. J. Rad. Res ., 39, 11-19, 1998. *Kyoto Prefectural University, Neurological Diseases and Geriatrics.

Nenoi, M., Mita, K., Ichimura, S. and Kawano, A: Higher frequency of concerted evolutionary events in rodents than in man at the polyubiquitin gene VNTR locus. Genetics, 148, 867-876, 1998

Ichimura, S., Hamana, K. and Nenoi, M.: Significant increases in the steady stated of putrescine and spermidine/spermine-N1- acetyltransferase mRNA in HeLa cells accompanied by growth arrest, Biochem Biophys Res Commun, 243, 518-521, 1998

Takahashi, A.*, Yano, T.*, Matsumoto, H.*, Wang, X.*, Ohnishi, K.*, Tamamoto, T.*, Tsuji, K.*, Yukawa, O. and Ohnishi, T.*: Effects of

accelerated carbon-ions on growth inhibition of transplantable human esophageal cancer in nude mice, Cancer Letters, 122, 181-186, 1998
*Departments of Biology, Surgery and Oncoradiology, Nara Medical University.

Ohnishi, T.*, Takahashi, A.*, Yano, T.*, Matsumoto, H.*, Wang, X.*, Ohnishi, K.*, Tamamoto, T.*, Tsuji, K.*, Furusawa, Y. and Yukawa, O.: Hyperthemic enhancement of tumour growth inhibitinob by accelerated carbon-ions in transplantable human esophageal cancer, Int. J. Hyperthmia, 14, 195-202, 1998
*Departments of Biology, Surgery and Oncoradiology, Nara Medical University.

Division of Radiobiology and Biodosimetry

Radiation effects on embryos of preimplatation. Wang, B. and Zhou, X.: Chinese Journal of Radiation Medicine and Protection, 17(6): 455-477, 1997.

Apoptosis induction in cultured mouse embryonic mid brain cells. Wang, B., Fujita, K., Watanabe, K., Mitani, H., Yamada, T. and Shima, A.: Radiat. Res. 147; 304-308. 1997.

Eguchi-Kasai, K., Murakami, M., Itsukaichi, H., Fukutsu, K., Yatagai, F., Kanai, T., Ohara, H. and Sato, K.: Repair of DNA double-strand breaks and cell killing by charged particles. Adv. in Space Res., 22(4): 543-549, 1998.

Fukumura, R., Araki, R., Fujimori, A., Mori, M., Saito, T., Watanabe, F., Sarashi, M., Itsukaichi, H., Eguchi-Kasai, K., Sato, K., Tatsumi, K. and Abe, M.: Leucine to proline substitution (3191) in DNA-PKcs affects the signal joint formation as well as coding joint formation of V(D)J recombination. J. Biol. Chem., 273, 13058-13064, 1998.

Kanda, R., Kobayashi, S. and Kanda, J.: Risk perception on industrial and social events among students of general education course in a Japanese University Japanese Journal of Risk Analysis, 8(2), 128-134, 1997. (*Shizuoka University)

Kusumoto, S.*, Jinnai, I.*, Matsuda, A.*, Murohashi, I.*, Bessho, M.*, Saito, M.*, Hirashima, K.*, Heshiki, A.* and Minamihisamatsu, M.: Bone marrow patterns in patients with aplastic anemia and myelodysplastic syndrome; observations with magnetic resonanece imaging. Eur. J. Haematol., 59, 155-161, 1997.(*Saitama Medical Scool)

Fukushima, S.*1, Ozeki, S.*1, Tang, T.J.,*1, Koizumi, M.,*1 Matsumura, S.,*1 lnoue, T.,*1 Inoue, T.,*1 Yamazaki, H.,*2 Murayama, S.,*3 Hatanaka, K.,*1 Ejiri, H.,*1 and Kasai, K.: Induction of p53 protein by carbon-ion and proton beamirradiation in two close human lymphoblastoid cell lines with different p53 status. Oncology Reports, 4: 481-484, 1977.
*1Osaka University, *2DUniversity of Pennsylvania, *3Nat. Cancer Center Hospital

Division of Radiotoxicology and Protection

Oghiso, Y., Yamada, Y. and Iida, H.: High frequency of leukemic lymphomas with osteosarcomas but no myeloid leukemias in C3H mice after 239Pu citrate injection. J. Radiat. Res., 38, 77-86, 1997.

Yamada, Y., Koizumi, A. and Fukuda, S.: Aerosolization of a Chelating Agent, Ca-DTPA, for Emergent Inhalation Therapy. J. Health Phys., 32, 167-172, 1997.

Fukutsu, K., Kanai, T., Furusawa, Y. and Ando, K.: Response of mouse intestine after single and fractionated irradiation with accelerated carbon ions with a spread-out bragg peak. Radiation Research, 148, 168-174, 1997.

Fukuda, S., Iida, H., Yamada, Y., Koizumi, A. and Ishigure, N.: Effects of DTPA therapy on removal of inhaled high-fired plutonium oxide in rats. J. Health. Phys., 32 383-386, 1997.

Ogiso, Y., Yamada, Y., Iida, H. and Inaba, J.: Differential dose responses of pulmonary tumor types in the rat after inhalation of plutonium dioxide aerosols. J. Radiat. Res., 39 61-72, 1998.

Division of Human Environment

Epidemiological study group on evaluation of individual doses (Y. Yoshimoto et al) : Reliability of individual doses relating to the epidemiological studies on nuclear industry workers in Japan (1) (in Japanese) , RADIOISOTOPES, 46, 833-843, 1997

Epidemiological study group on evaluation of individual doses (Y. Yoshimoto et al) : Reliability of individual doses relating to the epidemiological studies on nuclear industry workers in Japan (2) (in Japanese) . RADIOISOTOPES, 46, 917-932, 1997

Fujimoto, K.: Correlation between Indoor Radon Concentration and Dose Rate in Air from Terrestrial Gamma Radiation in Japan. Health Physics 75, 1-7; 1998.

Fujimoto, K.: Correlation between Nationwide Indoor Radon and Terrestrial Gamma Survey Data in Japan. Proceeding of the 7th Tohwa University International Symposium, Radon and thoron in the human environment, Oct. 23-25, 1997.

Fujimoto, K., Kobayashi, S., Uchiyama, M., Doi, M. and Nakamura, Y.: Nationwide Indoor Radon Survey in Japan, Hoken Butsuri 32, 41-51, 1997.
Iimoto, T., Tokonami, S. and Kurosawa, R.: Radiat. Prot. Dosim., 72, 55-60, 1997.

Iimoto, T., Fujimoto, K., Tokonami, S. and Kurosawa, R.: Characteristics of Major Filters Used for ^{222}Rn Progeny Measurements. Radiation Measurements, accepted. 1997.

Ishikawa, T. and Uchiyama, M.: Calculation of the counting efficiency for Cs-137 using voxel phantoms with lungs and a skeleton. Radiat. Prot.Dosim., 69; 199-204, 1997
.
Ishikawa, T. and Uchiyama, M.: Estimation of the counting efficiency for individual subjects in Cs-137 whole-body counting, using voxel phantoms. Radiat. Prot. Dosim., 71; 195-200, 1997.

Kakuta, I., Yukawa, M., and Nishimura, Y.: Effect of water salinity on the trace elemental composition of Otoliths from Tridentiger obscurus. Bull. Soc. Sea Water Sci. Jpn. 51: 388-394,1997

Kawamura, H.: 2.2 Organ mass measurement, in "Compilation of anatomical, physiological and metabolic characteristics for a Reference Asian Man, Vol. 1, Data summary and conclusions," IAEA-TECDOC-1005 (1998) , 27-55.

Nishimura, Y., Watanabe, Y., M, H. Jia., Takeda, H., Wada, and M. Yukawa,M.: Intestinal absorption of ^{14}C-Chitosan in Rats. Chitin and Chitosan Research, 3: 55-61, 1997.

Nishizawa K.: Dose estimation and risk-benefit analysis in mammography. Jpn. J. Med. Phys. Supplement 53; 17-32,1997

Sahoo, S. K. and Masuda, A.: Precise measurement of zirconium isotopes by thermal ionization mass spectrometry, Chem. Geol., 141, 117-126, 1997.

Shiraishi, K.: Sensitivity Comparison for electron spin resonance (ESR) on carbohydrates as dosimeter materials. Adv. ESR Appl., 13, 4-10, 1997.

Shiraishi, K., Tagami, K., Ban-nai, T., Yamamoto, M., Muramatsu, Y., Los, P., Phedosenko, G. V., Korzun, V. N., Tsigankov, N. Y., and Segeda, I. I.: Daily intakes of ^{134}Cs, ^{137}Cs, ^{40}K, ^{232}Th, and ^{238}U in Ukrainian males. Health Physics, 73, 807-812, 1997.

Tanaka, G., Kawamura, H. and Shiraishi, K: Physical, and anatomical data, and part of physiological and metabolic data for normal Japanese with special reference to establishing Reference Asian Man model for the anatomical characteristics, in "Compilation of anatomical, physiological and metabolic characteristics for a Reference Asian Man, Vol. 2, Country reports," IAEA-TECDOC-1005 (1998) , 95-112.

Tokonami, S., Takahashi, F., Iimoto, T. and Kurosawa, R.: Health Phys., 73, 494-497, 1997.
7. Matsusaka, N., Yamakawa, Y., Sato, I., Tsuda, S., Kobayashi, H., Nishimura, Y.: Organ distribution of ^{137}Cs in mice fetuses and their dams. Radioisotopes, 46: 219-225,1997.

Wada, M., Nishimura, Y., Watanabe, Y., Takita, T., and Innami, S.: Chitosan intake accelerates urinary calsium excretion in rats. Biosci. Biotech. Biochem., 6: 1206-1208, 1997.

Watanabe, Y., Nakamura, Y., and Ishii R.: Relationship between Starch Accumulation and Activities of the Related Enzymes in the Leaf Sheath as a Temporary Sink Organ in Rice Plant (Oryza sativa L.) . Australian Journal of Plant Physiology, 24: 563-569, 1997.

Yamamoto, M., Kofuji, H., Shiraishi, K., and Igarashi, Y.: An attemp to evaluate dry deposition velocity of airbore 816D816C8175Pb in a forest ecosystem. J. Radioanal. Nuc. Chem. Art., 227, 81-87,1998.

Yoshimoto, Y. and Yoshinaga, S.: Significance and limits ofmortality survey in the vicinity of nuclear power stations as a monitoring (in Japanese) . Proceedings of the Japan Radiation Research Society, the 40th annual meeting,88,1997.

Yoshinaga,S. Aoyama,T. and Yoshimoto,Y.: Significance and limitations of a cohort study of radiological technologists in Japan (in Japanese) .Journal of Epidemiology, 148, 7 , 1997.

Yukawa, M., Watanabe,Y., Nishimura, Y., Shiraishi, K., Kawamura, H., and Sakurai, S: Application of PIXE, NAA and ICP techniques to the determination of trace elements in food and diet samples. IAEA-SM-344/2: 435-446,1977.

Yukawa,M.: Proceedings of 34th Seminar on Science and Technology. Small Accelerators and Their Application: 151-161,1997.

Yukawa, M., Watanabe, Y., Nishimura, Y., Shiraishi, K., Kawamura, H., and Sakurai,S.: Proceedings of International Symposium on Harmonization of Health Related Environmental Measurements Using Nuclear and Isotopic Techniques: 435-446,1997.

Yukawa, M., Kimura, A., Watanabe, Y., and Sakurai, S.: Distribution of elements in beansprout determined by PIXE analysis. Int. J. PIXE, 5: 69- 77,1995.

Yukawa, M., Watanabe, Y., and Nishimura, Y.: Application of PIXE technique to determination of trace elements in diet and comparison with NAA and ICP-AES. Int. J. PIXE. 6: 395-403,1996.

Yukawa, M., Watanabe, Y., and Nishimura, Y.: Determination of trace elements in mate using PIXE analysis. Int. J. PIXE. 6: 505-509,1996.

Division of Radiation Health

Taki, S., T. Saito, K. Ogasawara, T. Fukuda, M. Sato, S. Hida, G. Suzuki,Mitsuyama, E.H.Shin, S. Kojima, T. Taniguchi, and Y. Asano: Multistage regulation of Thl-type immune responses by the transcription factor IRF-1. Immunity 6: 673-679, 1997

Hachiya, M., shimizu, S., Osawa, Y. and Akashi, M: Endogenous production of tumour necrosis factor is required for manganese superoxide dismutase expression by irradiation in the human monocytic cell line THP-1. Biochem. J 328, 615-623, 1997

Bioregulation Research Group

Onoda, M. and Inano, H.: Distribution of casein-like proteins in various organs of rat, J. Histochem. Cytochem., 45: 663-674, 1997

Furuse, M., Tsuneoka, K., Uchida, K*., and Nomoto, K*.: J. Rediat. Res., 38, 111-120, 1997. (*Yakult Central Institute for Microbiological Research)

Susa, N.*, Ueno, S.*, Furukawa, Y.*, Ueda, J., and Sugiyama, M.**: Potent protective effcct of melatonin on chromium (VI) -induced DNA single-strand breaks, cytotoxicity, and lipid pcroxidation in primary cultures of rat hepatocytes, Toxicol. Applied Pharmacol., 144 377-384, 1997. (*Kitazato Univ., **Asunaro Pharmacy)

Ueda, J., Hanaki, A.*, Yoshida, N.** and Nakajima, T.***: Proton nuclear magnetic resonance studies of the complexation of Zn (II) with histidine-containing peptides, L-histidylA059L-histidylglycylglycine and LA059histidylglycyl-LA059histidylgycine, Chem. Pharm. Bull., 45, 1108-1113, 1997. (*Shizuoka Univ., **Tokyo Med. Dent. Univ., ***Suntory Inst. for Bioorg. Res.)

Noda, Y.*, Anzai, K., Mori A.*, Kohno, M.**, Shinmei, **, Packer, L.*: Hydroxyl and superoxide anion radical scavenging activities of natural source antioxidants using the computerized JES-FR30 ESR spectrometer system. Biochem Mol. Biol. Internat., 42, 35-44-1997.
(*University of California, **JEOL)

Lee, S.*, Kiyota, T.*, Kunitake, T.*, Matsumoto, E.*, Yamashita, S.**, Anzai, K., Sugihara, G*: De Novo Design, Synthesis, and Characterization of a Pore Forming Small Globular Protein and Its Insertion into Lipid Bilayers. Biochemistry, 36, 3782-3791, 1997. (*Fukuoka University, **Kyushu Universtity)

Miura, Y., Anzai, K., Urano, S. *, Ozawa, T.: In vivo Electron Paramagnetic Resonance Studies on Oxidative Stress Caused by X- Irradiation in Whole Mice. Free Rad. Biol. Med.., 23, 533-540, 1997.
(*Tokyo Metropolitan Institute of Gerontology)

Matsuzaki, K.*, Yoneyama, S.*, Fujii, N.*, Miyajima, K.*, Yamada, K.**, Kirino, Y.***, Anzai, K.: Membrane permeabilization mechanisms of a cyclic antimicrobial peptide, tachyplesin I, and its linear analog.Biochemistry, 36, 9799-9806, 1997.(*Kyoto University, **Kyushu University, ***Tokyo University)

Inano, H., Suzuki, K., Onoda, M., and Wakabayashi, K[*].: Anti- carcinogenic activity of simvastatin during the promotion phase of radiation-induced mammary tumorigenesis of rats. Carcinogenesis, 18, 1723-1727, 1997. (Gunma University)

Suzuki, K. T.[*], Rui, M.[*], Ueda J. and Ozawa, T.: Production of ascorbate and hydroxyl radicals in the liver of LEC rats in relation to hepatitis. Res. Commun. Molec. Pathol. Pharmacol ., 96, 137-146, 1997. ([*]Chiba Univ.)

Miura, Y., Anzai, K., Takahashi, S. and Ozawa, T.: A novel lipophilic spin probe for the measuremect of radiation damage in mouse brain using in vivo electron spin resonance (ESR) . FEBS Lett., 419, 99-102, 1997

N. Ikota, J. Hirano, R. Gamage, H. Nakagawa, and H. HamaA059Inaba,Improved Synthesis of 1-Deoxynojirimycin and Facile Synthesis of Its Stereoisomers from (S) -Pyroglutamic acid Derivative. Heterocycles, 46,673-643 (1997).

Ishihara, H., & Tanaka, I.: Detection and cloning of unique integration sites of retrotransposon, intracisternal A-particle element in the genome of acute myeloid leukemia cells in mice. FEBS Letters, 418, (1997) 205- 209.

Kawai H:[*], Kitamura, Y.[**], Nikaido, O.[**], Tatsuka, M.[*], Hama-Inaba, H., Muto, M., Ohyama, H. and Suzuki, F.[*]: Isolation and Characterization of Apoptosis-resistant Mutants from a Radiosensitive Mouse Lymphoma Cell Line. Radiat. Res., 149, 41-51, 1998.
([*]Hiroshima University [**]Kanazawa University)

Hama-Inaba, H., Wang, B., Mori, M., Matsushima, T., Saitoh, T., Takusagawa, M., Yamada, T., Muto, M. and Ohyama, H.: Radiosensitive murine thymoma cell line 3SB. Characterization of its apoptosis-resistant variants induced by repeated X-irradiation. Mutation Res. 403, 85-94, 1998.

Genome Research Group

[*1]Zhao, J., [*1]Dynlacht, B., Imai, T., Hori, T., [*1]Harlow, E.: Expression of NPAT, a novel substrate of cyclin E-CDK2, promotes Sphase entry. Genes and Development 1998 Genes & Dev. 12, 456-461, 1998.([*1]Masachusetts Gen. Hosp.)

Saito, T., Seki, N., Yamauchi, M., Tsuji, S., Hayashi, A., Kozuma, S., Hori, T.: Structure, chromosomal location, and expression profile fo EXTR1 and EXTR2, new members of the multiple exostoses gene family. Biochemical and Biophysical Research Communications, 243: 61-66, 1998.

Hori, T., Seki, N., Ohira, M., Saito, T., Yamauchi, M., Sagara, M., Hayashi, A., Tsuji, S., Ito, H., Imai, T.: A distamycin A-inducible fragile site, FRA8E, located in the region of the hereditary multiple exostoses gene, is not involved in HPV16 DNA integration and amplification. Cancer Genetics and Cytogenetics, 101: 24-34, 1998.

Krien, M., S. Bugg, M. Palatsides, G. Asouline, M. Morimyo, and M. Connell, A NIMA homologue promotes chromatin condensation in fission yeast. J. Cell Sci., 1998. 111(7): p. 967-976.

*1Kawana, Y., *1Komiya, A., *1Ueda, T., *1Nihei, N., *1Kuramochi, H., *1Suzuki, H., *2Yatani, R., Imai, T., *3Dong, J-T., *4Imai, T., *4Yoshie, O., *5Barett, J. C., *5Isaacs, J. T., *1Shimazaki, J., *1Ito, H., *7Ichikawa, T.: Location of KAIl on the short arm of human chromosome 11 and frequency of allelicloss in advanced human prostate cancer. The prostate 32, 205-213, 1997.(*1Chiba Univ. School of Med, *2Fac. of Med, Mie Univ., *3Univ. of Virginia, *4Shionogi Inst. of Med. sci., *5Johns hopkins Univ. School of Med, *7Teikyo Univ. School of Med.)

*1Kitayama, E., *1Hosoda, F., *1Fukushima, M., *2Asakawa, S., *2Shimizu, N., Imai, T., *3Soeda, E., and *1Ohki, M.: A 3-Mbsequence ready contig map encompassing the multiple disease gene cluster on human chromosome 11 q13. 3. DNA Research, 4,281-289, 1997.(*1Radiol. Natl. Cancer Cntr Res. Inst, *2Keio Univ. Med., *3RIKEN Gene Bank)

Sugaya, K., Ajimura, M., Tsuji, H., Morimyo, M., Mita, K.: Alteration of the largest subunit of RNA polymerase II and its effect on chromosome stability in Schizosaccharomyces pombe. Mol. Gem. Genet., 258, 279- 287, 1998.

Sugaya, K., Sasanuma, S., Nohata, J., Kimura, T., Hongo, E., Higashi, T., Morimyo, M., Tsuji, H., Mita, K.: Cloning and sequencing for the largest subunit of chinese hamster RNA polymerase II gene: identification of a muration related to abnormal induction of sister chromatid exchanges. Gene 194, 267-272, 1997.

Space and Particle Radiation Science Research Group

H. Yamaguchi: Calculation of G-value of Fricke Dosimeter irradiated by photons 100 eV-10 MeV, "Microdosimetry-An Interdisciplinary Approach- ", Eds. by D. T. Goodhead, P. O'Neill and H. G. Menzel, PP. 97-100, The Royal Society of Chemistry 1997.

Suzuki, M., Kase, Y., Kanai, T., Yatagai, F. and Watanabe, M.: LET dependence of cell death and chromatin-break induction in normal human cells irradiated by neon-ion beams. International Journal of Radiation Biology, , 497-503, (1997).

Fukuda, S, Iida, H., Yamada, Y., Koizumi, A and Ishigure, H: Effects of DTPA therapy on removal of inhaled pultonium oxide in rats. J. Health Physics, 32 383-386, 1997.

Environment and Toxicological Sciences Research Group

Kubota, Y., Takahashi, S. and Sato, H.: Int. J. Radiat. Biol., 72, 71-78, 1997

Ban-nai, T., Muramatsu, Y. and Yoshida, S.: Health Physics, 72, 384-389, 1997

Uchida, S. and Tagami, K.: Separation and concentration of technetium using a Tc-selective extraction chromatographic resin. J. Radioanal. Nucl. Chem., 221, 35-39, 1997

Uchida, S. and Tagami, K.: Improvement of Tc Separation Procedure using a Chromatographic Resin for Direct Measurement by ICP-MS. Analytica Chimica Acta, 357, 1-3, 1997.

Ban-nai, T., Muramatsu, Y., Yoshida, S., Uchida, S., Shibata, S., Ambe, S., Ambe, F. and Suzuki, A.: Multitracer studies on the accumulation of radionuclides in mushrooms. J. Radiation Research, 38, 213-218, 1997

Kunst, F.[*1], Fuma, S. et al.: The complete genome sequence of the Gram-positive bacterium Bacillus subtilis. Nature, 390, 249-256, 1997.[*1]Institut Pasteur, France

Yanagisawa. K. and Muramatsu, Y.: Transfer of Technetium from Soil to Plant. Russian Journal of Radiochemistry, 39, 375-378, 1997

Yanagisawa. K., Muramatsu, Y. and Ban-nai T.: Behavior of Technetium in Paddy Soils. Journal of Radioanalytical and Nuclear Chemistry, 226, 221-223 (1997)

Sun, Xue Zhi, Inoue, M., Yamamura, H. and Fukui, Y.: Effects of prenatal treatment with tritiated water on the developing brain in mice.International Journal of Radiation Biology 71(3): 309-313, 1977

Sun, Xue Zhi, Inoue, M., Fukui, Y., Muramatsu, H., Muramatsu, T. and Yamamura, H.: Effects of different fixatived on immunohistochemical demonstration of midkine using quick-frozen mouse embryonic brains. Environmetnal Medicine. 41(2): 104-106 (1977)

Takahashi, S., Kubota, Y. and Sato. H.: Mutant Frequencies in lacZ Transgenic Mice following the internal Irradiation from ^{89}Sr or the External γ-Ray Irradiation. J. Radiat. Res., 39,53-60, 1998

Yoshida, S. and Muramatsu, Y.: Determination of major and trace elements in mushroom, plant and soil samples collected from japanese forests. Intern. J. Environ. Anal. Chem. 67, 49-58, 1997.
Sun, Xue Zhi, Inoue, M., Fukui, Y., Hisano, S., Sawada, K., Muramatsu,
H. and Muramatsu, T.: An immunohistochemical study of radial glial cells in the mouse brain prenatally exposed to γ-irradiation. J. Neuropathology and Experimental Neurology 56(12), 1339-1348, 1997.

Low Dose Radiation Risk and Carcinogenesis Research Group

Kobayashi, S., Nishimura, M., Shimada, Y., Suzuki, F.[*1], Matsuoka, A.[*2], Sakamoto, H.[*2], Hayashi, M.[*2], Sofuni, T.[*2], Sado, T., Ogiu, T.: Increased sensitivity of scid heterozygous mice to ionizing radiation. Int. J. Radiat. Res., 72, 537-545, 1997.([*1]CHiroshima Univ., [*2]Natl. Inst. Health Sci.)

Kinebuchi, M.[*], Matsuura, A.[*], Ogiu, T., Kikuchi, K. [*]: Deviated overexpression of TCR-β, TCR-γ, CD-4, and CD-8 on thymic lymphomas induced by 1-propy1-1-nitrosourea. J. Immunol., 159, 748-756, 1997. ([*]Sapporo Med. Univ.)

Takahashi, T.[*1], Yagi. T.[*1], Kakinuma, S., Kurokawa, A.[*1], Okada, T.[*1], Aizawa, S.[*2], Katagiri, T.[*1]: Supperession of autoimmune disease and of massive lymphadenopathy in MRL/Mp-lpr/lpr mice lacking tyrosine kinase fyn ($p59^{fyn}$). J. Immunol., 159, 2532-2541, 1997.([*1]Kitasato Inst., [*2]Kumamoto Univ.)

Sugaya, K., Sasanuma, S., Nohata, J., Kimura, T., Hongo, E., Higashi, T., Morimyo, M., Tsuji, H., Mita, K.: Cloning and sequencing for the largest subunit of Chinese hamster RNA polymerase II gene: identification of a mutation related to abnormal induction of sister chromatid exchanges. Gene,, 194, 267-272, 1997.

Nagasawa, M.[*], Watanabe, F., Suwa, A.[*], Yamamoto, K.[*], Tsukada, K.[*], Teraoka, H.[*]: Nuclear translocation of the catalytic component of DNA- dependent protein kinase upon growth stimulation in normal human T lymphocytes. Cell Struct. Funct. 22, 585-594, 1997.([*]Tokyo Med. Dent. Univ.)

Chibazakura, T. [*], Watanabe, F., Kitajima, S. [*], Tsukada, K. [*], Yasukochi, Y.[*], Teraoka, H.[*]: Phosphorylation of human general transcription factors TATA-binding protein and transcription factors TATA-bindingprotein and transcription factor IIB by DNA-dependent protein kinase synergistic stimulation of RNA polymerase IIB by DNA-dependent protein kinase - synergistic stimulation of RNA polymerase II basal transcription in vitro. Eur. J. Biochem., 247, 1166-1173, 1997 ([*]Tokyo Med. Dent. Univ.)

Nishimura, A.[*], Moriya, S.[*], Ukai, H.[*], Nagai, K.[*], Wachi, M.[*], Yamada, Y.[*]: Diadenosine 5', 5'''-Pl, P4-tetraphosphate (Ap4A) controls the timing of cell division in Escherichia coli. Genes Cells, 2, 401-413, 1997.([*]Natl. Inst. Genet.)

Division of Accelerator Physics and Engineering

Net-Ionization Cross Seetions of Rare Gases by Fully-stripped Heavy Ion impact: S. Makino, T. Matsuo, M. Mizutani. M. Sano, T. Kohno, T. Tonuma, H. Tawara, A. Kitagawa and T. Murakami; Phys. Seripta 73, (1997) 238-239.

Channeling with 290 MeV/u C^{6+}Ions in a Si Crystal: T. Ito, T. Azuma, K. Komaki, Y. Yamazaki, T. Murakami, E. Takada, A. Kitagawa, M. Torikoshi and M. Sano; Phys. Seripta 73, (1997) 345-346.

Medical Physics and Engineering Office

Endo, M., Yoshida, K., Kamagata, N.,[*1] Satoh, K.,[*2] Okazaki, T.,[*2] Hattori, Y.,[*2] Kobayashi, S.,[*2] Jimbo, M.,[*2] Kusakabe, M.[*2] and Tateno, Y.: Development of a 3D CT-scanner using a cone beam and video-fluoroscopic system. Radiation Medicine, 16, 7-12, 1998 ([*1]Univ. of Chiba, [*2]Sony Corp.)

Yoshida, K., Endo, M., Mori, K.,[*1] Katada, K.,[*2] Ueda, M.,[*3] Toriwaki, J.[*1] and Tateno, Y.: Virtualized angioscopy of the thoracic aorta in a rabbit model of atherosclerosis. Jpn. Circulation J., 62 198-200, 1998 ([*1]Univ. of Nagoya, [*2]Fujita Gakuen Univ., [*3]Osaka City Univ.)

Division of Radiation Medicine

Tsujii, H., Morita, S., Miyamoto, T., Mizoe, J., Mukai, M., Nakano, T., Kato, H., Kamada, T., Ishikawa, A. and Matsuoka, Y.: Preliminary results of phase I/II carbon-ion therapy at the national institute of radiological sciences. International Journal of Brachytherapy, 13(1), 1-8, 1997.

Yoshioka, H., Onaya, H., Itai, Y., Nishimura, H., Matsumura, A., Tsunoda, T., Kandatsu, S., Koga, M., Yoshikawa, K., Kato, H. and Tsujii, H.: Comparison between magnetization transfer contrast and fast spin-echo mr imaging of digenerative disease of the cervical spine at 0.3t.
Magnetic Resonance Imaging, 15(1), 37-45, 1997.

Ohara, K., Okumura, T., Tsuji, H., Chiba, T., Min, M., Tatsuzaki, H., Tsujii, H., Akine, Y. and Itai, T.: Radiation tolerance of cirrhotic livers in relation to the preserved functional capacity: analysis of patients with hepatocellular carcinoma treated by focused proton beam radiotherapy. Int. J. Radiat. Oncol. Biol. Phys., 38(2), 367-372, 1997.

Division of Accelerator Physics and Engineering

E. Urakabe. M. Inoue, Y. Iwashita. M. Kanazawa, T. Shirai, M. Torikoshi,
M. Tadokoro, M. Nishi, A. Noda, K. Noda. S. Yamada, and Y. Fujita: Parallel Plate Ionization Chanber for Studying The Time Structure of Slow extracted Beam; Beam Science and Technology, Vol. 2, p. 23-29, 1997.

Sato, Y. and Soga, F.: Analysis of Relative Biological Effectiveness of High Energy Heavy lons in Comparison to Experimental Data, J. Radit. Res., 38, 103-110, 1997.

Diagnostic imaging by energetic radiactive particle beams Nuclear Physics a616 (1997) 478-489.
AChatterjee, E. Takada, M. Torikoshi and
M. Kanazawa

Division of Advanced Technology for Medical Imaging

Iyo, M., Namba, H., Fukushi, K., Shinotoh, H., Nagatsuka, S., Suhara., T., Sudo, Y., Suzuki, K. and Irie, T.: Measurement of acetylcholinesterase by positron emission tomography in the brains of healthy controls and patients with Alzheimer's disease.: lancet, 349, 1805-1809, 1997.

K. Andoh[*1], K. Odagiri[*1], T. Matsumoto[*2], K. Yamashita[*1], I. Ogino[*1], T. Otsuka[*1]: Computed radiography excretory urography: Can the system sensitivity value be used as an image quality indicator?, J. Dig.Imag. 10(3), Aug., 1997: 132-136

Hasegawa, T[*1]., Murayama, H, Wada, Y.[*2]: Monte Carlo simulation of PET performance measurements for EXACT 47 at NIRS. Jpn. J. Med. Phys., 17 (72) , 83-93-1997.([*1]Kitasato Univ., [*2]Siemens-Asahi Medical Technologies Ltd.

Ikehira H, Obata T, Koga M, Yoshida K. Human hepatic carbohydrate metabolism. Dynamic observation using 13C NMR without proton decoupling. Acta Radiologica. 1997; 38: 998-1002

Morio S, Oh H, Endo N, Kawano E, Nakamura H, Asai T, Saito y, Uchida Y, Ikehira H, Yoshida K. Magnetc resonance imaging of reticulo- endothelial system in patients with itiopathic thrombocytopenic purpura. Am J Hematol 1997; 56: 52-58

Furuya Y, Ikehira H, Obata T, Koga M, Yoshida K. The measurement of blood flow parameter with deuterium stable isotope MR imaging. Annals Nucl Med. 1997; 11: 281-284

Endo M, Yoshida K, Kamagata N, Satoh K, Okazaki T, Hattori Y, Kobayashi S, Jimbo M, Kusakabe M, tateno Y. Development of a 3D CT- scanner using a cone beam and videofluoroscopic system. Radiation Medicine 1998; 16: 7-12

Yoshida K, Endo M, Mori K, Katada K, Ueda M, Toriwaki J, Tateno Y. Virtualized angioscopy of the thoracic aorta in a rabbit model of atherosclerosis. Jpn Circ J 1998; 62: 198-200

Suhara T, Sudo Y, Yoshida K, Okubo Y, Fukuda H, Obata T, Yoshikawa K, Suzuki K, Sasaki Y. Lung as a reservoir for antideressants in pharmacokinetic drug interactions. Lancet 1998; 351: 332-335

Haradahira, T., Inoue, O., Kobayashi, K., and Suzuki, K.: Synthesis and Evaluation of Carbon-11 Labeled Non-peptide Antgonists for Cholecystokinin (CCK) Receptors:[^{11}C]L-365, 260 and[^{11}C]L-365, 346 Nucl. Med. Biol. 25, 230-208, 1998

Namba, H., Iyo, M., Shinotoh, H., Nagatsuka, S., Fukushi, K. and Irie, T.: preserved acetylcholinesterase activity in aged human cerebral cortex lancet, 352, 881-882, 1998

Namba, H. Iwadate, Y., Iyo, M., Fukushi, K., Irie., T., Sueyoshi, K., Tagawa, M. and Sakiyama., S.: Glucose and methionine uptake by rat brain tumor treated with produg-activated gene therapy Nucl. Med. Biol., 25, 247-250, 1998

Laboratory for Radioecology

Yamada, M.: $^{239\text{-}240}$Pu and ^{137}Cs concentrations in salmon (Oncorhynchus keta) collected on the Pacific coast of Japan. J. Radioanal. Nucl. Chem., 223(1/2), 145-148, 1997.

Nozaki, Y.,^{*1}, Zhang, J. and Amakawa, H.^{*1}: The factionation between Y and Ho in the marine environment. Earth Planet. Sci. Lett., 148, 329- 340, 1997.(^{*1}Tokyo University)

Miyazaki, T., Masuda, R.^{*1}, Furuta, S.^{*2}, and Tsukamoto, K. ^{*1}: Laboratory Observation on the Nocturnal Activity of Hatchery-reared juvenile Japanese Flounder, Fisheries Science, 63(2), 205-210, 1997. (^{*1}Tokyo Univ. O. R. I, ^{*2}Tottori Prefectural Government)

Yamada, M., and Nagaya, Y.: Temporal variations of ^{137}Cs concentrations in the surface seawater and marine organisms collected from the Japanese coast during the 1980's. J. Radioanal. Nucl. Chem, 230(1/2), 111-114, 1988.

6.2 Organization and Staff

Status of March 31, 1998

Yasuhito Sasaki, M. D., Director-General

Masako Kimura, Secretary

Jiro Inaba, Ph. D., Deputy Director-General

Division of Technology and Safety

Ryutaro Oyama, Director

Section of Technical Maintenance

Hajime Sato, B.S., Section Head and 9 StaffMembers

Service for Radiotoxicology

Akira Koizumi, B.S., Head*1 and 4 Staff Members

Section of Safety Promotion

Yukihiko Nagai, Section Head and 14 Staff Members

Section of Radiation Safety

Masaharu Ishida, Section Head and 12 Staff Members

Division of Education and Sientific Services

Masayuki Tezuka, Director

Administrative Office

Mituru Kotoda, Head and 1 Staff Members

Education and Training

Hisamasa Joshima, Ph.D.,Head

Kiyoko Imai, Ph.D.*1

Infomation Network Promotion

Shozo Hongo, B.S., Head

Hiroshi Takeshita, B.S.,and 3 Staff Members

Kenjiro Fukuhisa, B.S.*1

Eiko Takeda*1

Hitoshi Imazeki*1

Laboratory Animal and Plant Sciences

Tsuneya Matsumoto, Ph.D.,Head

Junji Yamagiwa, D.V.M.,Ph.D.

Masayuki Kitazume, D.V.M.

Masanori Okamoto, Ph.D.

Akihiro Kawano, D.V.M. and 6 Staff Members

Hiroshi Suzuki, Ph.D.*6

Fumiaki Sato, Ph.D.*7

Division of Radiation Research

Jiro Inaba, Ph.D., Director

Mitsue Takeshita, Secretary

Fundamental Science

Takehiro Tomitani, Ph.D.,Head

Sado Shibata B.S.

Susumu Kinpara, Ph.D.

Radiation Protection

Jiro Inaba, Ph.D.,Head*1

Akihiro Shiragai, B.S.

Yutaka Noda, B.S.

Bio-Emission

Mikio Yamamoto, Ph.D., Head

Nakahiro Yasuda, Ph.D.*4

Masahiko Hirasawa, M.S.*7

Hideyuki Kokubo, B.S.*7

Mieko Kurano, B.S.

Tomoko Kokado, B.S.

Junko Taniguch, B.E.

Hideaki Sakaida, B.E.

Yoshio Machi, Ph.D.*7

Kimiko Kawano, B.S.*7

Keiichi Nishikawa, Ph.D.*4

Yohji Kaizuka, M.E.*4

Akira Watanabe, M.S.*4

Kensuke Kishi, M.S.*4

Masaharu Nakaawa, Ph.D.*6

Hiroyuki Takahashi, Ph.D.*6

Kouichi Ogura, Ph.D.*6

Tadayoshi Doke, Ph.D.*6

Karl-Ludwing Giboni, Ph.D.*7

Nobuo Fukuda, M.D.,Ph.D.*6

Medical Dosimetry

Takeshi Hiraoka, Ph.D.,Head

Akifumi Fukumura, B.S.

Kaname Omata, B.S.

Suoh Sakata, Ph.D.*4

Hiroki Ohtani, B.S.*4

Senior Research Counselor

Katsuhiro Kawashima, Ph.D.

Yoshikazu Kumamoto, Ph.D.

Division of Radiobiology and Biodosimetry

Isamu Hayata, Director

Takeko Odaka, Secretary

Proliferation and Differentiation Mechanisms

Eiichi Kojima, Ph.D.,Head

Kiyomi Eguchi-Kasai, Ph.D./td>

Kaoru Tanaka, B.S.

Molecular and Cell Biology

Harumi Ohyama, Ph.D.,Head

Hiromi Itsukaichi

Masahiro Murakami,Ph.D.

Masahiko Mori, Ph.D.

Kumiko Fukutsu, B.S.*1

Bing Wang, M.D.*4

Takashi Shimokawa, M.S.*4

Isao Shibuya, B.S.*4

Shigenari Hashimoto, B.S.*4

Tadashi Matsushima, B.S.*4

Cytogenetics and Cytometry

Isamu Hayata, Ph.D.,Head

Masako Minamihisamatsu, B.S.

Akira Furukawa, M.S.

Reiko Kanda, Ph.D.*1

Hiroshi Ohara, Ph.D.*1

Senior Research Counselor

Takaaki Ishihara, Ph.D.

Takesaburo Mori, M.D.

Koki Sato, M.D.

Division of Biology and Oncology

Kouichi Tatsumi, M.D.,Ph.D.,Director

Cellular and Moleular Respones to Radiation

Sachiko Ichimura, Ph.D.

Chidori Muraiso, B.S.

Tetsuo Nakajima, M.S.

Mitsuru Nenoi, Ph.D.

DNA Metabolism and Mutagenesis

Mitsuo Zama, Ph.D.,Head

Ikuko Furuno-Fukushi, Ph.D.

Masahiko Takahagi, Ph.D.

Yuko Houki-Fujimori, B.Ph.*8

Developmental Biology

Kouichi Tatsumi, M.D., Ph.D.,Head*1

Yuji Ishikawa, Ph.D.

Tomohisa Hirobe, Ph.D.

Immunology and Molecular Oncology

Masahiro Muto, Ph.D.,Head

Shiro Aizawa, Ph.D.

Eiko Kubo

Hitoko Kamisaku

Akira Fjimori M.D, Ph.D.*5

Yasuyoshi Kanari, Ph.D.*8

Susceptibility to Radiogenic Cancer

Kouichi Tatsumi, M.D., Ph.D.,Head*1

Hisako Sakiyama, M.D., Ph.D.

Takeshi Furuse, Ph.D.

Kazuko Yoshida, Ph.D.

Masumi Abe, Ph.D.

Yuko NOda

Ryoko Araki, M.D., Ph.D.*5

Semior Research Counselor

Toshihiko Sado, Ph.D.

Tamiko Iwasaki, M.D.

Hiroshi Tanooka, M.D., Ph.D.

Norikazu Yasuda, M.D.

Division of Radiotoxicology and Protection

Michikuni Shimo, Ph.D.,Director

Satoshi Fukuda, D.V.M., Ph.D.*1

Metabolism and Decorporatin

Michikuni Shimo, Ph.D.,Head*1

Hiroshi Sato, Ph.D.

Dosimetry of Internal Exposure

Nobuhito Ishigure, Ph.D.,Head

Takashi Nakano, Ph.D.

Hiroko Enomoto

Experimental Pathology

Yoichi Oghiso, D.V.M., Ph.D.,Head

Yutaka Yamada, D.V.M., Ph.D.

Haruzo Iida

Kumiko Fukutsu, B.S.

Safety Engineering

Akira Koizumi, B.S.,Head

Yuji Yamada, Ph.D.

Katsuhiro Miyamoto

Division of Human Radiation Environment

Masafumi Uchiyama.,Ph.D.,Director

Environmental Radiation Exposure

Kenzo Fujimoto, Ph.D.,Head

Masahide Furukawa, Ph.D.

Sinji Tokonami, Ph.D.

Takeshi Iimoto, Ph.D.*6

Biokinetics and Internal Dose Assessment

Yoshikazu Nishimura, D.V.M.,Ph.D.,Head

Masae Yukawa., Ph.D.

Yoshito Watanabe, Ph.D.

Shozo Hongo, B.S.*1

Internal Exposure and Human Models

Hisao Kawamura, B.S.,Head

Kunio Shiraishi,Ph.D.

Radiation Eposure Mitigation

Katsumi Kurotaki, Ph.D.,Head

Hidenori Yonehara, Ph.D.

Sarata Kumar Sahoo, Ph.D.

Kiyoko Imai, Ph.D.*1

Hiroshi Takeshita, B.S.*1

Sadao Shibata, B.S.*1

Population Dose Assessment

Kanae Nishizawa, Ph.D.,Head

Masaki Matsumoto, M.S.

Tetsuo Ishikawa, B.S.

Epidemiology and Risk Assessment

Yasuhiko Yoshimoto, Ph.D.,Head

Shinji Yoshinaga, M.S.

Senior Research Counselor

Toshiyuki Nakajima, Ph.D.

Masaharu Okano, Ph.D.

Visiting Scientist

Jia Ming Hong, Ph.D.

Yang Mingli(STA fellow)

Woon Hyuk Chung, Ph.D.

Young-ho Kim*3(STA fellow)

Division of Radiation Health

Hirohiko Tsujii, M.D.,Director

Clinical Hematology

Makoto Akashi, M.D., Ph.D.,Head

Satoshi Shimomura, M.D.

Yoshiko Kawase, B.S.

Misao Hachiya, Ph.D.

Yoshiaki Osawa, M.S.

Clinical Immunology

Gen Suzuki, M.D.,Ph.D.,Head

Masako Nose, B.S.

Kenichi Nakagawa, M.D., Ph.D.

Akiko Uzawa, B.S.

Yoshiro Aoki, M.D.*1

Yukiko Nakata, M.S.*7

Radiation Injury Control

Makoto Akashi, M.D. Ph.D.*1

Yasushi Yamamoto, M.D.

Nobuyoshi Kobayashi, M.D.

Bioregulation Research Group

Toshihiko Ozawa, Ph.D.,Supervising Researcher

Michiyo Takahashi, Seretary

Bioradical Research

Toshihiko Ozawa, Ph.D.,Head*1

Kiyoko Imai, Ph.D.

Jun-ichi Ueda, Ph.D.

Kazunori Anzai, Ph.D.

Yuri Miura, Ph.D.*5

Hideo Utsumi, Ph.D.*6

Mikinori Kuwabara, Ph.D.84DB*3

Expression of Bioregulator Gerech

Kazuko Tsuneoka, Ph.D.,Head

Hiroshih Ishihara, Ph.D.

Masako Furuse

Izumi Tanaka

Cytoregulation

Hiroshi Inano, Ph.D.,Head

Keio Suzuki, Ph.D.

Makoto Onoda, Ph.D.

Explorative Study of Bioregulation Substances

Nobuo Ikota, Ph.D.,Head

Hiroko Hama-Inaba, Ph.D.

Hidehiko Nakagawa, Ph.D.

Senior Research Council

Akira Hanaki, Ph.D.

Genome Research Group

Mitsuoki Morimyo, Ph.D.,Supervising Researcher

Genome Sequencing and Informatics

Kazuei Mita, Ph.D.,Head

Kimihiko Sugaya, Ph.D.

Genome Analysis on Model Organisms

Mitsuoki Morimyo, Ph.D.,Head*1

Tomoyasu Higashi, M.S.

Etsuko Hongo

Human and Mouse Genome Mapping

Takashi Imai, Ph.D., Head

Masashi Sagara, Ph.D.

Yasuharu Ninomiya, Ph.D.

Hiroko Ito

Human and Mouse Function

Mitsuoki Morimyo, Ph.D.,Head*1

Toshiyuki Saito, Ph.D.

Masatake Yamauchi, Ph.D.

Satsuki Tsuji

Mouse Gene Targeting

Tadahiro Shiomi, Ph.D.,Head

Yoshinobu Harada, Ph.D.

Manabu Koike, Ph.D.

Space and Particle Radiation Science Research Group

Kazunobu Fujitaka, Ph.D.,Supervising Researcher

Yutaka Noda*1, B.S.

Masahide Furukawa, Ph.D.*1

Kiyomi Eguchi-Kasai, Ph.D.*1

Experimental Radiotherapy

Koichi Ando, D.D.S., Ph.D.,D.M.Sc.,Head

Hideyuki Majima, D.D.S., Ph.D.

Sachiko Koike, B.S.

Kumie Nojima, B.S.

Hiromi Kanzaki

Eriko Sato

Kazumi Nakada

Soichiro Ando, M.D.

Particle Radiobiology

Kazunobu Fujitaka, Ph.D.,Head

Yoshiya Furusawa, Ph.D.

Masao Suzuki, Ph.D.

Marco Durante, Ph.D. STA fellow

Keiko Sekita

Space Radiation Environment

Hiroshi Yamaguchi, Ph.D.,Head

Hiroshi Yasuda, Ph.D.

Masashi Takada, M.S.

Tetsuya Sakashita, Ph.D.*4

Yukio Uchihori, Ph.D.*5

Joerg Siebers, Ph.D. STA fellow

Tadayoshi Doke, Ph.D.*3

Kazuko Kaiho

Michiko Takakura

Space bio-medicine

Satoshi Fukuda, D.V.M.,Ph.D.,Head

Yoko Sano

Environmental and Toxicological Sciences Research Group

Yuji Nakamura, Ph.D.,Supervising Researcher

Methodology Development

Yuji Nakamura, Ph.D.,Head*1

Masahiro Doi, Ph.D.

Tetsuya Sakashita, Ph.D.*1*3

Biogeochemical Research

Yasuyuki Muramatsu, Ph.D.,Head

Shigeo Uchida, Ph.D.

Satoshi Yoshida, Ph.D.

Keiko Tagami, Ph.D.

Tadaaki Ban-nai, M.S.*2

Model Ecosystem Studies

Hiroshi Takeda, Ph.D.,Head

Kiriko Miyamoto, Ph.D.

Kei Yanagisawa, Ph.D.

Shoichi Fuma, M.S.

Yoshito Watanabe, Ph.D.*1

Yoshikazu Inoue, M.S.*2

Environmental Toxicology

Sentaro Takahashi, Ph.D.,Head

Yoshihisa Kubota, D.V.M.

Hiroshi Sato, Ph.D.*1

X.Z.Sun, Ph.D.*4

Senior Research Counselor

Tetsuo Iwakura, M.S.

Zen-ichiro Kawabata, Ph.D.*6

Low Dose Radiation Risk and Carcinogenesis Research Group

Toshiaki Ogiu, M.D., Supervising Researcher*1

Low Dose Radiation Research

Shunsaku Sasaki, Ph.D., Head

Experimental Carcinogenesis

Toshiaki Ogiu, M.D., Head

Hiroko Ishii-Ohba, Ph.D.

Yoshiya Shimada, Ph.D.

Mayumi Nishihmura

Shizuko Kakinura, Ph.D.*6

Shigeru Kobayashi, M.D.*7

Fumio Suzuki, Ph.D.*3

Cancer Genetics

Hideo Tsuji, Ph.D.

Fumiaki Watanabe, Ph.D.*5

Hideki Ukai, Ph.D.*7

Director of Special Research

Tada-aki Hori, Ph.D.*1

Kiyomitsu Kawachi*1

Research Center of Charged Particle Therapy

Yasuhito Sasaki, M.D., Ph.D.,Director General

Section of Administrative Services

Hiyoshi Sato,Section Head and 9 Staff Members

Section of Accelerator Operation

Satoru Yamada, Ph.D.,Section Head*1

Takanobu Yamada, B.S.

Kazutoshi Suzuki, Ph.D.*1

Yoshikazu Kumamoto, Ph.D.*1

Yukio Sato, Ph.D.*

Akihiro Kohno*1

Kiyomi Kasai*1

Makoto Akashi*1

Misawo Hachiya*1

Koichi Ando*1

Masao Suzuki*1

Kumie Nojima*1 and 4 Staff Members

Accelerator Operation Office

Eiichi Takada, Ph.D.,Head and 3 Staff Members

Technical Management Office

Takeshi Murakami, Ph.D.,Head and 1 Staff Members

HIMAC Machine Time Coordinator

Yoshiya Furusawa, Ph.D.*1

Koji Noda, Ph.D. *1

Akifumi Fukumura, Ph.D.*1

Medical Information, Processing Office

Kenjiro Fukuhisa, B.S., Head

Toru Matsumoto, Ph.D.*1

Shinichiro Sato, M.D.,Ph.D.

Eiko Takeda

Medical Physics and Engineering Office

Masahiro Endo, Ph.D.,Head

Hiroko Koyama-Ito, Ph.D.

Nobuyuki Miyahara, Ph.D.*1

Shin-ichi Minohara, Ph.D.*1

Katsuyuki Nishimura, Ph.D.*6

Shigeo Furukawa*9

Division of Radiation Medicine

Hirohiko Tsujii, M.D.,Director

Section of Clinical Oncology

Shinroku Morita,M.D., Section Head

1st Room

Tadaaki Miyamoto, M.D.

Tadashi Kamata, M.D.

Hirotoshi Kato, M.D.

Shigeru Yamada, M.D.

Naoyoshi Yamamoto, M.D.

2Residential Doctors

2nd Room

Junetsu Mizoe, M.D.

Takashi Nakano, M.D.

Shosuke Matsuoka, M.D.

Hiroshi Tsuji, M.D.

Atsuko Abe, M.D. and

2 Residential Doctors

Clinical Radio-Technology

Kunio Sakashita and 10 Staff Members

Section of Clinical Diagnosis

Laboratory Examinations

Hidehumi Ezawa M.D.

Hiroko Moriya and 3 Staff Members

Imaging Diagnosis

Susumu Kandatsu, M.D.

Masakuni Kanai, M.D.

Kyosan Yoshikawa, M.D.

Masahisa Koga, M.D.

and 2 Residential Doctors

Section of Nursing

Mitsuko Matsuda, Section Head

Etsuko Okazaki

Fusako Kitane

Chiemi Murakami Fujiko Sugahara and 30 Staff Members with 4

Assistants

Pharmacy

Shin Watanabe and Hisashi Teshigawara

Division of Accelerator Physics and Engineering

Kiyomitsu kawachi, Ph.D.,Director

Low Energy Beam Research

Yukio Sato, Ph.D., Section Head

Toshihiro Honma, Ph.D.

Atsushi Kitagawa, Ph.D.

Takanobu Yamada, B.S.*1

Takeshi Murakami, Ph.D.*1

Kazutoshi Suzuki, Ph.D.*1

Daisuke Ohsawa, M.S.*6

High Energy Beam Research

Satoru Yamada, Ph.D.,Section Head

Masayuki Kumada, Ph.D.

Mitsutaka Kanazawa, Ph.D.

Koji Noda, Ph.D.

Eiichi Takada, Ph.D.*1

Kuninori Endo, Ph.D.*6

Tetsumi Tanabe, Ph.D.*6

Zhang Feng-ging*6

Medical Physics Research

Tatsuaki Kanai, Ph.D.,Section Head

Masami Torikoshi, Ph.D.

Shinichi Minohara, Ph.D.

Naruhiro Matsufuji, M.E.

Yasuyuki Futami, Ph.D.*1

Masahiro Endo, Ph.D.*1

Hiroko Koyama-Ito, Ph.D.*1

Nobuyuki Miyahara, Ph.D.*1

Akifumi Fukumura. B.S.*1

Haruo Yamashita, Ph.D.*5

Munefumi Shimbo, Ph.D.*8

Teiji Nishio, Ph.D.*6

Akio Higashi, Ph.D.*4

Takashi Akagi, Ph.D.*4

Akihumi Itano, Ph.D.*4

Division of Advanced Technology for Medical Imaging

Syuji Tanada, M.D.,Director

Taiko Joshima, Secretary

Keiko Yumino, Secretary

Imaging Physice and Tracer Chemistry

Kazutoshi Suzuki, Ph.D.,Head

Hideo Murayama, Ph.D.

Terushi Haradahira, Ph.D.

Toshihiko Kawakami

Eiichi Tanaka, Ph.D.*1*2

Norimasa Nohara, Ph.D.*1*2

Osamu Inoue, Ph.D.*1

Hinako Toyama, Ph.D.*7

Hiroyuki Shinohara, Ph.D.*7

Toshimitsu Fukumura, M.S.

Toshitaka Yamazaki*4

Akio Tsuchiyama*4

Yuko Tanaka*4

Yuichi Kimura, Ph.D.*4

Tomoyuki Hasegawa, Ph.D.*4

Akemi Uehara

Keiko Kawahara

Saeko Aoki

Radiopharmaceuticals and Radiopharmacology

Toshiaki Irie, Ph.D.

Kiyoshi Fukushi, M.S.

Hitoshi Shinotou, M.D.*4

Horoki Nanba, M.D.*4

Mika Yamaguchi, M.D.*4

Shinichiro Nagatsuka, M.S.*4

Clinical Imaging

Katsuya Yoshida, M.D.,Head

Toru Matsumoto, Ph.D.

Tetsuya Suhara, M.D.

Naoyuki Watanabe M.D.

Yukio Tateno, M.D.*1*2

Takeshi Iinuma, Ph.D.*1*2

Fumio Shishido, M.D.*1*2

Hiroshi Fukuda, M.D.*1

Hiroo Ikehira, M.D.*1

Yoshiro Okubo, M.D.*7

Takashi Okauchi, M.S.*4

Hiroyuki Tadokoro, M.D.*4

Kouji Suwa, D.D.S*4

Yoshihisa Akiyama, Ph.D.*4

Yuzuru Nakamura, Ph.D.*4/td>

Mikiyo Kitajima

Kinuko Doi

Reiko Mori

Kazuko Anami

Division of Planning and Coordination

Fuminori Soga, Ph.D.,Director

Noriko Shiomitsu, Section Head and 15 Staff Members

Division of Administration

Takayuki Shirao, Director

Section of General Affairs

Kazuo Hosokawa, Section Head and 13 Staff Members

Section of Accounting

Tadaatsu Suzuki, Section Head and 14 Staff Members

Laboratory for Radioecology

Kiyoshi Nakamura, M.S. Laboratory Director

Section of Administrative Services

Tomokichi Yamazaki, Section Head and 5 Staff Members

Geochemical Research

Shigeki Hirano, Ph.D., Section Head

Masatoshi Yamada, Ph.D.

Tatsuo Aono, Ph.D.

Jing Zhang, Ph.D.*4

Bio-concentration Research

Ryoichi Nakamura, B.S., Section Head

Motokazu Nakahara, B.S.

Toshiaki Ishii, B.S.

Mitsue Matsuba

Assessment of the Impacts of Environmental Radioactivity

Teruhisa Watabe, M.S., Section Head

Taeko Miyazaki, Ph.D.

Setsuko Yokosuka

*1 Dual Capacity

*2 On Leave of Absence

*3 Visiting Scientist

*4 Research Fellow

*5 National Institute Post Doctoral Fellow

*6 Guest Scientist

*7 Guest Research Associate

*8 Priority Research Supporting Staff

*9 Research Associate, Promotion of Charged Particle Therapy